Design of Sensory Display Technologies for a Laparoscopic Palpation System in Harmony with a Surgeon

(術者と調和した腹腔鏡下触診システムに向けた
感覚情報提示技術の構築)

2019

Tomohiro Fukuda

The work presented in this thesis has been supported by Japan Society for the Promotion of Science with Grant-in-Aid for JSPS Research Fellow and Grant-in-Aid for Scientific Research(A) (Grant numbers: JP16J08253 and JP17H01252).

Design of Sensory Display Technologies for a Laparoscopic Palpation System in Harmony with a Surgeon

by

Tomohiro Fukuda

A dissertation
submitted to the Department of Electrical and Mechanical Engineering,
Graduate School of Engineering, Nagoya Institute of Technology
in partial fulfillment of the requirements for
the degree of Doctor of Engineering

Abstract

Palpation is an important technique in the clinical field to obtain mechanical information about body tissue and to localize a hard mass such as a tumor within soft tissue. It relies on input from a surgeon's tactile sense; however, tactile input is rarely available in minimally invasive surgeries such as a laparoscopy. If the surgeon's tactile sense were compensated for by computer technologies, surgeons could perform intraoperative localization of the tumor immediately before a resection, which might reduce any unnecessary resection of normal tissue. In this thesis, it is aimed to achieve intraoperative localization of an early-stage gastric tumor that cannot be visually detected during laparoscopic surgery. The focus of this study is temporal information-based palpation, in which a single output is acquired from a direct-manipulating tactile sensor and fed back to the surgeon in real-time. This is advantageous because the use of a single output results in the overall simplicity of the palpation system, and the direct manipulation can be considered as a natural extension of current laparoscopic surgery techniques. Moreover, the real-time feedback is aimed at assisting with effective decision-making on the part of the surgeon. In this study, display methods for the sensor output to the surgeon were designed and evaluated to facilitate effective laparoscopic palpation. The ultimate goal was harmonization with the surgeon, i.e., maximizing both the performance of the surgeon (who possesses flexible sensory-motor control and decision-making capabilities based on his/her broad knowledge) and that of the system (which possesses superior computational capabilities over those of the surgeon). In addition, the goal includes the enhancement of the surgeon's confidence in his/her decision making over and above the enhancement of functional performance such as the reduction of localization errors.

Firstly, the visual and tactile feedback of the single sensor output were evaluated and discussed. As visual feedback, a line graph of the time-series output was prepared on an additional monitor to the laparoscopic monitor. As tactile feedback, a device that presents a normal force to the surgeon's foot was assembled. In addition, a psychophysical experiment that used four conditions (no feedback, visual feedback,

tactile feedback, and a combination of both types of feedback) was conducted to investigate the effects of the means of feedback on the users' detection performance of a phantom gastric tumor as well as their behavior during the detection. The results showed that the visual feedback was significantly more effective in detection than no feedback, whereas the tactile feedback did not significantly enhance detection. Moreover, both visual and tactile feedback led to safer manipulation with a significantly smaller load and lower scanning speed, respectively. The findings indicated the usefulness of visual feedback in laparoscopic palpation and the necessity for the redesign of the tactile feedback whereas both types of feedback contributed to the positive effect on the manipulation.

The previous findings suggest that visual feedback of the time-series sensor output is effective in detection. However, visual feedback can be problematic, as it requires an extra monitor which would occupy valuable space in the operating room. Furthermore, a major concern is the possibility of visual sensory overload since the surgeon should concentrate primarily on the laparoscopic image. An assistance algorithm was, therefore, proposed as the replacement for the surgeon's decision based on visual information. The algorithm was designed to analyze the time series of the sensor output and provide independent detection results from the surgeon. This approach is advantageous because the reliability and safety of the manipulation are ensured by a human operator, but a more effective detection might be expected from the collaboration between a human and the algorithm. The algorithm used a deep neural network to analyze the time-series of the sensor output. The algorithm was validated using the data acquired in the previous psychophysical experiment. The validation result supports the feasibility of the proposed algorithm for detection assistance during laparoscopic palpation.

Tactile feedback of the sensor output is advantageous in laparoscopic surgery because it avoids any possible sensory overload in comparison with visual feedback. However, the previous experiment showed no significant effect of the tactile feedback (provided by the device to the foot) on detection. To assess this issue, the spatial coincidence between the manipulating hand of the sensor and the feedback site was reconsidered. The contribution of the final part of this thesis is the development and evaluation of a pneumatic tactile ring, which is a clinically applicable tactile display

presenting pressure to one of the fingers on the manipulating hand. Since the tactile ring is driven by pneumatic power, it is lightweight, cost-effective, disposable, and sterilizable. The fundamental performance of the tactile ring was investigated, and a psychophysical experiment including a localization test of a phantom tumor was performed. The results of the experiment showed that the provided tactile feedback significantly reduced the absolute error of the tumor localization and increased participants' confidence in their answers. It was shown that the feedback through the tactile ring was effective in laparoscopic tumor localization. In addition, clinical tests with surgeons were conducted on actual patients with early-stage gastric cancer. The results of the tests suggested that the tactile ring is applicable to laparoscopic surgery and effective for the localization of an actual gastric tumor.

The results and findings in this thesis characterized our approach and showed its effectiveness. Moreover, they also may expand existing knowledge in the related research field. The characterization of the visual and tactile feedback of the time series of the sensor output provides suggestions for the design of sensory feedback in not only laparoscopic palpation but also other computer-aided surgery such as robot-assisted minimally invasive surgery. Moreover, the deep neural network-based assistance algorithm as the replacement for the surgeon's visually based decision exhibited a novel approach for the collaborative decision making between human and computer. Finally, the development and evaluation of the pneumatic tactile ring showed a valuable example of effective devices validated with clinical tests on actual patients.

Acknowledgements

I would like to thank many people for their support and encouragement during my doctoral research.

Firstly, I would like to express my gratitude to my advisor Professor Akihito Sano for giving me the opportunity to work in the doctoral course. He always gave me guidance and encouragement at each moment during my research. I am always impressed by his insightful and unique idea on research.

I would like to extend my gratitude to the internal examiners of the dissertation committee for their time and effort: Professor Manabu Yamada for his constructive comments and discussions, Professor Fumihiro Itoigawa for his helpful ideas and comment. I am sure that this thesis was made clearer and stronger thanks to them.

I would like to thank Assistant Professor Michitaka Fujiwara from Nagoya University for not only being the external examiner of the dissertation committee, but also keeping the collaboration on my research. He always gave me valuable comments on the research in the clinical point of view, and it would not have been possible to perform clinical evaluations that greatly strengthen this research without his great help.

I would like to thank Associate Professor Yoshihiro Tanaka for his insightful discussions, encouragement, and guidance. I have learned many from him; for instance, technical writings, ways for effective presentations, on research plannings, on budget applications, and so on. I would not fulfill the requirement for the doctoral degree (three journal papers) without his kind support.

I would like to thank Professor Astrid M. L. Kappers from Eindhoven University of Technology for her insightful discussions on psychophysics and kind support on my works. In particular, it was a valuable experience and nice memory for me to visit her laboratory for two months in 2015, and I have found how important, difficult, and interest psychophysics is.

I am grateful to the staffs of the laboratory: Ms. Reiko Nishimura for her many supports on budget management, Ms. Aiko Ito for her support on making something, and Ms. Aya Matsui for her support on research outreach.

I thank all members that I met during my six years in the laboratory. I was inspired many times by their fresh ideas during discussions. In particular, I thank Dr. Pham Quang Trung and Mr. Motoki Tachiiri to giving me valuable discussion and their heartfelt encouragement. I hope their researches will go well.

Finally, I thank my parents Shigeki and Hisae for their understandings and heartfelt support during my doctoral research. I am really happy to obtain the doctoral degree in engineering, which I have liked since my childhood.

Contents

List of Figures

Chapter 1

Introduction

1.1 Sensory input of clinicians

Clinicians use multiple sensory modalities to assess a patient's disease. Hippocrates (approximately 460–377 BC), known as the father of modern medicine [1], emphasized that *"It is necessary to study all that one can see, feel, and hear everything that one can recognize and use"* [2]. This statement indicates that clinicians have already been taking full advantage of their sensory input to diagnosis patients. Visual information is fundamental to gathering information on patients and their illness through their body features and color. When trying to assess the inner parts of a patient's body, however, a clinician cannot rely on visual information, and so, auditory information in the form of passive sound (by auscultation) or active sound (by percussion) from the body and tactile information by palpation are more effective. Palpation is a procedure used to assess the mechanical properties (i.e., the size, shape, or stiffness) of the organs and is based on a clinician's sense of touch. Hippocrates is depicted as demonstrating the use of palpation in Fig. 1.1 [3]. These methods of clinical examination based on a clinician's sensory inputs are still important in the current clinical field.

Palpation relies on the touch information obtained during the mechanical interaction between a clinician's finger/hand and the target tissue. It is, therefore, a straightforward way to obtain the mechanical properties of that target tissue. In particular, palpation is an effective method for the localization of a hard mass, such as a tumor, embedded in soft tissue whereas the same task would be rather difficult if relying on visual and auditory information.

After the diagnosis of a patient's disease, clinicians determine the appropriate clinical treatment of the disease. One of popular treatments is a surgery, which is a physical intervention on patient's tissues, e.g., cutting malignant tissues and closing

Fig. 1.1: Hippocrates palpates a young patient–a painting by Robert Thom, 1950s (reprinted from [3]).

wounds. Sensory input of clinicians is also important during a surgery to intraoperatively obtain the anatomical structure in order to perform the appropriate operations.

1.2 Minimally invasive surgery

In recent decades, minimally invasive surgery has become a standard operative treatment in place of open surgery. In minimally invasive surgery, surgeons make small incisions on the patient's abdomen and perform the operation with long thin instruments such as graspers, scissors, and staplers. Fig. 1.2 shows the setup and schematic representation of a laparoscopic surgery, which is an example of a minimally invasive surgery. It offers many benefits to the patient in comparison with traditional open surgery such as a shorter recovery time, reduced pain, and better cosmetic healing. Surgeons are, however, faced with some limitations. For instance, they must be able to manipulate long thin instruments whose rotational and insertion movements are restricted within a hole in the patient's abdomen. In particular, the surgeons' visual and tactile inputs are severely limited because they cannot directly see or touch the target tissue as a result of the laparoscopic setup.

Minimally invasive surgery is highly supported by computer technologies. Visual information during a minimally invasive surgery is provided by an endoscope, which

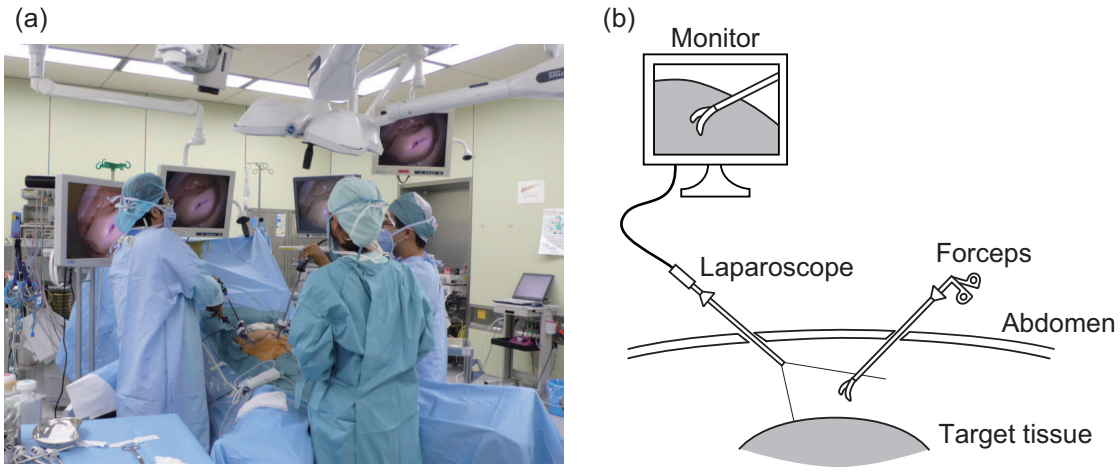

Fig. 1.2: Laparoscopic surgery: Surgeons open small holes in the patient's abdomen and use long thin instruments to manipulate the target tissue. The surgeons' visual sense is compensated for by the laparoscope (camera). (a) Setup for laparoscopy. (b) Schematic representation of the laparoscopy.

is a long thin camera. Although general endoscopes have issues such as a limited field of vision and a loss of depth information, these issues have been already overcome by recent vision technologies. For instance, high-definition and high-magnification endoscopes overcome the issue of the limited field and allow the acquisition of quite high-resolution images that cannot be achieved with human vision [4]. Stereoscopic imaging techniques can compensate for the depth information of an endoscopic image [5]. Recent computer technologies have, therefore, matured to the level that they can extend from compensation for to augmentation of the surgeons' visual capabilities.

In addition, robotic technologies have been applied to enhance surgeon's capability during a minimally invasive surgery. Robot-assisted minimally invasive surgery employs a master–slave setup, where a surgeon manipulates a master console to control surgical instruments at a slave side. da Vinci® (Intuitive Surgical Inc.) is a famous commercial robotic surgical system [6]. It offers an intuitive manipulation owing to 7 degrees-of-freedom of surgical instruments, and a surgeon can control the instruments in a similar way to his/her hand and finger. It also has functions of a tremor reduction and motion scaling to facilitate the dexterous manipulation by the surgeon. Recently,

autonomous surgery by robots has attracted attention. Yang et al. defined six levels of autonomy (0–5) for medical robots [7]. The level 0 indicates no autonomy, in which a surgeon directly manipulates surgical instruments or remotely operate a slave robot through a master console. Some research studies have tried to achieve a high level of autonomy; for instance, surgical robots with virtual fixtures [8] as an example of level 1 and autonomous suturing [9] as level 2 were developed.

In contrast to above-mentioned technologies, those for the compensation of the surgeon's tactile sense are now under development. For instance, da Vinci® does not have a function of haptic feedback. If the surgeon's tactile sense were substituted by computer technologies, the surgeon could perform dexterous manipulation and also intraoperatively localize a hard mass in the soft tissue, which could not be detected through the use of visual information. Intraoperative localization might lead to a reduction in the unnecessary resection of normal tissue with the complete resection of the malignant tissue. Furthermore, it might consequently contribute to a better quality of life for the patient with a shorter recovery time and a lower possibility of a recurrence of the disease.

1.3 Difficulty of surgical palpation

Computer technologies can be available to compensate for the surgeon's tactile sense in minimally invasive surgery. There is, however, no systematic method for the development of the devices for the compensation. There are some possible issues with the development of such kinds of devices. One issue is the insufficient understanding of human haptic perception and information processing during manual palpation. It is known that the mechanical interaction between the human skin and a target object is encoded by four mechanoreceptors (Meissner corpuscles, Pacinian corpuscles, Merkel cells, and Ruffini endings) in the skin as tactile information [10]. A neurophysiological study revealed that Merkel cells, which have a high spatial resolution, mainly contribute to the detection of a lump in soft objects during passive touch [11]. However, palpation relies on active touch, and it was also revealed that human uses complex modulation strategies during the localization of a lump by manual palpation [12]. Thus, other mechanoreceptors that mainly respond to a dynamic mechanical stimulus may also

contribute to lump detection. Moreover, the contribution of kinesthetic information, such as the finger position and posture, should be taken into account. It is, therefore, still unclear which haptic information is actually used and how the acquired information is processed for the localization of a hard mass in soft tissue. An additional difficulty is owing to the complex environment during a laparoscopic surgery. The organs have complex surfaces and can mostly be shifted and deformed during palpation; thus, the control of a sensing probe must be highly pliable and stable. Although several works have been attempted to achieve autonomous palpation by robots [13, 14], they were only successful under controlled conditions such as using known target tissues. Thus, it is challenging to apply robotic manipulation to the current minimally invasive surgery. Moreover, ethical and legal issues will be significant hurdles to overcome before widespread application is achieved.

For the above reasons, two big questions remain: how the tactile information should be acquired, and how the acquired information should be analyzed and presented to the surgeon. Moreover, the clinical applicability of such a device must first be considered. For instance, since palpation relies on mechanical interaction, sensing devices are required to be safe for patient's body tissue, e.g., no possibility of a leakage current. Being sterilization compatible is also mandatory for surgical applications. A low fabrication cost is also preferred in order to facilitate their use as disposable devices to increase the safety of the patients. The above-mentioned requirements increase the difficulty of the design of clinical devices for surgical palpation.

1.4 Objective of this thesis

1.4.1 Harmonization with a surgeon

This study aims to develop an assistive system for laparoscopic palpation utilizing computer technologies to enable the intraoperative localization of early-stage gastric tumors. The ultimate goal of this thesis is to achieve harmonization between the surgeon and the system. This harmonization refers to maximizing both performances by taking into account their characteristics. The surgeons are adept at the manipulation of surgical tools based on their sensory-motor control and wise decision-making

based on their broad knowledge and clinical experience. The system possesses superior computational abilities over those of a human being as well as the ability to perform quantitative data handling. The overall goal of the study also involves the enhancement of the surgeon's confidence in tumor localization over and above the enhancement of functional performance such as the reduction of localization errors. In other words, this study aims at making the overall surgical procedure more rewarding for the surgeons by developing a collaborative assistance system for laparoscopic palpation and does not intend to completely replace the palpation task with computer technologies.

1.4.2 Focuses in this study

To achieve the assistive system in harmony with a surgeon, the following points were focused in this study.

1) Use of a tactile sensor that is directly manipulated by the surgeon

The first point can overcome the difficulty in the control of a sensor probe during laparoscopic surgery which is a complex sensing environment. Surgeons are adept at the manipulation of tools despite this complex sensing environment as a result of their sensory-motor control. It is, therefore, reasonable to utilize their superior ability (in comparison to that achieved by a robot) for the manipulation of a sensor probe. Moreover, the use of a direct-manipulating tactile sensor is advantageous because it can be considered as a natural extension of the instruments required for laparoscopic surgery. Thus, additional training is not required in order to use the tactile sensor.

2) Use of the time series of a single output from the sensor

This point can result in the overall simplicity of the palpation system. As mentioned in the previous section, the clinical devices should have a low cost since they should be used in a disposable manner. Herein, the localization of a hard region is equivalent to the acquisition of the spatially distributed information of the target tissue; thus, it is generally required to use a sensor having multiple sensing elements. However, the tactile sensor with a single output can also acquire the information equivalent to the spatial distribution by dynamically scanning the sensor probe against the target tissue. In other words, using the time series of

the single sensor output is an effective and reasonable means to obtain the target information while maintaining the simplicity of the sensor. In a previous study, a forceps-type tactile sensor based on acoustic reflection has been developed [15]. The sensor has advantages for applications in laparoscopic surgery. The sensing technology for the palpation system has, therefore, been prepared.

3) Real-time feedback of information from the sensor to the surgeon

This point is mainly aimed at assisting with effective decision-making on the part of the surgeon. The surgeon most likely knows the internal model of the target tissue based on his/her broad knowledge and clinical experiences; thus, it can be expected that he/she can effectively interpret the feedback from the sensor. In addition, real-time sensory feedback might facilitate the improved manipulation of the sensor probe. Human sensory input and motor control are bidirectionally related; that is, whenever a movement is generated, sensory input is received as a result of that movement. Human then modifies the motor command to achieve the desired movement of his/her body/tools according to the sensory feedback. It can, therefore, be expected that providing real-time feedback from a sensor is informative for the more-stable and pliable manipulation of the sensor.

In this thesis, sensory display technologies for the single sensor output are designed and evaluated for the achievement of a palpation system in harmony with a surgeon according to the above-mentioned points. It offers the discussion about how the information measured by the direct-manipulating sensor should be presented to the surgeon in such a way that performance and effectiveness improve.

1.4.3 Target of palpation

The underlying scenario in this study is the laparoscopic resection of early-stage gastric cancer. Our target is a 0-IIc (superficial ulcerative) type tumor [16], which is the most common type of early-stage gastric tumor. The tumor is located on the mucosal side of the stomach wall and cannot be detected visually from the serosal side. Surgeons preoperatively observe the location of the tumor by peroral endoscopy; however, the preoperative information is not available during surgery. In the current procedure, there are several methods available to intraoperatively determine the location of the tumor

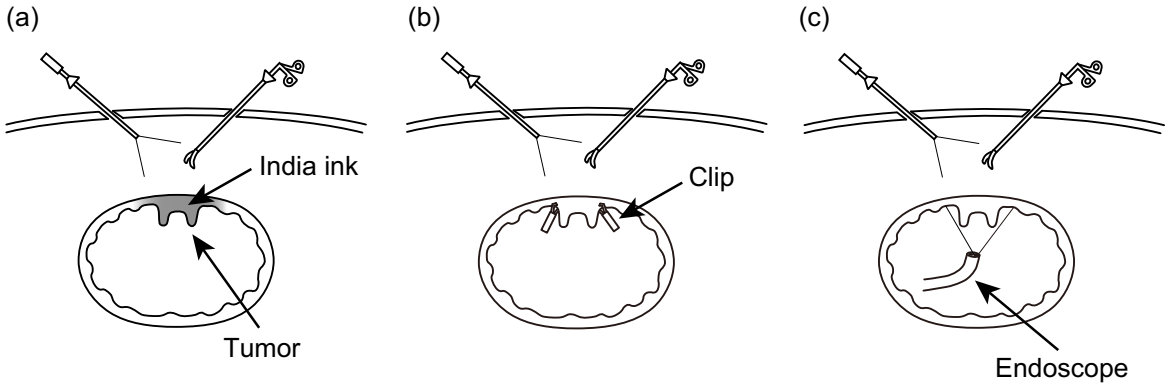

Fig. 1.3: Current technologies for intraoperative localization of early-stage gastric tumors. (a) Tattoing. (b) Clipping. (c) Intraoperative endoscopy.

such as preoperative endoscopic tattooing and clipping, and intraoperative endoscopy (see Fig. 1.3).

Endoscopic tattooing is a method to inject marker such as India ink to the tumor from the mucosal side under preoperative endoscopy and allows the surgeon to detect the marked region visually from the serosal side intraoperatively. However, it was reported that there have been some cases of undesirable spillage and spreading of the marker [17], which leads to the possibility of the mislocalization of the tumor. Another method is applying several clips to the mucosal surface under endoscopy, which the surgeons can then intraoperatively detect using ultrasonography [18] and radiography [19]. This method increases the complexity of the surgery owing to the additional procedures required to take transmission images and is not a straightforward localization method since the surgeons are required to interpret the acquired two-dimensional image in order to determine the tumor position. There is an additional method to intraoperatively locate the tumor before the resection using an endoscope [20]. This method requires an additional surgeon to operate the endoscope, and if the tumor boundary is unclear, the method will be not effective.

If intraoperative tumor localization by palpation with the aid of computer technologies were achieved, it might help the surgeon to determine the appropriate cut-line immediately before the resection by palpating the serosal surface of the stomach wall. Herein, there are cases of early-stage gastric cancer of small size and shallow invasion

depth that cannot be detected even through manual palpation in open surgery. In such cases, using preoperative clipping techniques, the surgeons might localize the tumors through the detection of the clips by palpation.

1.5 Organization of the thesis

This thesis is organized as follows:

In Chapter 2, recent technologies on sensing and displaying for clinical applications are summarized and categorized. Sensing technologies are summarized based on their principle and sensing information. Display technologies are categorized based on sensory modality. The advantages/disadvantages of the current technologies are discussed on the basis of clinical applications, and the details related to temporal information-based palpation, which is a focus of this thesis, are explained.

In Chapter 3, visual and tactile feedback of the time series of the sensor output were prepared and characterized through a psychophysical experiment with a detection task of a phantom early-stage gastric tumor under a simulated laparoscopic surgery setup. The effects of the visual and tactile feedback on the detection performance of participants and their detection behavior were investigated. The findings in this chapter indicate that both types of feedback are useful for laparoscopic palpation; however, their effects depend on the way in which they are presented.

In Chapter 4, an assistance algorithm using a deep neural network (DNN) is proposed as a replacement for the surgeon's visual-based decision. Although the visual feedback of the time series of the sensor output is effective in detection, it has the possible disadvantage of sensory overload. The algorithm is designed to assist the surgeon by analyzing the time series of the sensor output and providing independent detection results. The algorithm is validated using the data acquired from the experiment in Chapter 3, and the feasibility of the algorithm for detection assistance is shown.

In Chapter 5, a pneumatic tactile ring, which is a clinically applicable tactile device to provide instantaneous feedback from the tactile sensor, is developed. The findings in Chapter 3 exhibit no significant effect of the tactile feedback on detection, whereas the tactile feedback leads to safer manipulation with significantly lower scanning speed. It is assumed that the main issue is inferior spatial coincidence between

the manipulating hand of the sensor and the feedback site. To address this issue, we designed the tactile ring such that it presents pressure to the surgeon's finger pad on the manipulating hand. The tactile ring is lightweight, cost-effective, disposable, and sterilizable; thus, it has high applicability to surgical situations. The fundamental performance of the tactile ring is investigated, and the effect of the feedback through the tactile ring on tumor localization is investigated through a psychophysical experiment. It is shown that the tactile feedback through the ring is effective in laparoscopic tumor localization. Furthermore, this chapter mentions the details and results of clinical tests on actual patients for the localization of an early-stage gastric tumor.

In Chapter 6, the results and findings from the previous chapters are summarized, and the future orientations of the study are then discussed.

Chapter 2

Related works

This chapter summarizes the state-of-the-art sensing and sensory display technologies in manipulation and palpation with respect to their clinical applications. Sensing technologies are classified based on their principles and sensing information, and display technologies are categorized based on the sensory modality for receiving information. Moreover, the detail of the focus in this thesis, temporal information-based palpation, is discussed.

2.1 Introduction

Surgical skills involve manipulation and palpation. Manipulations such as a needle insertion, making incisions, or suturing a wound, are based on the surgeon's sensory-motor control for achieving the desired movements with surgical instruments, or handling of target tissue. Palpation is also based on sensory-motor control, but ultimately, it is aimed at obtaining information about the target tissue, or detecting hard masses such as tumors in soft tissue. These skills, therefore, rely on sensory inputs from the visual, auditory, and tactile channels [21] as mentioned in Chapter 1, and a surgeon efficiently integrates these sensory inputs. However, in laparoscopic surgery, there are difficulties in dexterous manipulation and palpation owing to the limitation of the surgeon's tactile sense. Computer technologies can compensate for the surgeon's tactile sense and overcome these difficulties.

Many researchers have tried to compensate for the surgeon's tactile sense in minimally invasive surgeries such as a laparoscopy. Various devices for the acquisition of tactile information and for displaying sensory information to the surgeon have been developed. In this chapter, the current technologies of sensing and sensory display for not only achieving palpation but also achieving enhanced manipulation are summa-

rized, and their characteristics are discussed from the point of view of their clinical application.

2.2 Review on sensing technologies

There are many devices aimed at the acquisition of tactile information such as force and vibration during minimally invasive surgery. Firstly, the current sensors using various principles are listed, and advantages/disadvantages of each sensing principle for clinical applications are discussed. The sensors are then classified into two categories based on the information acquired.

2.2.1 Sensing principles

Using electrical elements

A straightforward way to acquire tactile information is using conventional electrical sensing elements such as commercial force sensors [22, 23], strain gauges [24–28], piezoelectrical materials [29–32], piezoresistive materials [33], capacitive sensors [34], Hall effect sensors [35], and differential coil sensors [36]. These kinds of sensing elements tend to have high sensitivity, resolution, and repeatability owing to well-designed and improved sensing principles in the engineering field. It is possible to miniaturize a sensing element by employing MEMS (micro electro mechanical systems) technologies and to integrate multiple elements into a single package (i.e., [37–39]). Moreover, it is popular to use an array-type sensor to obtain distributed information [40–44]. To obtain tactile information, which is a direct mechanical interaction with the target tissue, a frequent design is to put elements quite near to the position of the interaction site. This design reduces the electrical safety for the patient's body tissue. Moreover, such sensors tend to be structurally complex owing to the need for electrical wiring, which is a disadvantage with respect to their being used in a disposable manner. Furthermore, it is also possible that these sensors can be affected by noise from other electrical surgical instruments such as an acusector inside the patient's abdomen.

Without electrical elements

Considering the electrical safety of sensors for the body tissue is mandatory for clinical applications. There are many studies aimed at the development of clinically applicable sensors. Firstly, it is popular to use the vision-based principle, which relies on camera images to acquire the displacement of markers owing to the mechanical interaction with the target tissue [45–48] or the deformation of the target tissue [49–56]. Although this principle is effective in obtaining spatially distributed information, it is not cost-effective and tends to be bulky owing to the use of cameras. A similar principle is the optically-based principle, in which the displacement of the sensing part is measured via changes of intensity of reflected light using a photodetector [57, 58]. Optical fibers are commonly used to separate optical sensors and the sensing site [59–65]. This design is electrically safe for the body tissue because any electrical parts are kept outside of the patient's abdomen. It is also a compatible principle for the design of a long thin probe like surgical instruments. Another method is to measure force/pressure mediated by a fluid such as water [66] and air [67]. This approach has the same advantage as using optical fibers in that it can sense information at a distance. Moreover, it was shown that these methods can be used to actuate an end effector [66] and change the size of a sensing part [67] as well as the sensing functions. The above-mentioned sensors without electrical elements have the great advantage of electrical safety for the body tissue; however, they also have some complexity, which can impede their use in a disposable manner.

Another type of sensor without electrical elements is visualization. For instance, Takaki et al. used a Moiré fringe to visualize the grasping force of surgical instruments [68]. Watanabe et al. developed a silicone retractor to visualize the retraction force from deformation of markers on the silicone body [69]. Visualization techniques require no electrical elements and tend to be structurally simple; thus, they are advantageous in clinical applications. Such techniques, however, cannot offer quantitative sensing information. Moreover, there are studies aimed at the estimation of the reaction force at the end effectors in teleoperation [70–72]. Although these methods do not need any sensing elements, they cannot acquire actual information owing to mechanical interaction and can also be affected by inertia, gravity, or frictional forces on a slave robot.

2.2.2 Sensing information

This section classifies the current sensors developed for clinical applications based on sensing information and discusses the advantages/disadvantages of each type of sensor.

Spatial information-based sensing

The first group of sensors is those that acquire spatial information. It is popular to obtain spatially distributed information using a sensor array [40–44] and camera images [49–56, 63, 64]. Since the information of a certain area can be obtained at the same time, the sensing movement is mainly the vertical pressing against the target, and lateral dynamical scanning is not needed. The sensing information is, therefore, not largely affected by sensing conditions such as a pressing force and a posture of a sensor probe. A main issue of spatial information-based sensing is that the sensors tend to have complex structures owing to the use of multiple sensing elements.

Temporal information-based sensing

Another group is sensors that have a single sensing element [22–28, 34, 35, 57, 59–61, 65–67]. This sensing method is popular for the purpose of the enhancement of dexterous manipulation. For the localization of tumors, such sensors should be dynamically and laterally scanned against the target tissue, and the time series of the sensor output is analyzed to obtain the information about the target tissue. They tend to be structurally simple, which leads to high cost-effectiveness, in comparison with spatial information-based sensors. The sensing information can, however, be largely affected by sensing conditions; thus, stable and dexterous control of the sensor probe is required.

2.3 Review on sensory display technologies

How the information obtained is displayed is just as important as the sensing technologies. This section summarizes different methods based on the sensory modality used for the display.

2.3.1 Visual feedback

It is popular to use the surgeon's visual channel for displaying the sensor output. There are studies aimed at providing sensory information through the visual channel using a color map [73–76], a color bar [77, 78], or a sequential lamp [79]. Visual feedback is advantageous because it can offer intuitive interpretation of the display information thanks to various presentation parameters such as color, shape, and position. For instance, a color map overlaid on an endoscopic image is effective because surgeons can easily find a hard portion through its color distribution and localize the projected position to the actual tissue [80, 81]. However, a general issue of using visual feedback is the possibility of sensory overload [82]. In minimally invasive surgery, surgeons fully rely on their visual input and, therefore, providing additional information through the visual channel might degrade the original information such as the endoscopic image and surgeons' performance during the surgery. Braun et al. showed that force feedback during robot-assisted surgery significantly reduced the surgeons' visual stress and fatigue [83]. This finding implies the possibility of visual sensory overload, and also the necessity for an appropriate design for the visual feedback of sensory information during minimally invasive surgery.

2.3.2 Force/Tactile feedback

To prevent sensory overload, it is effective to use a different sensory input of the surgeon. Force (kinesthetic) feedback is popular in robot-assisted minimally invasive surgery [84–90]. Although it is a straightforward way to compensate for the lack of kinesthetic information during surgery, it can affect the manipulation of the sensor probe or the stability of the control loop in teleoperation [91].

An alternative method is tactile feedback. For instance, devices to present displacement [92, 93], multi-degree-of-freedom displacement [94], distributed pressure or displacement [95–99], vibration [100–103] and contact force and posture [104]. These devices are advantageous because they are independent of the visual channel and do not interfere with the surgeon's manipulation. Devices providing tactile feedback should meet the same requirements for clinical applications as sensors because the devices are in direct contact with the surgeon's body.

2.3.3 Auditory feedback

Another feedback method is using the auditory channel but few studies have been conducted. For instance, there are devices that provide sounds related a force measured by a microforceps [105] and a sequential tone according to an insertion force of a microcatheter during endovascular coil embolization [106]. It might be a simple feedback method since an audio cue is easily provided by a speaker from a distance but the audio feedback might interfere with alarms from other surgical equipment and conversation between surgeons. In addition, Koehn et al. investigated surgeons' and non-surgeons' preference of tactile and auditory feedback of instrument vibration during robotic surgery, and they showed that tactile feedback resulted in the participants being more careful and aware of tool contacts in comparison with the auditory feedback [107]. This suggests the necessity and difficulty of an effective design for auditory feedback methods in clinical situations.

2.4 Temporal information-based palpation

Three focus points in this thesis to achieve a laparoscopic palpation system in harmony with a surgeon were described in Chapter 1. We refer to these points as temporal information-based palpation, in which a single output is acquired from a direct-manipulating sensor and fed back to the surgeon in real-time. In a previous study, we have developed a forceps-type tactile sensor based on acoustic reflection aiming at intraoperative tumor localization in laparoscopic surgery [15]. The sensor uses a long thin acoustic cavity with a deformable part as a sensing area. It can respond to a uniaxial deformation applied to the sensing area as a result of contact with the target tissue. If the surface of the target tissue is continuously scanned by the tactile sensor, therefore, tumor localization can be conducted on the basis of temporal change in the sensor output. Our sensor can, thus, be categorized as temporal information-based sensing. As mentioned above, a main issue of temporal information-based sensing is that the sensing information can be largely affected by sensing conditions such as pressing force and posture of the sensor probe. To address this issue, we designed the sensor such that it is directly manipulated by the surgeon. Laparoscopic surgeons are

adept at manipulating long thin instruments like forceps; thus, we aimed to introduce the surgeons' manipulation skill into our palpation system. Moreover, in our palpation system, tumor localization is performed by the surgeons based on provided information from the sensor in real-time. Thus, simplicity of the entire palpation system can be guaranteed owing to the use of single sensor output, but effective tumor localization can be expected as a result of the surgeons' manipulation skills and their decision-making abilities based on their clinical experiences.

In this thesis, we focus on visual and tactile feedback of temporal information from the sensor. Although auditory feedback can be one of feedback means, it is not considered because of the possibility of interference with alarms from other surgical equipment and the surgeons' conversation. Moreover, we neglected auditory feedback to make room for the further improvement of our palpation system. As summarized in the previous section, each feedback method has advantages and disadvantages for clinical applications, and they should be appropriately designed. We, therefore, firstly characterize visual and tactile feedback of the sensor output in Chapter 3, and then, we discuss the solutions to overcome the issues of each type of feedback in Chapters 4 and 5.

2.5 Summary

In this section, we summarized the state-of-the-art sensing and display technologies for the compensation of surgeons' tactile sense in minimally invasive surgery. The current sensing principles were firstly classified based on whether or not electrical elements are used for sensing. With respect to clinical applications, sensing technology that does not require electrical elements is preferred to ensure the safety of the body tissue such that there is no possibility of a leakage current. The current sensors were then classified as follows based on their sensing information: spatial information-based and temporal information-based sensing. Sensory display technologies were summarized based on the following sensory modalities: visual, force/tactile, and auditory feedback. The use of each modality for presenting sensing information has advantages and disadvantages with respect to clinical applications. Thus, the sensory display technologies for clinical applications should be appropriately designed. Finally, we mentioned our focus in this

thesis: temporal information-based palpation. In this palpation, a single output is acquired from a sensor and presented to the surgeon; therefore, it has the important advantage of simplicity. We have already developed the tactile sensor with clinical applicability for temporal information-based palpation. In this thesis, sensory display technologies for the output from the tactile sensor are developed and evaluated.

Chapter 3

Characterization of the visual and tactile feedback of single sensor output

In this chapter, visual and tactile feedback of the time-series sensor output are prepared and characterized through a psychophysical experiment that consists of four feedback conditions (no feedback, visual feedback only, tactile feedback only, and a combination of visual and tactile feedback). The effects of each type of feedback method on participants' detection performance of a phantom early-stage gastric tumor and detection behavior are investigated. The advantages/disadvantages of each type of feedback are then discussed in relation to its clinical application.

3.1 Introduction

Sensory feedback, such as visual, auditory, and tactile feedback, of information to human users is an effective method to augment their functional performances. For example, there are studies to investigate the effect of sensory feedback in user interfaces such as a mouse-type device [108], a touchscreen [109], and a floating virtual screen [110]. Moreover, it was reported that there are many studies to investigate the effects of vibrotactile feedback on various task performances of the users [111]. For instance, it was shown that providing tactile feedback on events occurring in a virtual environment improves the performances in a grasping and holding task [112], a balancing task [113], and a paddle juggling task [114]. In addition to the functional performances of various tasks, it is known that sensory feedback affects users' behavior. A popular application is walking navigation; for instance, there are studies aimed at controlling pedestrians' walking direction by providing a dynamic visual stimulus such as a moving

stripe pattern on the ground [115] and a cropped real-world image on a head-mounted display [116]. There are also examples to achieve walking navigation by providing vibrotactile feedback with rhythmic patterns [117] by multiple vibrators [118], and those that induce an illusory pulled sensation [119]. Although the above-mentioned studies on navigations utilized the positive effects of sensory feedback, they also imply that sensory feedback for the improvement of task performances might unintentionally affect users' behavior at the same time. Thus, in the design of sensory feedback, it is important to not only evaluate the effect on performances but also the effect on behavior.

We aim to achieve laparoscopic palpation by providing sensory feedback according to the information acquired by a tactile sensor in real-time. An important research question is how the information should be fed back to the surgeon in such a way that performance and effectiveness improve [120]. In master–slave surgical systems, there are studies to investigate the effectiveness of various means of feedback. For instance, Gwilliam et al. investigated the effects of haptic and visual force feedback on performance in identification of an embedded rigid object and on exploratory movements [121]. Tavakoli et al. compared visual and force feedback in terms of performance in lump localization, exploration time and energy supplied to the tissue [79]. On the other hand, in palpation systems with a directly manipulated tactile sensor, there are few studies considering the use of tactile feedback whereas visual feedback is popular as mentioned above. To the best of our knowledge, there is no study comparing the effects of various means of feedback on system performance and exploratory movements for palpation systems with direct sensor manipulation.

In this chapter, we aim to design and evaluate means of feedback from the tactile sensor for laparoscopic tumor detection. We considered two means of feedback that could be of use in surgical applications. One is visual feedback through an extra monitor placed next to the laparoscope monitor. The other is tactile feedback; we developed a tactile display using a voice coil motor for presentation of a normal force to the surgeon's foot, which is a so-called unclean area. Thus, the tactile display does not need to be sterilized for clinical use. A psychophysical experiment with a detection task using phantoms of the stomach wall with/without a tumor was conducted in a simulated laparoscopic setup for four conditions regarding feedback from the tactile sensor: no

feedback, only visual feedback, only tactile feedback, and a combination of both visual and tactile feedback. During the experiment, the pressing force and sensor position were measured to analyze the behavior of participants. Moreover, we conducted a few informal trials with four expert surgeons to assess the practical effectiveness of the sensory feedback. The findings in this chapter offered good suggestions for the design of the feedback methods for laparoscopic tumor detection.

3.2 Methods

3.2.1 Tactile sensor

We have developed a tactile sensor using acoustic reflection for laparoscopic tumor detection [15]. The sensor uses a long thin acoustic cavity with a deformable part as a sensing area, a speaker and a microphone. A sinusoidal acoustic wave with a single frequency is continuously inserted into the acoustic cavity. The sensor can detect the magnitude of deformation due to the force applied to the sensing area by measuring the amplitude of the acoustic wave in the cavity. The sensor does not have any electrical elements within the part that is inserted into a patient's body. It has high applicability to laparoscopic surgery because it has suitable dimensions and electrical safety for body tissue. It can also be used in a disposable manner because of its low fabrication costs.

Fig. 3.1 shows the tactile sensor for laparoscopic tumor detection. The sensor is composed of a sensor tip having the sensing area, an aluminum tube and a handle in which the speaker and the microphone were embedded. We used a sinusoidal acoustic wave with a frequency of 3065 Hz, which was determined according to results of theoretical analyses [15] and the experimental resonance characteristics of the sensor used. The sampling frequency of the sensor is 1 kHz. The sensor detects a uniaxial force applied to the sensing area, which is located on the side of the tip. Thus, if the surface of the target tissue is continuously scanned by the tactile sensor, tumor detection can be conducted on the basis of the temporal change in the sensor output.

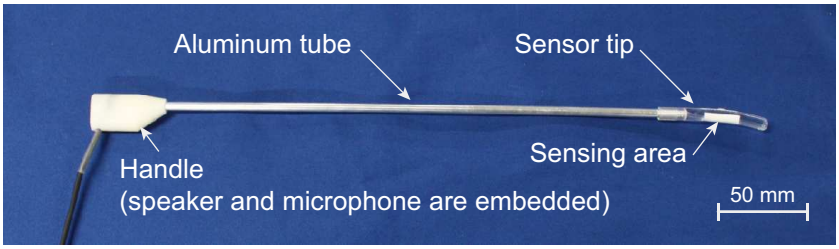

Fig. 3.1: Forceps-type tactile sensor using acoustic reflection.

3.2.2 Means of feedback of the sensor output

Visual feedback

A line graph on a monitor is offered to the user. The height of the line graph on the monitor $h(x,t)$ at a time t is given by the following equations:

$$\text{if } t \leq T$$

$$h(x,t) = \begin{cases} C_{\mathrm{v}} e_{\mathrm{v}} \left(\dfrac{T}{L} x \right) & \left(x \leq \dfrac{L}{T} t \right) \\ 0 & \text{otherwise} \end{cases} \tag{3.1}$$

$$\text{if } t > T$$

$$h(x,t) = C_{\mathrm{v}} e_{\mathrm{v}} \left(t - T \left(1 - \frac{x}{L} \right) \right), \tag{3.2}$$

where $x \in [0, L]$ shows the horizontal axis on the monitor, $L = 238$ mm is the width of a presenting area, and $C_{\mathrm{v}} = 159$ mm/V is the gain of the visual feedback. The line graph offers the time history for $T = 5$ s. $e_{\mathrm{v}}(t)$ is the sensor output smoothed by a low-pass filter with a cut-off frequency of 10 Hz to reduce noise. Fig. 3.2 shows the typical visual feedback when the user scans phantoms of the stomach wall with/without a tumor. The user can see two peaks if they appropriately scan the outside surface of a phantom with the tumor in a lateral direction. The tumor has a toroidal shape (details are provided in Section 3.3.2), and the sensor responds with two small peaks in this case. The typical sensor output was about 0.03 V peak to peak; thus, the height of the peaks was about 4.8 mm on the monitor. The typical distance between the monitor and participants' eye-position was about 1 m.

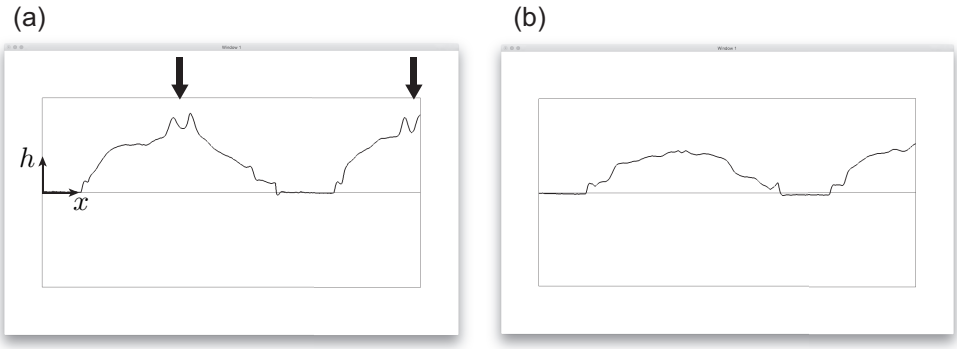

Fig. 3.2: Typical visual feedback when a user scans a phantom of the stomach wall. (a) Visual feedback for a phantom with tumor. (b) Visual feedback for a phantom without tumor. The horizontal axis shows time. The vertical axis shows the sensor output. Black arrows indicate the peaks that mark the tumor.

Tactile feedback

The body part to which the tactile feedback will be applied is an important factor to consider in the design of a clinical device. Although the finger has better tactile sensitivity than other areas of the body, the necessary sterilization of a tactile display on the finger imposes serious design issues. The foot is a better choice because it is an unclean area of surgeons, and a tactile display for the foot does not need to be sterilized. Schoonmaker et al. attempted vibrotactile feedback to the bottom of the foot according to forces measured at a surgical tool tip for minimally invasive surgery [122]. They showed that the addition of vibrotactile feedback provided better control of force application.

In this chapter, we developed a tactile display using a voice coil motor for the user's foot. The tactile display was designed to present a normal force to the upper side of the foot (instep) since this area has higher tactile sensitivity to static pressure than other areas [123]. Fig. 3.3 shows the tactile display for the instep. It is composed of a voice coil motor (AVM30-15, Akribis Systems Japan Co., Ltd), a linear guide, a rubber hemisphere, a flexible stand, and a base. The display can be fixed by placing the user's foot on the base. The rubber hemisphere guarantees stable contact with the instep.

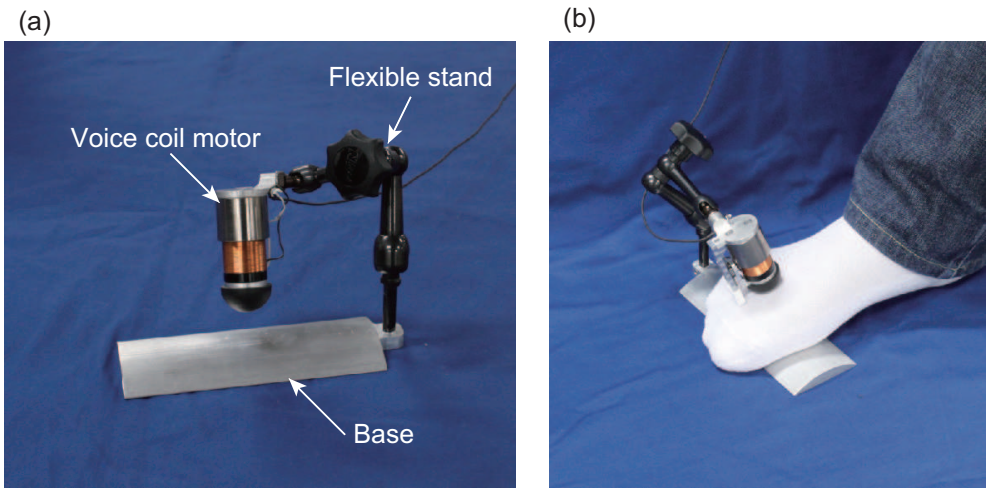

Fig. 3.3: Tactile display presenting a normal force to the user's instep. (a) Composition of the tactile display. (b) Usage of the display.

The tactile display presents a force on the basis of the sensor output as shown by the following equation:

$$f(t) = C_{\mathrm{t}} e_{\mathrm{t}}(t), \tag{3.3}$$

where $C_{\mathrm{t}} = 196.9$ N/V is the gain of the tactile feedback. If the typical sensor output is obtained as shown in Fig. 3.2(a) (0.03 V peak to peak), the tactile display presents a force of 5.9 N peak to peak. The gain was determined on the basis of a preliminary experiment so that participants clearly felt the change in force due to the tumor but did not feel pain. If the user appropriately scans the phantom with the tumor, they can feel two sequential peaks in the same way as the visual feedback. The refresh rate of the force presentation is 250 Hz. $e_{\mathrm{t}}(t)$ is the sensor output filtered by a bandpass filter with a bandwidth of 0.5–10 Hz. According to Weber's law [124], a just noticeable difference in a stimulus is proportional to the intensity of the standard stimulus. If the tactile feedback is linear for the sensor output, the offset force during contact with a phantom brings less sensitivity for small changes in force due to the tumor. Thus, the high-pass portion of the filter acts to reduce the offset of the sensor output.

3.3 Psychophysical experiment

We investigated the effects of the means of feedback on user performance and exploratory movements through a psychophysical experiment. Our scenario in this chapter is that surgeons preoperatively know the position of the tumor by peroral endoscopy. Then, the surgeons intraoperatively determine a region of interest based on known information, and they inspect the region with the tactile sensor to determine whether the region includes the tumor or not. Thus, we employed a detection task to assess the fundamental effect of the sensory feedback on discrimination of two types of stimuli with different subsurface features (with/without the tumor).

3.3.1 Participants

Twelve persons (6 male and 6 female, age range 18–24, mean 21) were paid to participate in this experiment. All participants were strongly right-handed according to Coren's test [125]. They did not have any medical background. They gave their written informed consent before participation. The experimental procedure was conducted in accordance with the ethical standards of the Helsinki Declaration and approved by the Ethical Committee of the Nagoya Institute of Technology.

3.3.2 Stimuli

The detection target is a 0-IIc (superficial ulcerative) type tumor [16], which is the most common type of early-stage gastric cancer. The tumor is located on the mucosal side of the stomach wall and cannot be detected visually from the serosal side in laparoscopic surgery. We designed phantoms of the stomach wall with/without the tumor on the basis of the typical dimensions and softness of the actual stomach wall and the 0-IIc type tumor. Figs. 3.4(a) and (b) show the phantoms used in the experiment. The phantoms had a length of 180 mm, a width of 120 mm and a thickness of 9 mm. They have two layers made of two different polyurethane gels. One layer is a harder sheet made of a gel with the hardness of Asker C 2 (Hapla Pudding Gel, PL-5, Polysis Co., Ltd), imitating the serosa of the stomach wall. The other layer is a softer sheet having folds made of a gel with the hardness of Asker C 0 (Hapla Pudding Gel, PL-00, Polysis

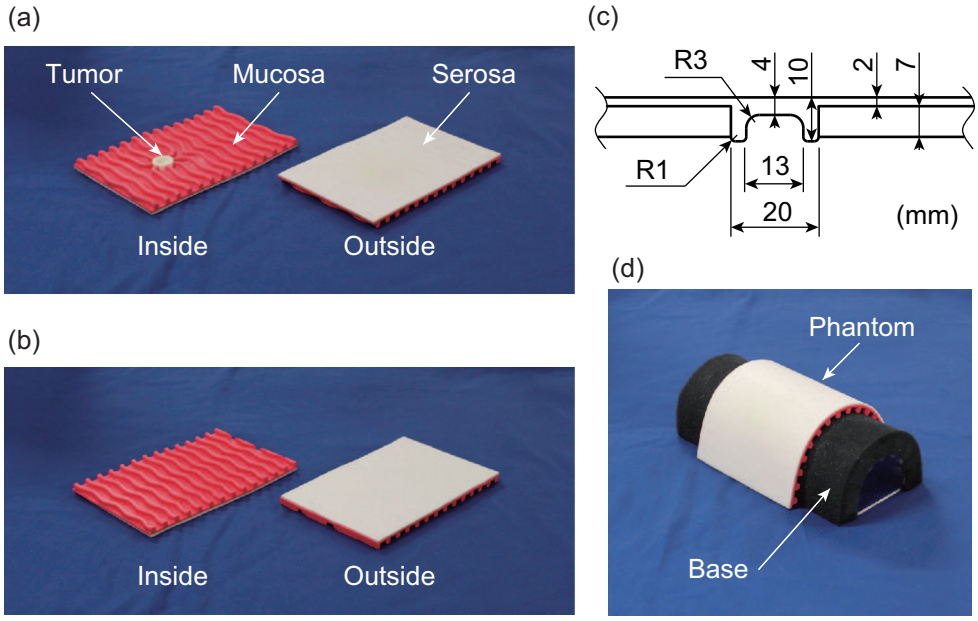

Fig. 3.4: Stimuli for the psychophysical experiment. (a) Phantom of the stomach wall with tumor. (b) Phantom without tumor. (c) Cross-sectional drawing of the phantom with the tumor. (d) The phantom was placed on a semicylindrical sponge in the experiment.

Co., Ltd), imitating the mucosa. The tumor is made of the same gel as the harder layer. The thicknesses are 2 mm and 7 mm for the harder and softer layers, respectively. The tumor has a toroidal shape, and the cross-section of the phantom with the tumor is shown in Fig. 3.4(c). The outer diameter of the tumor is 20 mm, the inner one is 13 mm, and the height is 8 mm. We compared the stiffness of surgically resected stomachs and the phantom through the measurement with a durometer (Asker Durometer Type FP, Kobunshi Keiki Co., Ltd). The stomachs and phantom were placed on a rigid plate, and the durometer was pressed against them from the mucosal side. For the actual stomachs, the mean stiffness was Asker FP 34 (value range 0–68) for the normal area and Asker FP 44 (value range 20–100) for the tumor area. The mean stiffness of the phantom was Asker FP 63 for the normal area and Asker FP 81 for the tumor area. Although the phantom has higher stiffness than the actual stomach and tumor, these values are not greatly different because they lie in the stiffness range of the actual

stomach and tumor. Each phantom was placed on a base, where a urethane sponge with a thickness of 20 mm was stuck on the surface of a semicylindrical acrylic base with a radius of 30 mm, as shown in Fig. 3.4(d) to mimic the fact that the stomach does not have flat surfaces. Moreover, the stomach is located on the ventral side of the pancreas, which is a harder organ than the stomach and fixed to the retroperitoneum with minimal deformation. Thus, we assumed that the phantom on a sponge created a condition similar to that of the actual one.

3.3.3 Setup

Fig. 3.5 shows the experimental setup. It was composed of a laparoscopic training box (Endowork-Pro II, Kyoto Kagaku Co., Ltd), a 12-mm trocar (Endopath XCEL CB12LT, Ethicon Inc.), a camera, a monitor for displaying the camera image, the tactile sensor, a laptop PC for the visual feedback and the tactile display. The participants stood in front of the training box during the experiment. They were asked to wear headphones playing white noise to avoid hearing sound from the acoustic tactile sensor although the sound was barely audible. All participants wore the same socks prepared for the tactile display. The participants used their right hand for manipulation of the sensor and always placed their right foot on the base of the tactile display. They could always see the monitor that presented the camera image regardless of the experimental condition. To avoid visual detection of the tumor, the training box was covered with a black cloth and the camera image was blurred a little by adjusting the focus. A marker (black circle) was attached above the sensing area for easy observation of the sensor position.

The stimuli were placed on a three-axis force sensor (Gamma SI-32-2.5, ATI Industrial Automation, Inc.), and they were fixed to the inside of the training box to keep their position constant regardless of random stimulus presentation. The position and posture of the sensor were measured by a motion capture system (OptiTrack, NaturalPoint, Inc.) with six cameras, which were located above the experimental setup and the participant. A custom-made marker set (four spherical infrared markers) was fixed to the sensor for rigid-body registration of the sensor. The force exerted and sensor movements were measured at sampling frequencies of 1 kHz and 120 Hz, respectively.

The experiment consisted of the following four conditions regarding the feedback

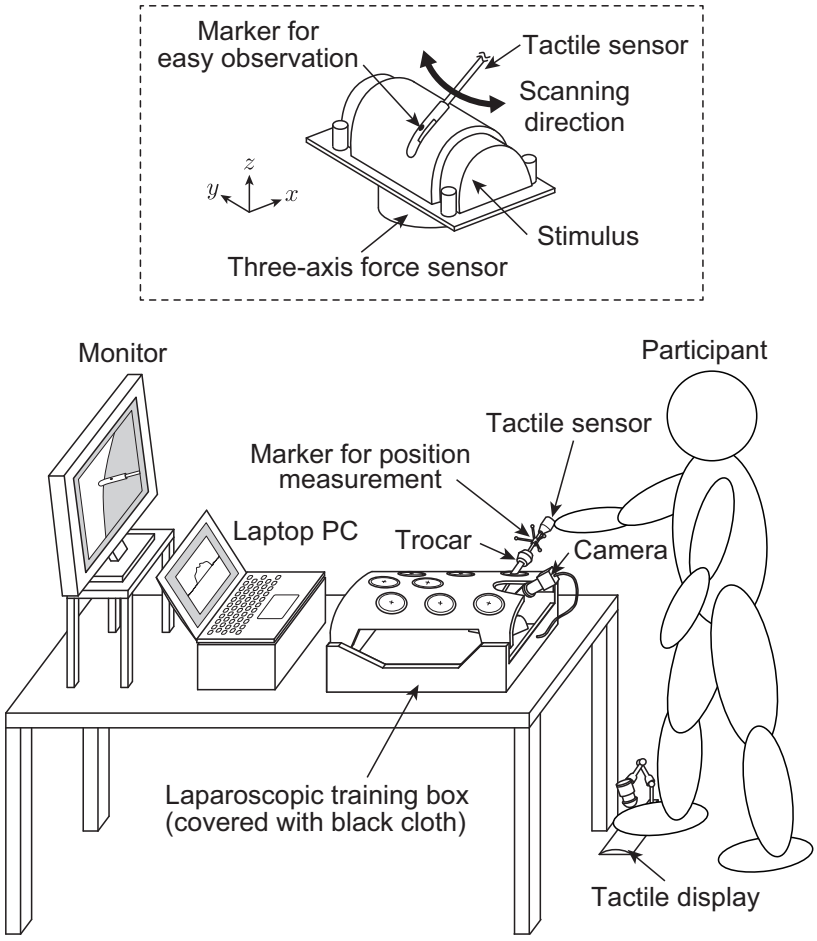

Fig. 3.5: Experimental setup. The dashed rectangle shows the inside of the training box.

from the tactile sensor: no feedback (N), visual feedback (V), tactile feedback (T), and combined visual and tactile feedback (VT). Under condition N, the participants did not receive any feedback from the sensor. Under condition V, the laptop PC presented the line graph according to Eqs. (3.1) and (3.2) but the tactile display did not work during the experiment. Under condition T, the tactile display presented the normal force according to Eq. (3.3). The laptop PC did not present any meaningful information and showed only a constant line graph at zero regardless of the sensor output. Under condition VT, the participants received both visual and tactile feedback. Under

the all conditions, direct haptic information was always available because participants physically interacted with the stimuli through the rigid sensor probe.

To reduce learning effects, each condition was conducted on a different day. Fig. 3.6 shows an example of the experimental procedure for one participant. The interval between conditions was more than 24 hours, and all participants completed the four conditions within three weeks. The order of the conditions was counterbalanced across the participants. Each experimental day consisted of a practice session and an experiment session.

3.3.4 Experimental design

Practice session

The participants practiced the sensor manipulation under the corresponding condition. They were asked to memorize the difference in the corresponding feedback when they palpated the stimulus with/without the tumor using the sensor. They were informed that the tumor was always located at the horizontal center of the phantom, and they were allowed to switch the stimulus with/without the tumor if they wanted. The practice session consisted of the following two parts.

The first practice was conducted outside the training box. The main purpose of the first practice was to become familiar with the characteristics of the tactile sensor. The participants were instructed to laterally and continuously scan the surface of the phantom using the sensor. They were informed that the sensing area is located at the side of the sensor tip, and they were instructed to adjust the longitudinal sensor position if they could not perceive the feedback from the sensor. The time limit of the first practice was 5 min. The time limits in the practice session were determined on the basis of a preliminary experiment so that the participants had sufficient time for their practices.

In the second practice, the participants practiced the sensor manipulation inside the training box. The main purpose was to practice the sensor manipulation in the actual experimental situation. The participants could not directly see the stimulus and the sensor movement, and could see only through the camera image. The time limit for the second practice was 10 min.

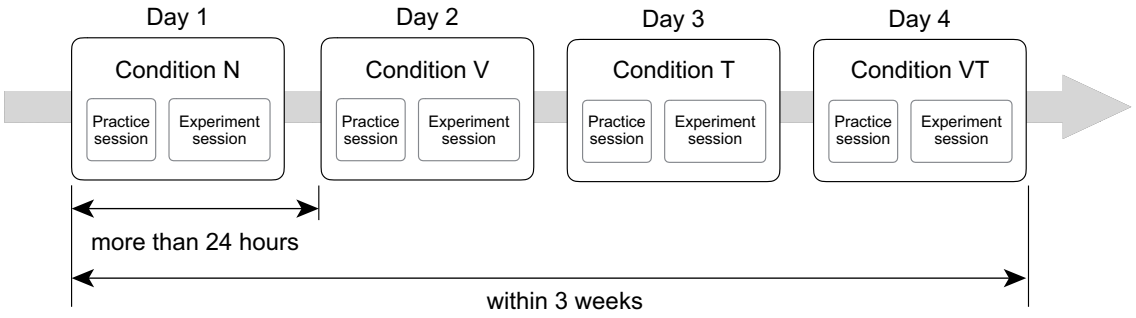

Fig. 3.6: Example of the experimental order. To reduce learning effects, each condition was conducted on a different day, and the order was counterbalanced across all participants.

Experiment session

In the experiment session, a two-alternative-forced-choice procedure was employed. The participants were asked to answer 'yes' (tumor was present) or 'no' (tumor was absent) on the basis of the corresponding feedback. Each trial had a limit of 30 s. They were asked to discriminate the stimulus as quickly as possible and also to grade their confidence in their answer on a scale between 1 (not confident at all) and 100 (very confident). The response time was measured with a stopwatch. If the participants overran the time limit, they were forced to stop the sensor manipulation, and then to report a binary answer and a confidence rating. This session contained 50 trials in total. The first 10 trials were treated as practices, and the participants received the correct answer after each trial. Five of each stimulus type (with/without tumor) were randomly presented in these 10 trials. If the percentage correct was less than chance level (50%), the participants were allowed to practice again inside the training box with a limit of 5 min, except for the no-feedback condition. After the extra 5-min practice, no further practice trials with feedback were given. Five of the participants needed these extra 5 min. The remaining 40 trials were actual trials, and the results were used for analyses. Twenty of each stimulus type were randomly presented. In the actual trials, the participants were allowed to have breaks of about 5 min after every 10 trials.

3.3.5 Data analysis

Detection sensitivity

In this chapter, we aimed to reveal the sensitivity of the participants in distinguishing the stimuli with/without tumor. In a yes–no experiment, a hit rate $H \in [0, 1]$ (the proportion of 'yes' responses when the tumor is present) and a false-alarm rate $F \in [0, 1]$ (the proportion of 'yes' responses when the tumor is absent) can be calculated. If participants achieve better sensitivity, the hit rate and the false-alarm rate approach 1 and 0, respectively. Here, using either the hit rate or the false-alarm rate as the detection sensitivity is inappropriate because they are contaminated by participant's criterion (willingness to say 'yes'). Thus, applying signal detection theory [126] is one solution by which remove the influence of the criterion, where both the hit rate and the false-alarm rate are considered for calculation of a sensitivity index.

In addition, the detection strategy of participants can be analyzed through curves of the receiver operating characteristic (ROC), which show pairs of (F, H) for different criteria. When the criterion increases or decreases, a point on a ROC curve approaches $(0, 0)$ or $(1, 1)$, respectively. Here, the basic detection theory assumes normal distributions of internal response against repeated presentations of the stimulus, and an entire ROC curve can be estimated from a single pair of (F, H) (an example is shown in Fig. 3.7 as a black dashed line). However, preliminary analyses revealed that underlying distributions were no longer normal; thus, we tried to plot empirical ROC curves from binary responses and confidence ratings of the participants. There were $2N$ $(= 200)$ possible responses (binary answers $\times$ the total number of levels on the rating scale) from a participant for each trial. Since confidence ratings indicate participants' criteria [126], we can derive multiple pairs of $(F_i, H_i), (i = 1, \cdots, 2N - 1)$. The empirical ROC curve can be drawn by plotting and connecting all pairs of (F_i, H_i) on the ROC space (an example is shown in Fig. 3.7 as a black solid line). Then, the area under the empirical ROC curve can be used as a sensitivity index without any model assumption. To calculate the area under the ROC curve, the areas under a series of trapezoids were summed up as the sensitivity index A_{g} as follows [127]:

$$A_{\mathrm{g}} = \frac{1}{2} \sum_{i=0}^{2N-1} (F_{i+1} - F_i)(H_{i+1} + H_i), \tag{3.4}$$

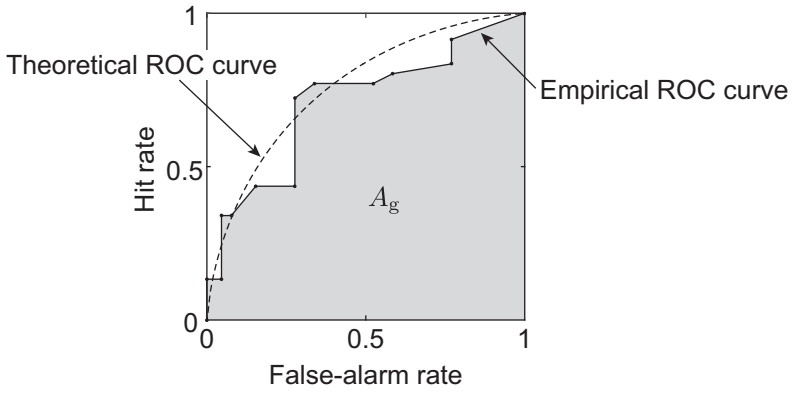

Fig. 3.7: ROC curves on an (F, H) space. The dashed line shows a ROC curve with the assumption of normal distributions. The solid line shows an example of an empirical ROC curve. The area under the empirical ROC curve A_g was used as a sensitivity index in this chapter.

where (F_0, H_0) equals $(0, 0)$, and (F_{2N}, H_{2N}) equals $(1, 1)$. A_g ranges from 0 to 1, and the chance level is 0.5.

Data extraction

We calculated the average normal force and scanning speed during each trial in the experiment sessions. Here, the left–right, front–back and vertical directions of the force sensor were defined as the y-, x- and z-axes, respectively, as shown in Fig. 3.5. The force along the y-axis was defined as tangential force. The resultant of the forces along the x- and z-axes was defined as normal force. All forces were smoothed by low-pass filters with a cut-off frequency of 10 Hz. We used the tangential force to extract each lateral scanning, and the threshold was set to 10% of the maximum tangential force during each trial because the range of the tangential force varied widely between participants. The motion capture system provided the position and posture of the marker set, which was fixed near the handle of the sensor. The three-dimensional position of the center of the sensing area was calculated from the positional relationship between the sensing area and the marker set. The scanning speed at the center of the sensing area was calculated by using the sampling period (1/120 s). The calculated scanning speed was

filtered with a low-pass filter with a cut-off frequency of 5 Hz to reduce numerical noise.

Statistical test

Effects of the experimental condition on detection performance and the exploratory movements were investigated through statistical tests. The significance level was set to 0.05. Before analyses, a Shapiro–Wilk test was conducted to check whether all the dependent parameters were distributed normally. If the assumption of normality was violated, a non-parametric Friedman test was conducted to compare the parameters obtained between the four conditions. In the case when a significant result was obtained, post-hoc six Wilcoxon signed rank tests for all possible combinations were conducted with Holm–Bonferroni correction. If the assumption of the normal distribution was confirmed, Mauchly's sphericity test was conducted to confirm the assumption of homogeneity of variance. Then, a one-way repeated ANOVA was conducted with experimental condition as a factor. If the assumption of homogeneity of variance was violated, Greenhouse–Geisser correction was applied. In the case when a significant result was obtained, post-hoc six paired t-tests were conducted with Holm–Bonferroni correction.

3.4 Results

3.4.1 Detection performance

Fig. 3.8 shows empirical ROC curves for each experimental condition. The area under the ROC curve A_g was calculated as the detection sensitivity for each participant. Fig. 3.9 shows the detection sensitivity, the confidence in the answer, and the response time for all participants. White, light grey, dark grey, and black bars indicate the results for conditions N, V, T, and VT, respectively. Statistical tests were conducted to investigate the effect of the condition (and the experimental order) on the detection sensitivity, the confidence rating, and the response time.

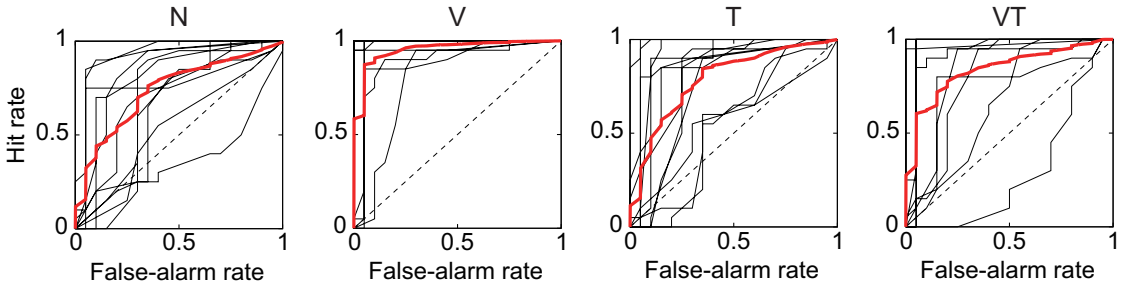

Fig. 3.8: Empirical ROC curves for experimental conditions. Black solid lines show ROC curves for 12 participants. Red solid lines show the average ROC curves of the participants. Black dashed lines show the chance level.

Sensitivity

Fig. 3.10(a) shows the detection sensitivity for the experimental conditions. The horizontal line inside each box shows the median. The top and bottom of each box show the upper quartile $Q3$ and lower quartile $Q1$, respectively. The upper and lower whiskers show the maximum and minimum values within $[Q1 - 1.5\,\mathrm{IQR}, Q3 + 1.5\,\mathrm{IQR}]$, where $\mathrm{IQR} = Q3 - Q1$ is the interquartile range. Open circles show outliers. A non-parametric Friedman test on the detection sensitivity for the experimental condition showed a significant influence of condition ($\chi^2(3) = 11, p = 0.011$). Wilcoxon signed rank tests showed a significant difference between conditions N and V ($W(12) = 5, p = 0.029$). This result shows that the detection sensitivity in condition V is significantly higher than that in condition N.

Fig. 3.10(b) shows the detection sensitivity for the experimental order. A Friedman test on the detection sensitivity for experimental order showed no significant influence of the order ($\chi^2(3) = 3.8, p = 0.28$). This result indicates that the order of the conditions did not significantly affect the sensitivity.

Confidence in the answer

Fig. 3.10(c) shows the confidence rating for each condition. An ANOVA showed a significant influence of condition ($F(1.8, 20) = 6.6, p = 0.0078$). Paired t-tests showed a significant difference between conditions N and V ($t(11) = 3.3, p = 0.042$). This

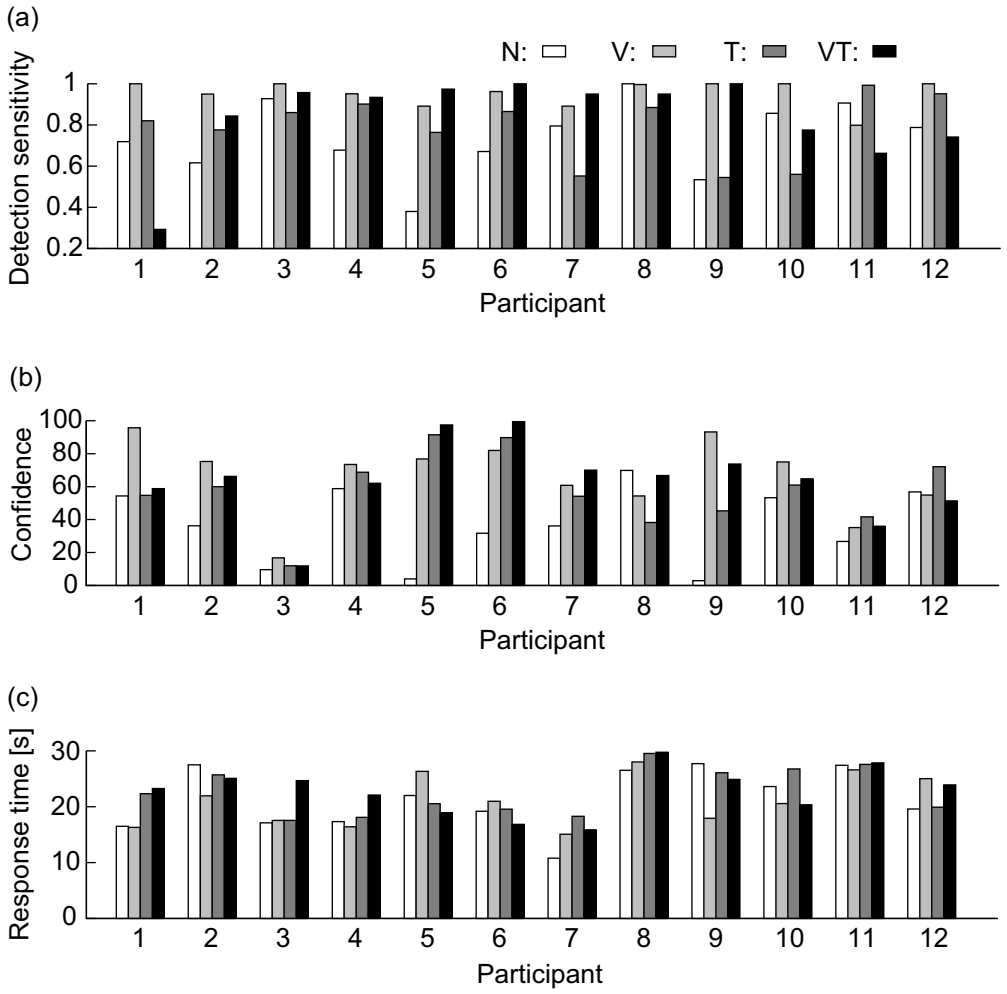

Fig. 3.9: Detection performance in individual participants. White, light grey, dark grey, and black bars indicate the results for conditions N, V, T, and VT, respectively. (a) Detection sensitivity. (b) Confidence ratings. (c) Response time.

result is similar to that of the detection sensitivity for each condition.

Response time

Fig. 3.10(d) shows the response time for each condition. An ANOVA showed no significant influence of condition ($F(3, 33) = 1.2, p = 0.32$). This result shows that the

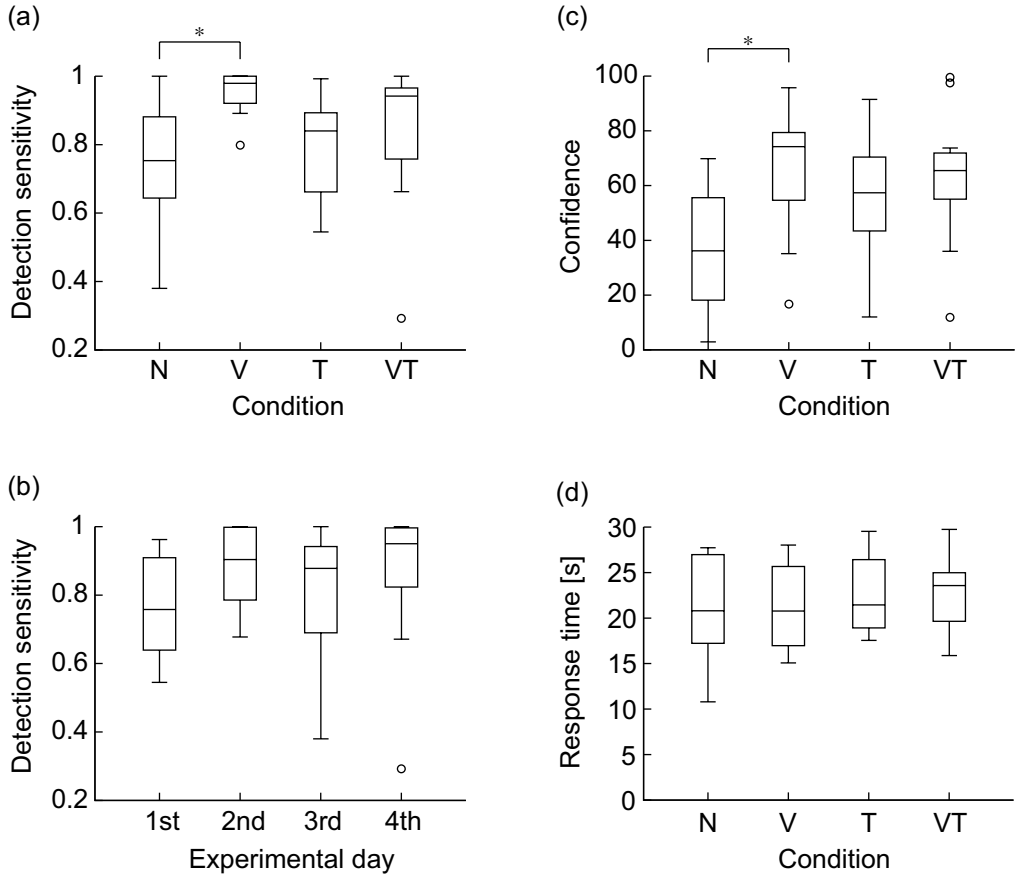

Fig. 3.10: Summary of detection performance. (a) Detection sensitivity for the condition. (b) Detection sensitivity for the experimental day. (c) Confidence ratings for the condition. (d) Response time for the condition. * indicates $p < 0.05$ with post-hoc Wilcoxon signed rank tests or t-tests with Holm–Bonferroni correction.

condition did not significantly affect the response time.

3.4.2 Exploratory movements

Fig. 3.11 shows the normal force and the scanning speed for all participants. Statistical tests were conducted to investigate the effect of condition on the exploratory movements.

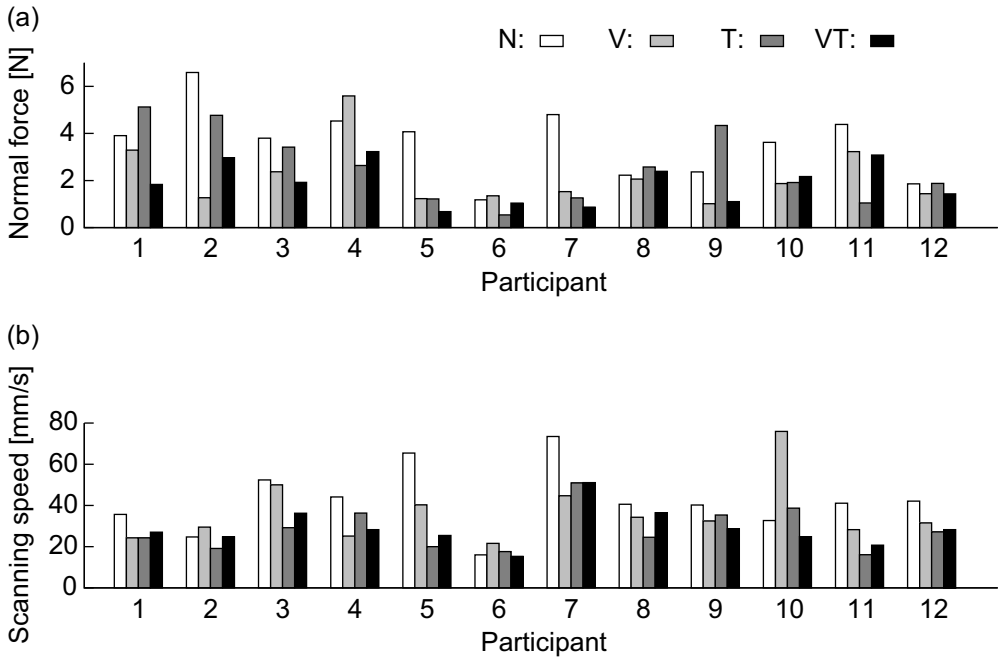

Fig. 3.11: Exploratory movements in individual participants. White, light grey, dark grey, and black bars indicate the results for conditions N, V, T, and VT, respectively. (a) Normal force. (b) Scanning speed.

Normal force

Fig. 3.12(a) shows the normal force for each condition. A Friedman test showed a significant influence of condition ($\chi^2(3) = 11, p = 0.014$). Wilcoxon signed rank tests showed significant differences between conditions N and V ($W(12) = 71, p = 0.046$) and between conditions N and VT ($W(12) = 76, p = 0.0014$). This result shows that the normal forces in the conditions V and VT are smaller than those in condition N.

Scanning speed

Fig. 3.12(b) shows the scanning speed for each condition. A Friedman test showed a significant influence of the condition ($\chi^2(3) = 13, p = 0.0053$). Wilcoxon signed rank tests showed significant differences between conditions N and T ($W(12) = 73, p = 0.024$) and between conditions N and VT ($W(12) = 77, p = 0.0059$). This result shows

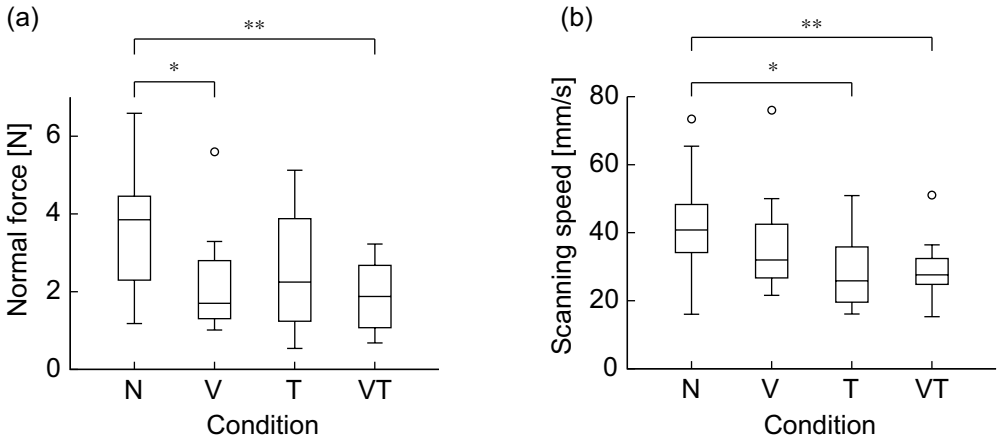

Fig. 3.12: Summary of exploratory movements. (a) Normal force for the condition. (b) Scanning speed for the condition. * indicates $p < 0.05$ and ** $p < 0.01$ with post-hoc Wilcoxon signed rank tests with Holm–Bonferroni correction.

that the scanning velocities in the conditions T and VT are smaller than those in condition N.

3.5 Informal trials with expert surgeons

To assess the practical effectiveness of the feedback of the sensor output in laparoscopic tumor detection, we conducted a few trials with expert surgeons.

Four very experienced laparoscopic surgeons participated voluntarily. The experimental setup was almost the same as that described in Section 3.3.3, but no visual feedback was offered because surgeons always see the endoscopic monitor during laparoscopic surgery, and it is not practical to see an extra monitor during the operation. Three stimuli with different tumor positions were prepared by shifting the position of the phantom of the stomach wall on the semicylindrical sponge. One of the stimuli was randomly put inside the training box, without fixing it; thus, stimulus position and posture could be freely changed by the participant. Two surgeons–an operator and an assistant–stood on the left and right sides of the laparoscopic training box. The operator manipulated the tactile sensor with his/her dominant hand to scan the surface

of the stimulus, with a forceps in the other hand to adjust the position and posture of the stimulus. The assistant surgeon cooperated with the operator manipulating the sensor. Before the actual scanning of the tumor in the training box, the operator felt the tactile feedback outside the training box for several tens of seconds to familiarize him/herself with the feedback as a rehearsal. Then, the surgeon tried to identify the position of the tumor in the phantom inside the training box.

Three out of four expert surgeons could correctly localize the phantom tumor in the first trial. The fourth surgeon firstly pointed out an incorrect position, but could correctly localize the tumor in the second trial. This surgeon commented that s/he mistook the fold of the phantom stomach for the tumor in the first trial. Other surgeons commented that they could find the position of the tumor through the tactile feedback from the sensor. They also commented that for optimal performance, they should become more familiar with the tactile feedback because some specific skills for the sensor manipulation should be acquired.

3.6 Discussion

First, we will discuss the procedure and setup for the psychophysical experiment with novice participants. Fig. 3.10(b) shows that the detection sensitivity did not significantly depend on the experimental order. This validates the experimental design, in which the order was counterbalanced across participants, and time intervals were inserted between the experimental conditions to reduce learning effects. Regarding the detection sensitivity, the median for the condition N was 0.75 and the exceeded chance level (0.5). This indicates that the participants could utilize the direct haptic information to distinguish the stimuli. Some participants commented that the camera image could also be used as the cue for detection because a small change in the sensor movement or the deformation due to the tumor could be observed. In addition, participants tended to use a larger normal force in condition N as shown in Fig. 3.12(a), which places higher stress on the tissue. This might indicate that participants tried to increase the intensity of direct haptic information. The stimuli used in the experiment were fixed in the training box whereas the actual stomach wall often shifts according to the applied tangential force. Thus, direct haptic information might be less informa-

tive, and the feedback from the sensor output might be more efficient in a real surgical situation. Regarding the response time, it did not significantly depend on condition. It is possible that an effect of condition did not show up because of the short time limit (30 s).

In the following sections, we will discuss the effects of each type of feedback on the detection sensitivity and the exploratory movements, and their characteristics from the point of view of clinical applications. Moreover, we will finally discuss the practical effectiveness of the sensory feedback from the tactile sensor according to the results of the informal trials with expert surgeons.

3.6.1 Visual feedback

The experimental results show that visual feedback is sufficient for tumor detection. Visual feedback was the line graph, which offered the time history of the sensor output for 5 s. Thus, participants could discriminate the tumor on the basis of the shape of the line graph as shown in Fig. 3.2. We have hypothesized that the visual channel might be overloaded in condition V because the camera image and the line graph were simultaneously presented on two different monitors. However, the participants did not frequently need to pay attention to the camera image once they learned the appropriate manipulation of the sensor.

Regarding the exploratory movements, the visual feedback has the effect of decreasing the normal force for tumor detection. This is probably because of the visual feedback provided by the quantitative sensor output through the line graph; thus, the participants could adjust the normal force on the basis of the height of the line graph. In addition, if the normal force was too large, the line graph was out of range on the PC monitor. This might have worked as an implicit indication of excessive normal force. Thus, the gain of the visual feedback might affect the range of normal force used.

From the point of view of clinical applications, decreasing the normal force has a positive effect because it places less mechanical stress on the tissue. Moreover, the advantage of visual feedback is that surgeons can share the sensing information, and this might make the decision more transparent. On the other hand, the visual feedback needs extra space for the extra monitor in addition to the laparoscopic one. A possible solution to this issue is to superimpose the sensor output information on the camera

image [80, 81]. However, this makes the surgical field less visible. In addition, the possibility of overloading the visual channel [82] remains because the surgeons should pay attention to the laparoscopic image in actual surgery. In future work, we will improve the visual feedback to address these issues.

3.6.2 Tactile feedback

The detection sensitivity showed no significant difference between conditions T and N. There were some possible sources providing confusing tactile feedback to the participants. For instance, the participant could feel a force fluctuation due to the fold of the inside of the stimuli when they used a large normal force. It has also been reported that the benefit of force feedback in a teleoperation system depends on experience in robot-assisted minimally invasive surgery [128]. All participants were novices in laparoscopic surgery, and they could not interpret the tactile feedback accurately. Moreover, some participants who achieved better performance in condition N commented that the tactile feedback somewhat interfered with the direct haptic information from the sensor probe. Thus, the means of tactile feedback should be considered carefully in a laparoscopic palpation system, where users can receive direct haptic information. A possible solution is to optimize the gain for each participant so that the tactile feedback appropriately augments the direct haptic information.

The tactile feedback has the effect of decreasing the scanning speed. A possible reason for the low speed is that the participants tried to recognize the shape of the tumor through tactile feedback. The tumor used in the experiment has a toroidal shape, and the typical sensor output during the scanning has two peaks, as shown in Fig. 3.2(a). Regarding tactile performance in temporal discrimination, humans can definitely perceive two sequential stimuli when the interval between them exceeds 100 ms for electrical stimulation [129]. Thus, a low scanning speed might help to perceive two sequential force stimulations due to the tumor. On the other hand, the tactile feedback has no effect on the normal force. This might be because the tactile feedback presented the high-passed sensor output; thus, the participant could not know the quantitative sensor output through the tactile display. In future work, we will continue to improve the means of tactile feedback toward more efficient tumor detection.

The effect of decreasing the scanning speed might bring less risk of accidents such

as an undesired collision between the sensor and the tissue. In addition, the tactile display developed in this chapter is highly applicable to surgical situations because the display was designed for the foot, where sterilization is not necessary. When the surgeons conduct palpation, they have only to insert their foot into the display; thus, the display does not disturb the surgeon during other surgical tasks. However, the surgeon should take off their footwear for this, and this inconvenience remains when they need to move their foot to operate other surgical instruments through foot pedals. When designing an improved version of our tactile display, we will take this aspect of inconvenience into account.

3.6.3 Combination of visual and tactile feedback

The detection sensitivity showed no significant difference between conditions VT and N. We have hypothesized that the combination of the two types of feedback could achieve the highest detection sensitivity due to maximum likelihood integration [130]. Fig. 3.9(a) shows that some participants increased their sensitivity in condition VT. However, the overall tendency shows that condition V achieved the highest performance, and the integration of visual and tactile feedback yielded lower performance, as shown in Fig. 3.10(a). A possible explanation is a cross-modal masking effect. Ide et al. demonstrated experimentally that tactile stimulation can suppress visual perception [131]. If the participant could not interpret the tactile feedback appropriately as mentioned in the previous section, the tactile feedback might degrade the visual feedback and introduce uncertainty to the tumor detection.

The combination of the visual and tactile feedback has the effect of decreasing both the normal force and the scanning speed. This means that the effects of each type of feedback did not interfere in terms of the exploratory movement. Decreasing both normal force and scanning speed supplies less energy to the tissue, which might produce less damage to it [79]. Thus, if the tactile feedback were improved, better detection with a decreasing effect of normal force and scanning speed could be achieved by utilizing both visual and tactile feedback.

In this chapter, we revealed that the type of signal processing of the feedback (such as clipping and filtering) as well as the modality affects the exploratory movements in our laparoscopic palpation system. This indicates that the participants reasonably

changed their behavior according to the characteristics of the feedback information and modality.

3.6.4 Practical effectiveness

The results of the informal trials with expert surgeons indicate that the feedback from the tactile sensor might be effective for practical use in laparoscopic surgery. Whereas the surgeons could find the position of the tumor through the tactile feedback from the sensor, they commented that they should become more familiar with the tactile feedback because some specific skills for the sensor manipulation should be acquired. In future work, we will try to seek more effective and even more intuitive ways to provide the feedback.

3.7 Summary

In this chapter, we designed and evaluated means of feedback from a direct-manipulating tactile sensor for laparoscopic tumor detection. We used a previously developed simple and biocompatible tactile sensor using acoustic reflection. As one type of feedback, a monitor presenting a line graph of the low-pass-filtered sensor output ($<$ 10 Hz) was prepared as visual feedback. As another type of feedback, we developed a tactile display for the upper side of the user's foot. It presents normal force that relates to the high-pass-filtered sensor output (0.5–10 Hz). The tactile display has advantages for surgical applications because the foot is in the unclean area of a surgeon and does not need to be sterilized. Thus, the whole system is highly applicable to clinical situations.

A psychophysical experiment was conducted in a setup simulating laparoscopic surgery for 12 novices. Four feedback conditions (no feedback, only visual feedback, only tactile feedback, and a combination of the visual and tactile feedback) were compared in terms of detection sensitivity and exploratory movement. We employed signal detection theory to analyze participants' sensitivity and measured normal force and scanning speed during the experiment. The experimental results showed that the visual feedback can achieve significantly higher sensitivity and greater confidence of

participants in their answers compared to no feedback. The tactile feedback has no significant effect on the sensitivity. In addition, visual feedback has the effect of decreasing normal force, and tactile feedback has the effect of decreasing scanning speed. Interestingly, the combination of the two types of feedback has both effects. Moreover, a few informal trials with four expert surgeons were conducted. The surgeons could localize the correct position of a phantom tumor according to the tactile feedback provided.

We will improve the means of visual and tactile feedback with the aim of providing better and even more intuitive tumor detection with small normal force and low scanning velocity. Moreover, the end goal of our research is intraoperative tumor localization; thus, we will also investigate how the means of feedback affect performance in tumor localization.

Chapter 4

DNN-based detection assistant as replacement of visual feedback

This chapter proposes a novel assistance algorithm based on a deep neural network for laparoscopic tumor detection. It was found that visual feedback is effective in tumor detection, but problematic for clinical applications owing to the possibility of sensory overload. The proposed algorithm is designed to analyze the time series of the sensor output in real time and to provide independent detection results from the surgeons. This approach, therefore, allows for the removal of the visual feedback while keeping its effectiveness in detection. The feasibility of the algorithm is validated using the data acquired in the previous chapter.

4.1 Introduction

In recent years, deep neural networks (DNNs) have achieved remarkable results in medical image analyses. For example, annotation [132], segmentation [133–137], and diagnosis [138–140] of medical images were developed by using DNNs. These studies aimed to assist in diagnosis or planning before a surgical procedure, based on preoperatively acquired medical images. Through using DNN, some of these studies detected changes in the mechanical properties of tissue, such as cerebral microbleeds, brain tumors, breast lesions, lung nodules, and pulmonary nodules. Moreover, analysis techniques have been developed where laparoscopic images are used to classify surgical events [141, 142], and track [143] or classify [144] surgical instruments. These studies targeted postoperative objectives, such as assisting in medical training, analyses, and compiling databases of recorded endoscopic images. These studies exhibit that possibility of the replacement of human decision-making based on information from a visual channel with DNN techniques.

The previous chapter concluded that the visual feedback of the time series of the sensor output is significantly effective in tumor detection; however, the visual feedback is possible to occur the visual sensory overload and occupies a valuable space in the operating room. In this chapter, we propose an assistance algorithm for laparoscopic tumor detection by employing DNN technique. Our scenario is that the surgeon manipulates a sensor probe and makes a decision based on the temporal sensory feedback given by a tactile display, and simultaneously the assistance algorithm performs detection based on the time series of the sensor output. Thus, the algorithm assists in the decision-making process of the surgeon, by providing independent detection results. This method is advantageous because the reliability and safety of the manipulation are ensured by a human operator, but a more effective detection might be expected from the collaboration between a human operator and the algorithm. In our temporal information-based palpation, if the detection performance of the algorithm could achieve a level comparable with that of the human operator, then it would imply that visual feedback could be replaced by the algorithm. This would avoid any possible sensory overload. Moreover, decision support systems, where clinical information analyzed by a computer is provided to the surgeon, can reduce clinical error and improve patient outcomes [145]. Thus, our proposed algorithm has the advantages of enhancing detection performance, improving the confidence of the surgeon, and removing visual feedback.

We propose to use a DNN model with three hidden layers to segment whether the sensor output at each sampling included the information on the tumor and a method for inputting the sensor output to the DNN model considering real-time analysis. Moreover, the method of determining the detection criterion is proposed, by investigating the relationship between accuracy and various detection criteria. In this chapter, we aim to investigate the feasibility of the proposed algorithm by using the data acquired in the previous psychophysical experiment. In this experiment, 12 novice participants were asked to detect a phantom of an early-stage gastric tumor, under various conditions of sensory feedback. We used the obtained sensor outputs, which were not analyzed in the previous study, as a dataset. In addition to the accuracy, the potential detection performance of the model was analyzed by employing signal detection theory. Then, we conducted two types of cross-validation: within-participant and across-participant

validation. The accuracy and potential detection sensitivity of the DNN model were compared with the performance of the participants, which was analyzed in the previous chapter.

4.2 Data preparation

In Chapter 3, we conducted a psychophysical experiment to investigate the effect of using sensory feedback on tumor detection performance and manipulation behavior. Twelve participants without any medical background participated in the experiment. The participants were asked to discriminate a phantom of the stomach wall with/without a tumor, by scanning with a sensor probe and receiving sensory feedback from the sensor in a simulated laparoscopic environment. Four conditions for the method of feedback were set: no feedback, visual feedback, tactile feedback, and a combination of visual and tactile feedback. Under the no feedback condition, the participants did not receive any feedback from the sensor. Under the visual feedback condition, a line graph of the sensor output on a monitor was provided to the participants. Under the tactile feedback condition, our developed tactile display provided a force against the upper side of the participant's foot according to the sensor output. Under the combination condition, the participants received both visual and tactile feedback simultaneously. It was shown that the visual feedback was significantly effective in the tumor detection. In this chapter, we used the data acquired under the condition of visual feedback, because we aimed to replace the participants' decision through visual channel with the algorithm. The following paragraph presents how the sensor output was collected under the visual feedback condition.

The experimental setup is shown in Fig. 4.1. The participants manipulated a long, thin tactile sensor that was previously developed [15]. The sensor only detected a single force applied on the side of the sensor tip. The sensor output was filtered by a low-pass filter with a 10 Hz cut off frequency. This data was then presented on a laptop PC as a line graph, for a time series of 5 s. The laptop PC was placed next to a monitor that displayed the camera image inside the laparoscopic training box. The participants scanned a phantom of the stomach wall, using the sensor in a rotational direction. There were no restrictions on either the force exerted to the

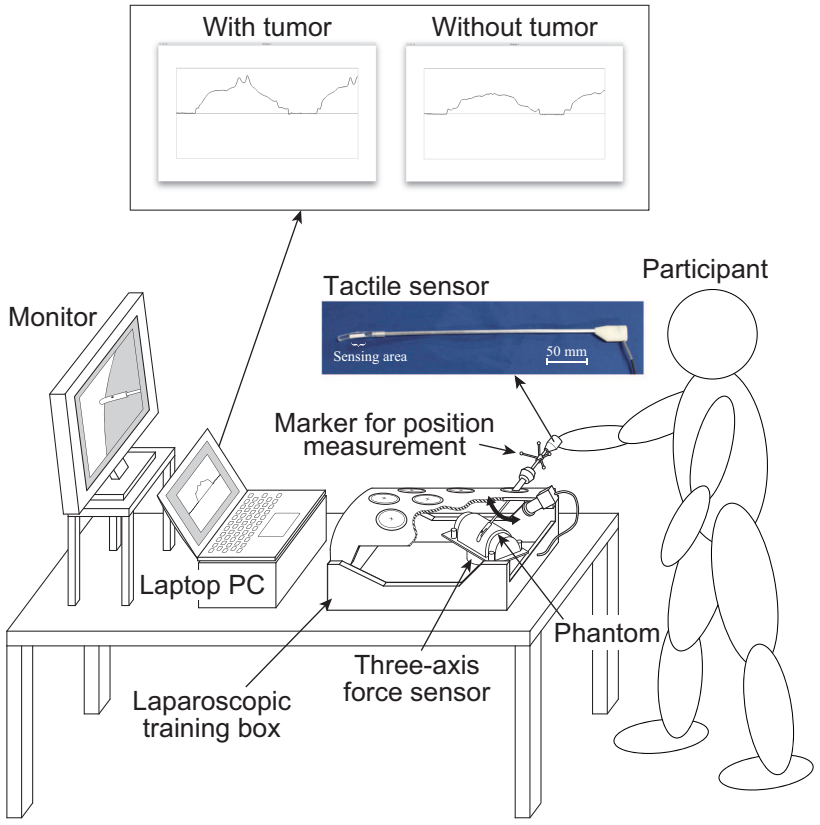

Fig. 4.1: Setup of the psychophysical experiment conducted in the previous chapter. Participants scanned the phantom by the forceps-type tactile sensor in a rotational direction, (shown by a black bold arrow), and determined the presence of a tumor in the phantom. The rectangle shows two typical line graphs provided as visual feedback when a participant scanned a phantom with/without the tumor.

phantom or the scanning speed of the sensor. The rectangle in Fig. 4.1 shows the typical visual feedback when a participant appropriately scanned the phantom with/without a tumor. The participants could distinguish the presence or absence of a tumor based on the shape of the line graph, when they appropriately scanned the phantom. Before the detection trials, the participants were asked to practice the manipulation of the sensor probe, and to memorize the differences in visual feedback when scanning the phantom with/without the tumor. Then, the participants conducted 40 detection tasks

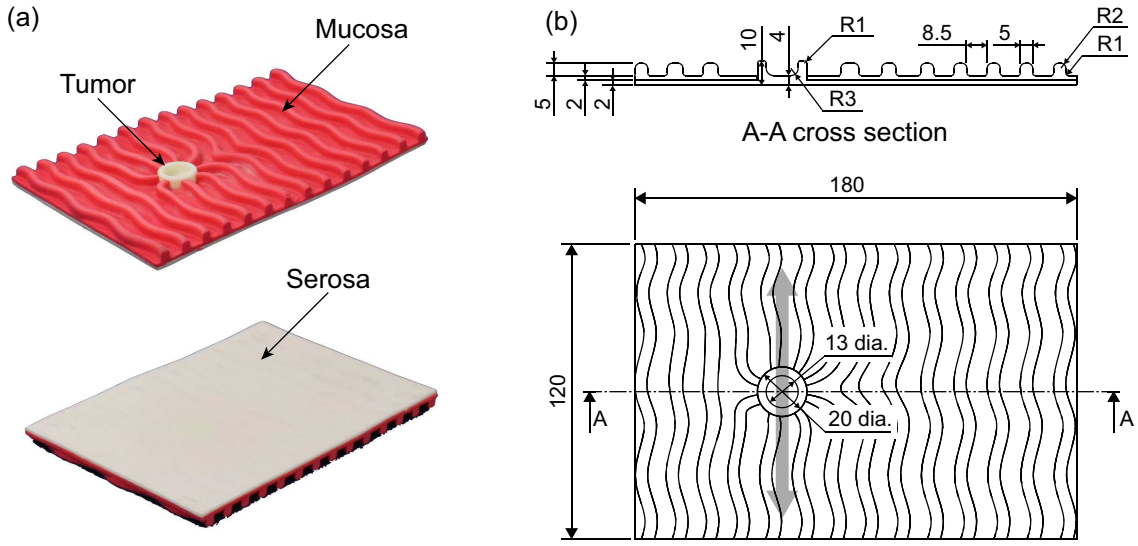

Fig. 4.2: Phantom of the stomach wall used in the previous psychophysical experiment. The phantom was placed on a semi-cylindrical sponge as shown in Fig. 4.1. (a) Photographs of the phantom. The serosal side (smooth side) was scanned by the sensor. (b) Structure of the phantom. The dimensions are indicated in millimeters. The light gray arrow indicates that the back was scanned in the direction indicated. Thus, the typical sensor output had two small peaks, owing to the toroidal shape of the tumor.

comprising 20 of each scenario (presence/absence of the tumor) which were randomly generated. The force applied on the phantom was measured by a three-axis force sensor placed under the phantom, and the position and orientation of the sensor were measured by a motion capture system using a maker set attached to the sensor. The sensor output and the applied force were recorded at sampling frequencies of 1 kHz, and sensor movements were recorded at 120 Hz.

Fig. 4.2 shows the details of the phantom stomach wall with a tumor used in the experiment. The target tumor was a 0-IIc (superficial ulcerative) type tumor [16], which is the most common type of early-stage gastric cancer. The geometry of the phantom and the tumor were based on the typical features of the actual stomach wall and tumor. Whereas the stiffness of the phantom was within the stiffness range of the actual stomach wall and tumor, the anatomical structures and boundary conditions

were not completely the same. The tumor has a toroidal shape, therefore the sensor output typically responded with two peaks that corresponded to the two edges of the toroidal tumor, as shown in Fig. 4.1. The phantom was placed on a semi-cylindrical sponge to simulate a stomach that does not have flat surfaces.

4.3 Methods

4.3.1 Data extraction

A method to input the temporal sensor output to a DNN model is important for achieving real-time analysis. For example, the use of a single sample of the sensor output is not sufficiently informative to facilitate tumor detection. Therefore, a time series with a certain length is required to compare the relative differences in sensor output. However, waiting to obtain a long length of sensor output signals leads to a reduction in the refresh rate. We propose using a region of interest to extract the sensor output, and then shift the region so that it overlaps with the previous extraction. Thus, more efficient detection can be expected by the model, while maintaining a sufficient refresh rate for detection. Fig. 4.3 displays the procedure for data extraction. The top panel in Fig. 4.3 shows an example of the sensor output acquired during the detection experiment. The sensor output was extracted for a time width of $T_{\mathrm{w}} = 1.0$ s, then the extraction area was shifted so that it overlapped the previous extraction for $T_{\mathrm{o}} = 0.9$ s. Thus, the refresh rate of the estimation achieved by the model was 10 Hz, because the data was prepared every 0.1 s and the sensor output at each sampling was included in the ten independent extractions.

For training of the DNN model, a binary label was prepared for the sensor output at each sampling to identify the sensor located above the tumor. It was calculated on the basis of both the measured position and orientation of the sensor during the experiment. The label was '1' while the center of the sensing area was in the tumor area, and '0' while in the other areas. The binary label was also extracted in the same way as for the sensor output. Thus, the extracted output $\boldsymbol{x}$ and the corresponding label $\boldsymbol{t}$ had the same dimension. Moreover, the time for each scanning was extracted according to the tangential force applied on the phantom tumor during the experiment.

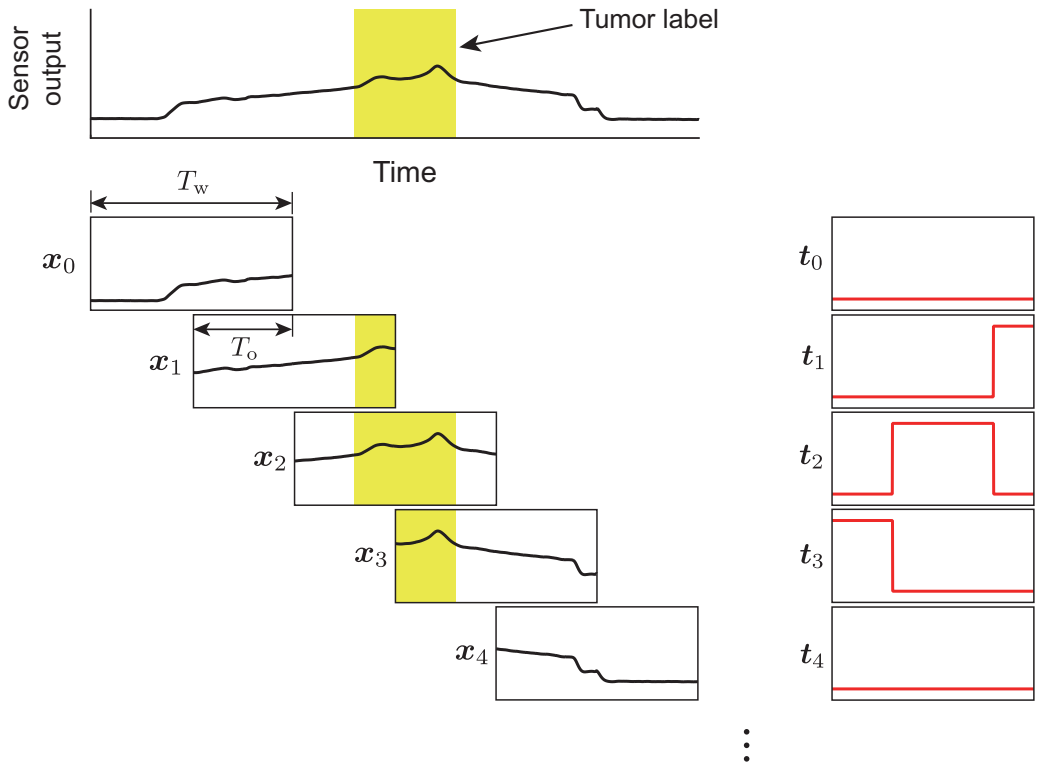

Fig. 4.3: Procedure for the data extraction. Yellow areas show the tumor label, which was calculated on the basis of the sensor position measured by the motion capture system. The region of interest with a time width of T_w was shifted with the overlap time of T_o. The terms $\boldsymbol{x}_k$ and $\boldsymbol{t}_k$ are the extracted sensor output and corresponding label, respectively. Pairs of $(\boldsymbol{x}_k, \boldsymbol{t}_k)$ were used for training the DNN model.

The scanning times were used in the validation of the proposed DNN model.

4.3.2 DNN model

We used a deep neural network with three hidden layers. Input vector $\boldsymbol{x} \in \mathbb{R}^{1000}$ is the extracted sensor output. Output vector $\boldsymbol{y} \in \mathbb{R}^{1000}$ is the estimated tumor label corresponding to the sensor output at each sampling. The values at each hidden layer

$\boldsymbol{h}_i$, ($\boldsymbol{h}_0, \boldsymbol{h}_4 \in \mathbb{R}^{1000}$ and $\boldsymbol{h}_1, \boldsymbol{h}_2, \boldsymbol{h}_3 \in \mathbb{R}^{2000}$) are shown by the following equation:

$$\boldsymbol{h}_i = \boldsymbol{\sigma}\left(\boldsymbol{W}_i \boldsymbol{h}_{i-1} + \boldsymbol{b}_i\right), (i = 1, 2, 3, 4), \tag{4.1}$$

where, $\boldsymbol{W}_1 \in \mathbb{R}^{1000\times2000}, \boldsymbol{W}_2, \boldsymbol{W}_3 \in \mathbb{R}^{2000\times2000}$, and $\boldsymbol{W}_4 \in \mathbb{R}^{2000\times1000}$ are the weight matrices, and $\boldsymbol{b}_i \in \mathbb{R}^{1000}$ is the bias vector. $\boldsymbol{h}_0$ is equal to $\boldsymbol{x}$. $\boldsymbol{\sigma}$ indicates an element-wise activating function (rectified linear unit [146]) as follows:

$$\boldsymbol{\sigma}(\boldsymbol{z}) = \max(\boldsymbol{z}, \boldsymbol{0}). \tag{4.2}$$

The output $\boldsymbol{y}$ was derived by applying an element-wise sigmoid function to $\boldsymbol{h}_4$ as follows:

$$\boldsymbol{y} = \frac{1}{1 + \exp(\boldsymbol{h}_4)}. \tag{4.3}$$

The sigmoid function was inserted to transform the value from the model to be within 0 and 1; thus, the value of each component in the output vector can be interpreted as a probability that the sensor output at corresponding sampling includes information on the tumor. The model was implemented using Chainer [147].

4.3.3 Learning

Dataset $(\boldsymbol{x}, \boldsymbol{t})$, which is the pair of sensor output and correct label, was used to optimize the model parameters ($\boldsymbol{W}_i$ and $\boldsymbol{b}_i$). We used cross-entropy E between the correct and estimated labels for the optimization as follows:

$$E = -\sum_k t_k \ln y_k, \tag{4.4}$$

where, t_k and y_k are k-th correct label and estimated label, respectively. For the initialization of the parameters, the method proposed by He et al. [148] was employed. The parameters were updated to minimize the cross-entropy according to Adam method [149] with a mini-batch size of 100. The update was conducted for 200 epochs.

4.3.4 Detection algorithm

As described in Section 4.3.1, the sensor output was extracted by a window of 1.0 s, and the window was shifted with an overlap time of 0.9 s. Thus, the proposed algorithm

could provide the estimation score every 0.1 s. On the other hand, we validated the proposed algorithm by using a pre-acquired dataset; thus, we added a procedure to calculate a representative score for each experimental trial, because the participants scanned the phantom multiple times in each trial, and the number of scannings varied between participants.

Fig. 4.4 illustrates two examples of the sensor output and the estimation score for a single detection trial. The mean of the ten independent outputs from the DNN model was calculated for each sampling of the sensor output, as shown by the red solid lines in Fig. 4.4. The yellow areas depict the binary label, calculated from the measured positions of the sensor. The gray areas show the extracted scanning times, based on the tangential force applied to the phantom. The maximum estimation score within each scanning was calculated as shown in the upper portion of Fig. 4.4. Then, the mean of the maximum scores for all the scanning was calculated, and used as a representative estimation score for each trial. If the representative score was larger/smaller than the detection criterion, it was considered that the DNN model did/did not detect the tumor, respectively. This procedure allowed us to consider that the DNN model outputted a single score for each trial in a similar way to the previous experiment, where the participant's response was recorded for each trial. We used accuracy ACC (the ratio of the number of correct detections to the number of total detection trials) as an index of the detection performance. For the determination of the detection criterion, we first investigated the relationship between the accuracy and criterion for each trained DNN model. Multiple accuracies ACC_j were calculated based on the estimated scores for multiple detection criteria c_j from 0 to 1, with 0.01 increments ($j = 0, \cdots, 100$). The relationship between the accuracy and detection criterion was derived as shown in Fig. 4.4. Subsequently, the threshold detection criterion c_{th} was calculated on the basis of the following equations:

$$ACC_{\mathrm{th}} = \max(ACC_j) - \frac{\max(ACC_j) - 0.5}{10}, \tag{4.5}$$

$$c_{\mathrm{th}} = \frac{c_{\mathrm{u}}(ACC_{\mathrm{th}}) + c_{\mathrm{l}}(ACC_{\mathrm{th}})}{2}, \tag{4.6}$$

where ACC_{th} is the threshold of the accuracy to obtain upper criterion $c_{\mathrm{u}}(ACC_{\mathrm{th}})$ and lower criterion $c_{\mathrm{l}}(ACC_{\mathrm{th}})$, as shown in Fig. 4.5. Threshold criterion c_{th} was calculated

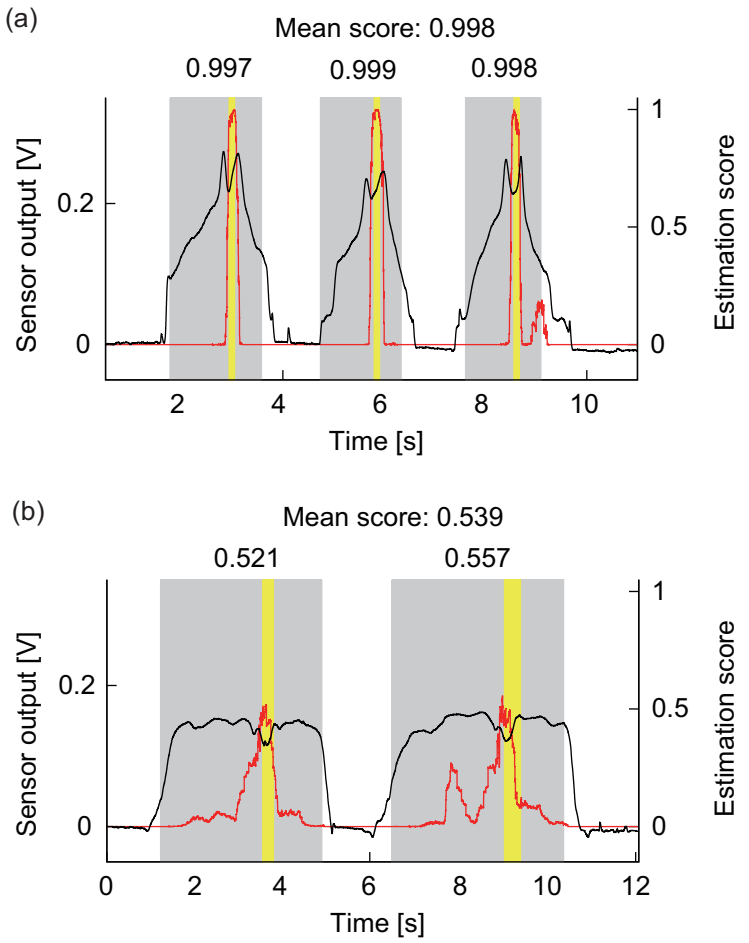

Fig. 4.4: Examples of the sensor output (black lines) during a single detection trial and the estimated score (red lines) by the DNN model. Yellow areas show the time when the sensor scanned the tumor. Gray areas show the scanning time that was calculated based on the applied tangential force. The maximum estimation score within each scanning time was extracted as shown in the upper side of the gray areas. Next, the mean of the scores was calculated and used as a representative score for this trial. (a) and (b) show the data from participants 9 and 4, respectively.

as the mean of the upper and lower criteria. The equation to calculate ACC_{th} was experimentally determined. The threshold detection criterion determined by this method leads to the maximum accuracy for the dataset used in the model construction.

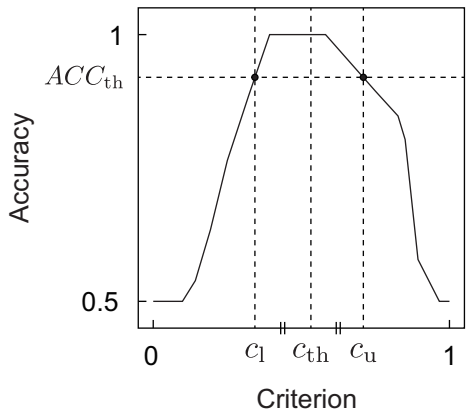

Fig. 4.5: Example of the relationship between the detection criterion and accuracy. Detection criterion c_{th} was determined on the basis of this relationship.

4.3.5 Potential sensitivity

When investigating the detection outcomes of the proposed DNN model, it is important to evaluate the accuracy. However, accuracy does not explicitly reveal how a classifier has the potential to distinguish between two situations, because the detection criterion also affects the accuracy. Thus, we additionally analyzed the detection results based on signal detection theory [126] to assess the potential detection performance. Hit rate $H \in [0, 1]$ (the number of detections divided by the total number of trials in which the tumor was present) and false alarm rate $F \in [0, 1]$ (the number of detections divided by the total number of trials in which the tumor was absent) were calculated for multiple detection criteria c_j. Hence, multiple pairs of hit and false alarm rates (F_j, H_j), $(j = 0, \cdots, 100)$ were derived. Then, a receiver operating characteristic (ROC) curve was drawn by plotting and connecting all the pairs of the hit and false alarm rates for the different detection criteria on the (F, H) space. The area under the ROC curve A_{g} was calculated as follows:

$$A_{\mathrm{g}} = \frac{1}{2} \sum_{j} (F_{j+1} - F_j)(H_{j+1} - H_j) \tag{4.7}$$

Here, A_{g} indicates the potential sensitivity of a classifier, A_{g} lies within $[0, 1]$, and the chance level is 0.5.

4.3.6 Validation

Two types of validation were conducted on the basis of a dataset used for model training. One is within-participant validation, where the data obtained from one participant is used for both training and testing the model. The other is across-participant validation, in which to perform the detection test for the data from a single participant, the data from all other eleven participants were used in the model construction. The details of the data preparation for each validation are presented in the following sections.

Within-participant validation

A four-fold cross-validation was performed within the data for each participant. Fig. 4.6(a) shows the procedure for the preparation of the data used for the within-participant validation. The data from one participant was divided into four groups, and each group contained the data for ten trials. The data in one group was used for the detection test (dataset #1). The data in the remaining three groups were used for the model construction (dataset #2). Moreover, dataset #2 was divided into two groups: one was for the training of the DNN model (dataset #2-1) that included 20 trials from ten of each type of trial in which the phantom with/without the tumor was presented, and the other was for the determination of the detection criterion (dataset #2-2) including ten trials from five of each. The division of dataset #2 was randomly conducted five times, regardless of the first grouping. The within-participant validation was independently conducted for 12 participants.

First, the DNN model was trained by using a pair of $(\boldsymbol{x}, \boldsymbol{t})$ in dataset #2-1. Then, estimated label $\boldsymbol{y}$ was obtained against sensor output $\boldsymbol{x}$ in dataset #2-2 by the trained model. The estimation score was calculated from estimated label $\boldsymbol{y}$ for each trial in dataset #2-2. Accuracies ACC_j for the multiple detection criteria were calculated, and the threshold detection criterion c_{th} was determined based on ACC_j. This procedure was repeated five times because the random separation of dataset #2 was conducted five times, and the mean threshold detection criterion for the five times repetition was

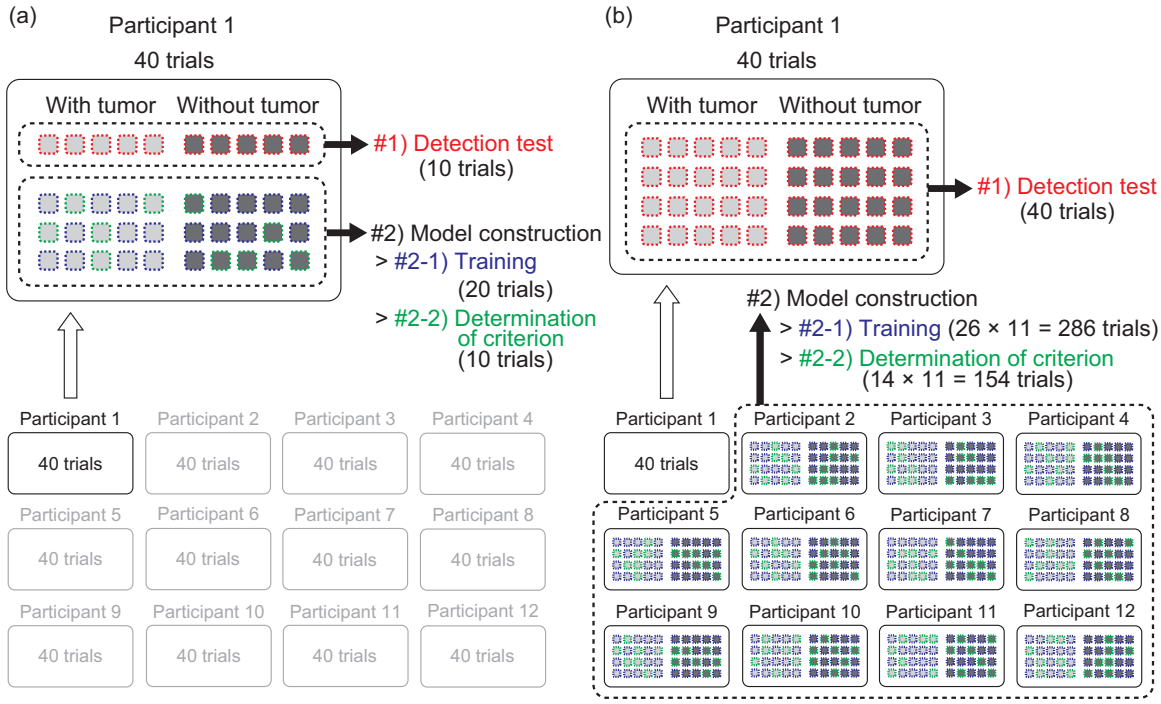

Fig. 4.6: Preparation of the dataset for the two types of validations. Light and dark gray filled rectangles indicate the data acquired at a single detection trial where the tumor was present and absent, respectively. Red, blue, and green dashed lines indicate that the data was assigned for detection test, model training, and determination of the detection criterion, respectively. (a) Within-participant validation. Four-fold cross-validation was conducted within the data for each participant. (b) Across-participant validation. Leave-one-out cross-validation was conducted against data for all the participants. Both validations were conducted independently, 12 times along all the participants.

calculated. Estimated label $\boldsymbol{y}$ was obtained against sensor output $\boldsymbol{x}$ in dataset #1, and the estimation score was calculated. Accuracy ACC was calculated by applying the mean threshold detection criterion to the estimation scores. Moreover, false alarm rates F_j and hit rates H_j were calculated, then ROC curves were plotted from (F_j, H_j). This procedure was repeated four times by changing dataset #1 for each participant, and the mean of accuracy ACC and the area under the curve A_{g} were calculated for

four times validation.

Across-participant validation

Leave-one-out cross-validation was conducted against the data for all the participants. Fig. 4.6(b) shows the procedure for the data preparation. The data for all the 40 trials from a single participant were used for the detection test (dataset #1). The remaining data were from 11 out of the 12 participants, and used for the model construction as dataset #2. Dataset #2 was divided into two groups: for the training (dataset #2-1) and for the determination of the detection criterion (dataset #2-2). For datasets #2-1 and #2-2, 26 trials from 13 of each type of trial, and 14 trials from 7 of each, were randomly selected from each participant, respectively. The entire procedure (training, determination of the criterion, detection test, and drawing of the ROC curves) was similar to the within-participant validation. The across-participant validation was independently conducted 12 times by changing dataset #1 along the participants.

4.4 Results

4.4.1 Within-participant validation

Detection performance

Fig. 4.7 displays the relationship between the accuracy and detection criterion for each participant. This result was obtained against dataset #2; thus, it indicates the performance of the constructed model. The black and red solid lines show the results for four times validation and the mean, respectively. If a criterion has ultimate values (such as 0 or 1), the accuracy has the chance level of the detection (0.5). It can be seen that the relationship curve was different for the participants. Dashed vertical lines in Fig. 4.7 represent the mean of the determined detection criteria. A higher accuracy is obtained at a criterion closer to the determined value.

The accuracy was compared between the human participants and DNN model. Fig. 4.8 shows the results of the comparison. The accuracy for the DNN model was obtained against dataset #1; thus, it indicates the detection performance of the model

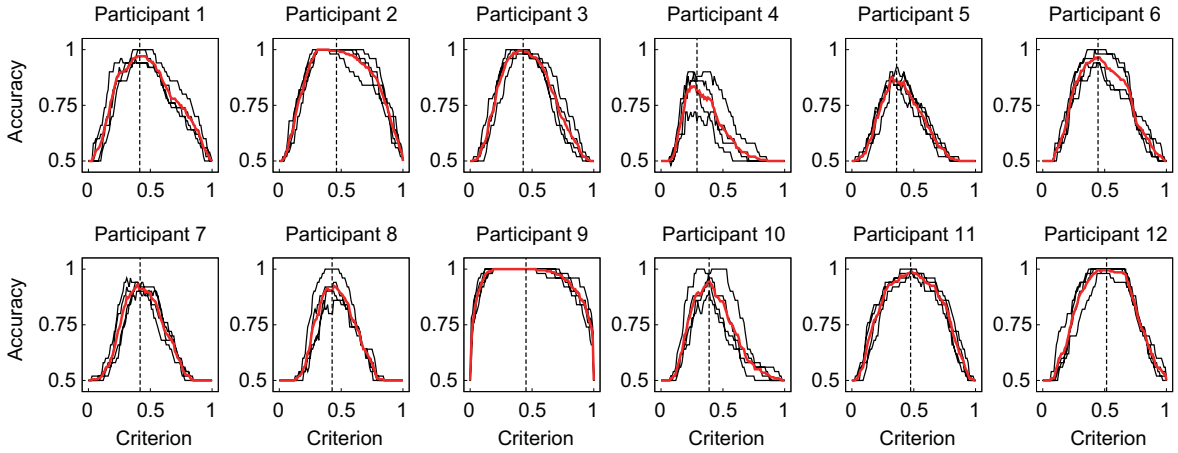

Fig. 4.7: Relationship between the accuracy and detection criterion for each participant obtained in the within-participant validation. Black lines indicate each data for the 4-fold cross-validation, and red lines indicate the mean of four data. Black vertical dashed lines indicate the mean threshold criterion.

for the unknown dataset. The accuracy for the human participants was calculated based on the data obtained in our previous chapter. Statistical tests were conducted to compare the accuracy of the human participant and DNN model. Before the analysis, a Shapiro–Wilk test was conducted to confirm that the all-dependent parameters were normally distributed. Because the assumption of the normal distribution was violated, a Wilcoxon signed-rank test was conducted to compare the accuracy for the human participants and DNN model in the within-participant validation. The statistical test showed no significant difference in the accuracy of the human participants and DNN model ($W(12) = 23, p = 0.37$). This indicates that the median of the accuracy for the human participants and proposed DNN model were not different in the within-participant validation.

ROC curve

Fig. 4.9(a) depicts the ROC curves obtained against dataset #2 in the within-participant validation from all participants. Each curve is drawn based on the estimation by the DNN model, trained by the data from each participant. The black

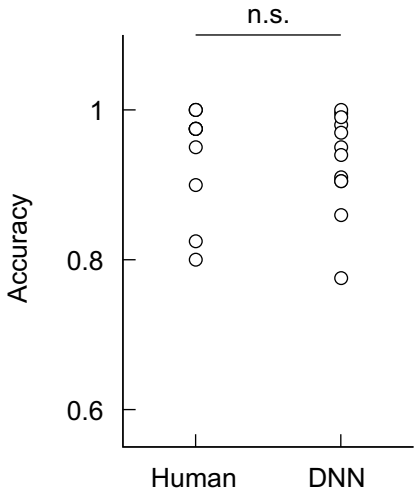

Fig. 4.8: Comparison of the accuracy of the human participants and DNN model in the within-participant validation. The performance of the human participants was calculated based on the data in Chapter 3. Label n.s. indicates no significant difference at the 0.05 level with a Wilcoxon signed-rank test.

and red solid lines show the ROC curves for the four-fold cross-validation and mean curves, respectively. If an ROC curve approaches the top left part, the curve indicates that the DNN model has a higher potential sensitivity. In particular, the ROC curves based on the data from participants 2, 9, and 12 indicate that the model achieved the ultimate potential sensitivity ($A_{\mathrm{g}} = 1$) because the curves form a unit square.

The potential detection sensitivity A_{g} was compared for the human participants and DNN model. Fig. 4.9(b) shows the comparison of A_{g}. The values for the human participants were obtained in our previous study. A Wilcoxon signed-rank test showed no significant difference in the potential sensitivity between the human participants and DNN model ($W(12) = 33, p = 0.21$). It indicates that the median of the potential sensitivity for the human participants and proposed DNN model was not different in the within-participant validation.

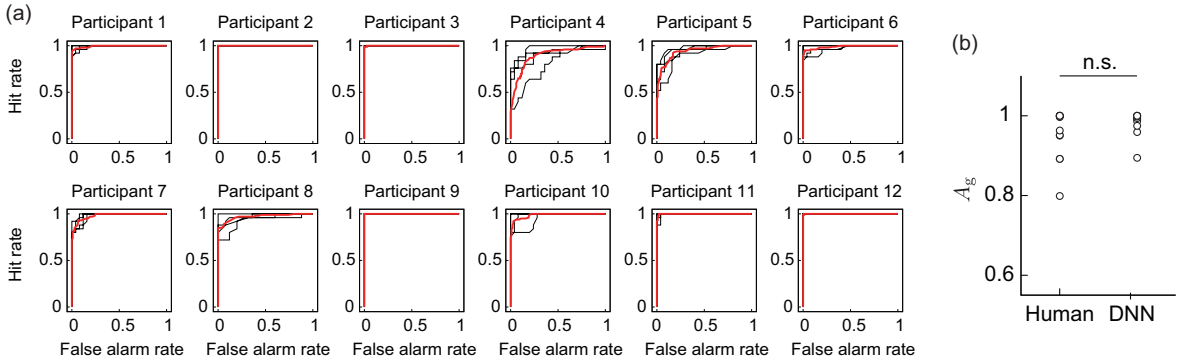

Fig. 4.9: Potential detection performances of the DNN model constructed in the within-participant validation. (a) ROC curves. Black lines indicate each data for the 4-fold cross-validation, and red lines indicate the mean. (b) Comparisons of the area under the curve A_g of the human participant and DNN model. The performance of the human participants was obtained in Chapter 3. Label n.s. indicates no significant difference at the 0.05 level with a Wilcoxon signed-rank test.

4.4.2 Across-participant validation

Fig. 4.10(a) exhibits the relationship between the accuracy and detection criterion in the across-participant validation. As the result was obtained against dataset #2, it indicates the performance of the constructed model. The black and red solid lines show each curve for 12 times validation and the mean curve, respectively. The mean and standard deviation of the determined criterion are represented as $c_{\mathrm{th}} = 0.38 \pm 0.014$, for which the detection performance of $ACC = 0.95 \pm 0.0093$ was achieved.

Fig. 4.10(b) shows a comparison of the accuracy for the human participants and DNN model in the across-participant validation. The accuracy of the model was calculated for dataset #1; thus, it indicates the performance of the model for the unknown dataset. A Wilcoxon signed-rank test showed a significant difference in the accuracy for the human participants and DNN model ($W(12) = 74, p = 0.006$). This result indicates that the median of the accuracy for the DNN model was significantly smaller than that for the human participants. Moreover, a one-sample Wilcoxon signed-rank test against 0.5 (the chance level of the detection) was conducted, and a significant difference was shown ($W(12) = 78, p = 0.002$). This indicates that the median of the

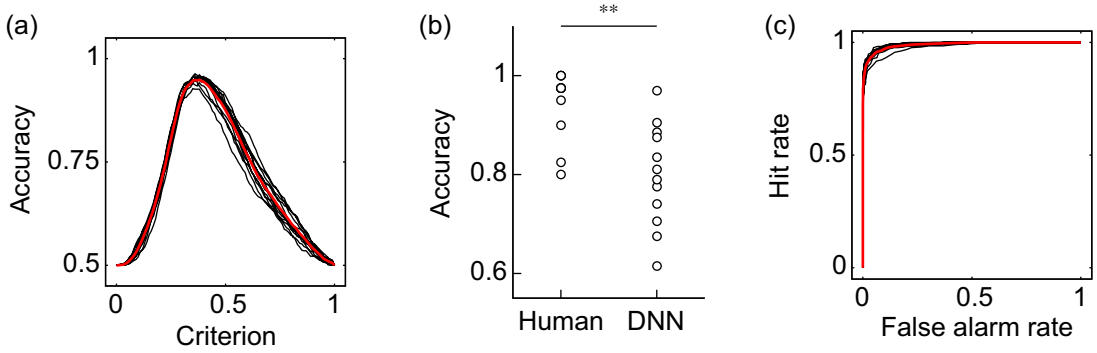

Fig. 4.10: Results of the across-participant validation. (a) Relationship between the accuracy and detection criterion. Results of 12 independent validations shown by the black solid line, and their mean was shown by a red solid line. (b) Comparison of the accuracy for the human participants and DNN model. The accuracy for the human participants was calculated in Chapter 3. Here, ** indicates $p < 0.01$ with a Wilcoxon signed-rank test. (c) ROC curves.

accuracy for the DNN model was higher than the chance level.

Fig. 4.10(c) shows the ROC curves obtained in the across-participant validation. This result was obtained against dataset #2. The black and red solid lines exhibit the data for each independent validation and mean of the results, respectively. The mean and standard deviation of the area under the curve were $A_{\mathrm{g}} = 0.99 \pm 0.0037$.

4.5 Discussion

The experimental results of the within-participant validation showed no significant difference in the accuracies obtained for the human participants and proposed DNN model. This result indicates the possibility of replacing the detection by the participants based on visual feedback with the DNN model. Fig. 4.7 shows that the relationship curve between the accuracy and various criteria were different for the participants. This difference might be due to a large variation in sensor output. In Fig. 4.4 it can be seen that the sensor output that indicates the presence of a tumor was different for the participants, despite the same tumor being scanned. Moreover, we discovered in

the previous chapter that the applied force and scanning speed varied between participants. Thus, the variation for the participants suggests a necessity for an appropriate determination of the detection criterion. We proposed usage of the relationship curve to determine the detection criterion. Here, Fig. 4.9(b) shows that the potential sensitivities for the human participants and DNN model were similar in the within-participant validation. Even if the trained model has a high potential sensitivity, a high accuracy is not obtained until the detection criterion is not appropriate. This suggests that the proposed method to determine the criterion was appropriate. Moreover, Fig. 4.7 shows that the relationship curve for participant 12 had more peaky shape in comparison with that for participant 9, whereas their potential detection sensitivities (ROC curves) were similar (Fig. 4.9(a)). The more peaky shape suggests that the accuracy was more sensitive to changes in detection criterion. Thus, the relationship curve also reveals the robustness of the detection to a change in the detection criterion.

A comparison of Figs. 4.8 and 4.10(b) shows that the accuracy for the DNN model in the within-participant validation tended to have a higher value than in the across-participant validation. Moreover, the accuracy for the model in the across-participant validation was significantly smaller than that for the human participants, whereas the mean potential detection sensitivity (area under the curve) of the constructed model was 0.99. This indicates that the model constructed in the across-participant validation achieved inefficient detection with unknown datasets. The inferior performance suggests that the use of data from the same participant is more effective in the training of the model. It could also be attributable to a variation in the appropriate detection criterion for the participants, as discussed in the above paragraph. In the across-participant validation, the criterion was determined from the data obtained from the other 11 participants. Thus, using the determined detection criterion might not be optimal for detection by the remaining participant, whose data was not used in the model construction. In contrast, the accuracy for the model was significantly higher than the chance level of the detection (0.5). Therefore, in practical applications it might be effective to use the data from the other users in the pre-training. This could contribute to more effective detection with low computational cost during the model update.

Next, we will discuss the future works toward clinical applications. Experiments

with expert surgeons are necessary to investigate the applicable range and conditions of the proposed assistance algorithm at the next stage. Herein, the stiffness of the phantom used in the experiment lies within the stiffness range of the actual stomach wall and tumor; however, it did not have exactly the same anatomical structures and boundary conditions found in reality. In the experiment, it was shown that the novice participants could discriminate the phantom with/without the tumor after sufficient practice. Further, some participants achieved a complete detection performance. Thus, the experiment with expert surgeons in the current setup might not bring valuable discussion toward practical applications. In future work, we will investigate the applicable range and conditions of the algorithm through the sensor manipulation by expert surgeons in an in-vivo setup. In addition, it is important to consider the method of generating the tumor label for model training. The label was calculated according to the measured positions of the phantom tumor and sensor. However, in surgical situations, it would be difficult to make the label in the same way, because the correct position of the tumor is not available during surgery. One solution is to record the time when the surgeon intraoperatively finds a tumor, according to feedback from the tactile sensor. If it is found in the postoperative examination that the position intraoperatively indicated by the surgeon is correct, then the label can be generated based on the recorded time and used for model training. Moreover, tumors vary in dimensions and stiffness, therefore it might be effective to input the preoperatively acquired features of the tumor to achieve more robust detection, regardless of tumor differences. In future work, we will develop a methodology for data acquisition considering surgical applications.

In our scenario, the user manipulates the tactile sensor and make a decision according to tactile feedback from the sensor, and the DNN model conducts the detection according to the sensor output in real-time. Thus, the proposed assistance algorithm is collaborative, and the surgeon should appropriately manipulate the sensor to scan the target tissue so that the effective detection by the model is achieved. Thus, it is necessary to optimize the tactile feedback of the sensor output to the surgeon, for more effective detection by both the surgeon and DNN-based assistant. Although our previous study showed that tactile feedback was only effective for a safer manipulation, effective tumor detection could be achieved by introducing the proposed assistance algorithm. We will also continue to improve the tactile display for sensory feedback,

to improve decision making and sensor manipulation by the surgeon. Moreover, an important design factor for the data-driven assistant is the interaction between the surgeon and assistant. A possible method to realize this is by using an audio channel that is independent from the visual and tactile channels. Furthermore, the use of an audio channel would imitate the interaction between a surgeon and human assistant. Therefore, we will consider different approaches for achieving this interaction. Moreover, we will investigate the effect of this interaction on decision making and sensor manipulation by the surgeon.

4.6 Summary

We proposed an assistance algorithm using a deep neural network for laparoscopic tumor detection. The algorithm uses the temporal output from a tactile sensor that is directly manipulated by a surgeon. Thus, safe and dexterous manipulation of the sensor is ensured by the surgeon, and the decision of the surgeon is assisted by the algorithm that performed the tumor detection simultaneously with and independently from the surgeon. This chapter was motivated by the previous psychophysical experiment, in which the participants had to detect a phantom of the stomach wall with/without a tumor based on visual feedback (a line graph based on the temporal sensor output). It was determined that providing visual feedback to an operator significantly enhanced the detection performance. However, using a visual channel for the sensory feedback was problematic because of the possibility of sensory overload, and of using valuable space in the operating room by the extra monitor. Thus, the proposed assistance algorithm in this study was intended to replace visual feedback.

A DNN model with three hidden layers was used to segment the sensor output, to identify whether the output included information on the tumor at each sampling. We proposed methods to input the temporal sensor output to the model considering real-time analysis, and to determine the detection criterion based on the relationship between accuracy and the various detection criteria. Moreover, signal detection theory was employed to assess the potential detection sensitivity of the model. Subsequently, two types of validation (within-participant and across-participant validation) were conducted to assess the effectiveness of the proposed model. Further, the detec-

tion performances were compared for the DNN model and human participants, which were obtained in our previous study. The results of the within-participant validation showed no significant differences in the accuracy and potential sensitivity for the human participants and DNN model. Thus, the possibility of replacing the detection by a user with a DNN-based algorithm was shown. Although the results in the across-participant validation showed that the accuracy of the DNN model was significantly less than that of the human participants, the performance was significantly higher than the chance level of the detection. Thus, this suggests that the data obtained from other users might be used in pre-learning of the model.

In future work, we will investigate the applicable range and conditions of the proposed algorithm. Moreover, we will consider a method for data collection in surgical situations. We will also develop an effective method to interact with the DNN-based assistant, and investigate the effects of the assistant on decision and sensor manipulation by the surgeon.

Chapter 5

Pneumatic tactile ring for instantaneous feedback

This chapter describes the development and evaluation of a pneumatic tactile ring, which is a clinically applicable tactile display to present pressure against the finger pad of a surgeon. The experiment in Chapter 3 showed no significant effect of the tactile feedback on detection. We assume that the main issue is the inferior spatial coincidence between the manipulating hand of the sensor and the displaying site. The tactile ring is designed to wear on one of the fingers of the manipulating hand. Fundamental characteristics of the tactile ring are investigated, and the effectiveness of the tactile ring in tumor localization is validated through a psychophysical experiment. In addition, clinical tests with surgeons are conducted to assess the clinical applicability and effectiveness of the tactile ring for the localization of the actual tumor.

5.1 Introduction

Tactile feedback of the acquired information is a reasonable mean in surgical situations because it is independent of other sensory channels. Moreover, tactile feedback is also advantageous because it does not interfere with the surgeon's manipulation in comparison with force feedback. There are many tactile displays that provide sensory feedback to the surgeon in minimally invasive surgery, robot-assisted minimally invasive surgery, and surgical training. Various types of actuation principles have been employed; for instance, pneumatic-driven tactile displays with multiple balloons [150,151], integrated capacitive sensors for three-axis deformation control [152], and granular jamming chambers to change its stiffness [153] have been developed. Those that supply an air jet to the finger pad have also been created [154]. There are tactile displays that use multiple servomotors to actuate a pin array directly [155–157], to drive a pin array through

a flexible tendon and conduit [158], and to control a planar platform [159]. In addition, there are several other principles employed in tactile displays such as the use of shape memory alloys [160,161], magnetorheological fluid [162–164], and microhydraulic actuators [165]. These tactile displays aim to supply rich tactile information such as spatially distributed pressure, stiffness, and multiple degrees of freedom of deformation. Although such tactile displays might be intuitive to use, they tend to have complexity due to the need of multiple displaying elements. This might result in high fabrication costs, which impedes their being used as disposable devices as well as their widespread application.

We have focused on temporal information-based palpation, in which a single output is acquired from a sensor and instantaneously fed back to the surgeon. A temporal information-based palpation system has the important advantage of simplicity since only a single sensing element and displaying element are needed unlike systems that use spatially distributed information. Yao et al. have developed a hand-held instrument with an embedded accelerometer and a vibrator to detect small cracks on objects in arthroscopic surgery [166]. This device detects a vibration at its tip while probing objects and presents amplified vibration to the tool body. An assistance device for needle insertion into soft tissues has been developed by Lorenzo et al. [167]. The device detects a force applied at the needle tip and transmits the magnified force to the operator. These studies showed that the detection and display of even a single output were effective in specific tasks. However, these devices were not designed for laparoscopic tumor localization, in which a long thin probe is manipulated to detect a hard mass within soft tissue. Devices for this purpose should be lightweight, and the means of feedback should be appropriately designed so as not to impede the manipulation of the probe. Moreover, some issues regarding their clinical application, such as reduced cost-effectiveness, disposability, and sterilizability, remain.

In Chapter 3, we developed a tactile display for the user's foot, where sterilization is not needed, to present a single force related to the sensor output and investigated the effects of visual and tactile feedback from the tactile sensor on ability of the user to detect a phantom tumor and on the user's behavior. It was found that the tactile feedback from the sensor had a positive effect on the sensor manipulation; however, the effect was not significant with respect to tumor detection. This might be because

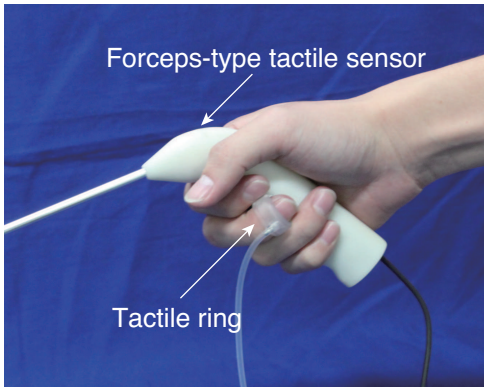

Fig. 5.1: Tactile ring to provide instantaneous feedback from the forceps-type tactile sensor.

the selected feedback site was the foot, which is quite a distance from the hand manipulating the tactile sensor. The feedback to the foot may, therefore, not be informative enough for laparoscopic tumor detection. The devices that use only simple information were designed such that a sensor and an actuator are embedded in the same hand-held tool [166], and a needle and manipulation point are coaxially aligned [167]. Spatial coincidence between the manipulating hand and the feedback site might, therefore, facilitate the sensory-motor integration and the interpretation of the given feedback.

The contribution of this chapter is the development and evaluation of a pneumatic tactile ring, which is a clinically applicable tactile device to provide instantaneous sensory feedback during laparoscopic tumor localization. To address the issue of spatial coincidence, tactile stimulation is transmitted to one of the fingers on the manipulating hand. The tactile ring was designed to present pressure to the surgeon's finger pad (see Fig. 5.1). Since it is driven by pneumatic power, it is lightweight, cost-effective, disposable, and sterilizable. It also hardly impedes the manipulation of the tactile sensor due to its wearability and means of stimulation. We also developed a compact pneumatic drive unit that consists of a diaphragm pump and a voice coil motor to control the inner pressure of the tactile ring continuously and quickly. The static and dynamic responses for the pressure controlled by the drive unit were investigated. Moreover, we performed a psychophysical experiment with 12 participants who had no medical background. Firstly, just noticeable differences (JNDs) for the pressure

were measured to quantitatively evaluate how the tactile ring presents the pressure perceived by the user and validates the signal processing applied to the sensor output. A localization test of a phantom early-stage gastric tumor was then conducted in a simulated laparoscopic setup. Localization performances were compared between the conditions with and without tactile feedback.

5.2 Tactile ring using pneumatic power

5.2.1 Design concept

We aimed to develop a tactile device that is worn on the finger of the hand used to manipulate a tactile sensor. Placing the tactile device on the finger results in high spatial coincidence between the manipulating hand and the feedback site. Additionally, the device should not impede the sensor manipulation; in particular, it should not have a weight large enough to affect the sensor manipulation due to its large inertia. Thus, high wearability is required. It is also inevitable to meet requirements for clinical application [120]. Sterilization adaptability is a major factor for a device in contact with the surgeon's hand. Furthermore, a low-cost device means that it can easily be used in a disposable manner. To put an actuator, such as a motor and a vibrator, on an adjacent part of the finger will result in reduced wearability, sterilizability, and disposability. Thus, using pneumatic power is a reasonable choice for the development of a clinically applicable tactile device. Pneumatic power can be generated at a distance and has a high power-to-volume ratio. The body of the tactile device can, therefore, be lightweight, which causes less interference with the sensor manipulation. In addition, its low-cost fabrication allows for its use as a disposable device.

An important design factor is how a reaction force against the stimulation of the finger pad is grounded. Fingernail-grounded tactile devices are suitable to achieve better wearability than grounded and body-grounded devices [168]. There are many fingernail-grounded devices that achieve high wearability such as those in [169], [170], and [171]. In this study, we designed a pneumatic tactile ring, which is a ring-type device for pressure presentation. A ring is a reasonable shape to use to ground the reaction force. There are relevant studies on the development of tactile devices em-

ploying a ring shape to achieve high wearability [172–175]. However, these devices are not currently applicable to surgical situations because of the disadvantages related to the use of electrical elements. We designed the tactile ring to be rigid; thus, the surgeon can easily wear the device by just inserting it onto the finger, and the reaction force against the pressure presentation is grounded on the back of the finger pad and the nail. Moreover, we developed a pneumatic drive unit to supply air pressure. Many related studies on pneumatic tactile displays have mainly focused on their body; however, fewer studies have been conducted to reduce the overall size of the driving unit. It is popular to use a commercial air compressor, a tank, and a pneumatic valve, which tend to be bulky and are not optimized for specific applications. We aimed to control the inner pressure of the tactile ring continuously and quickly (at least a bandwidth of 1 Hz) with a compact setup.

5.2.2 Tactile ring

The tactile ring is shown in Fig. 5.2(b), and its composition is shown in Fig. 5.2(c). It contains a cavity, which is opened at the inner lower side of the ring. A silicone rubber membrane with a thickness of 0.5 mm was stuck to the opened portion to form the presenting area of pressure. A sponge was attached to the inner upper side of the ring to address individual differences of finger size. The cavity was connected to a silicone rubber tube with a length of 3 m, and an inner and an outer diameter of 2 mm and 3 mm, respectively. Another tube end was connected to a luer-lock needle, which can easily be attached to/detached from a luer-lock coupling in the pneumatic drive unit. The total weight and cost of the tactile ring including the rubber tube are approximately 17 g and US$ 4.5, respectively.

5.2.3 Pneumatic drive unit

The pneumatic drive unit is shown on the right side of Fig. 5.2(a), and its composition is shown in Fig. 5.2(d). The drive unit mainly consists of a diaphragm pump (DSA-2F-12, DENSO SANGYO Co., Ltd.) and a voice coil motor (AVM20-10, Akribis Systems Japan Co., Ltd.). The pump can supply a maximum of approximately 90 kPa. The voice coil motor has a force sensitivity of 2.0 N/A. A silicone rubber sheet with a

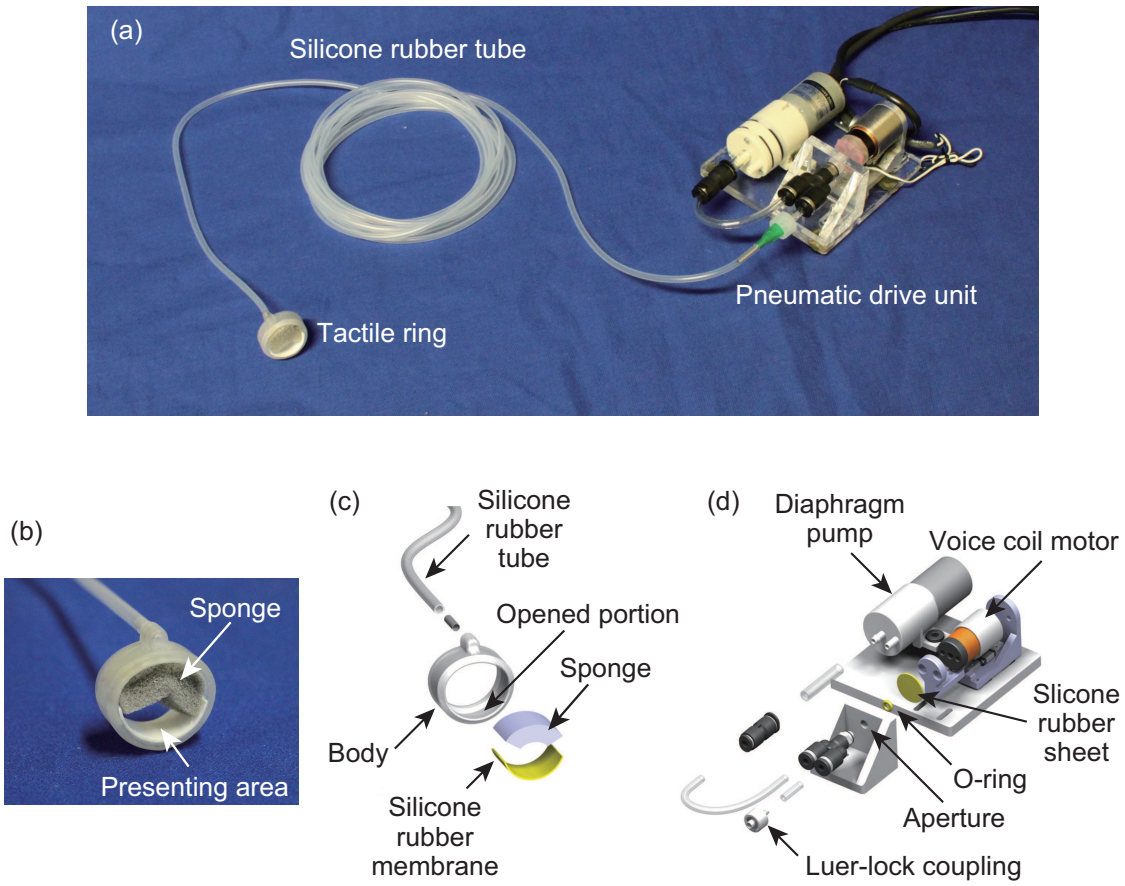

Fig. 5.2: Details of the tactile ring using pneumatic power. (a) Overview of the entire system. (b) Close-up of the tactile ring. (c) Expanded view of the tactile ring. (d) Expanded view of the pneumatic drive unit. Note that the scales in the two expanded views are not same.

thickness of 1 mm was attached to the top of the movable part of the motor. Air is supplied at a constant flow rate to the tactile ring from the pump via an aperture with a diameter of 5 mm. An O-ring with the inner and outer diameters of 4.8 and 8.6 mm, respectively, was attached coaxially to the aperture. The voice coil motor presses the silicone rubber sheet against the aperture with the O-ring. This portion acts as a proportional flow valve because the air leakage rate from the aperture varies according to the pressing force of the motor. The dimensions of the unit are $120 \times 80 \times 43$ mm

including the protruding portions.

5.3 Fundamental characteristics

5.3.1 Procedure

To investigate the pressure response at the presenting area in the tactile ring, a pressure sensor (AP-13A, KEYENCE Corp.) was connected to the pneumatic drive unit via the silicone rubber tube instead of the tactile ring. The pressure was recorded at a sampling frequency of 1 kHz.

The relationship between the input current to the voice coil motor and the inner pressure was investigated. The inner pressure was measured for eight input currents ($0.22, 0.45, 0.69, 0.92, 1.15, 1.39, 1.63$, and 1.86 A). Moreover, the step and frequency responses were measured to assess the dynamic performance of the drive unit. The inner pressure was measured for different step inputs that were switched on at 0.5 s and off at 2.5 s with eight target currents. For the measurement of the frequency responses, sinusoidal currents i_{in} with different frequencies (0.1–1.0 Hz with a 0.1 Hz increment and 1–10 Hz with a 1 Hz increment) were used as inputs to the voice coil motor, as follows:

$$i_{\mathrm{in}} = 0.5 I_{\mathrm{A}} \left\{ \sin\left(2\pi f t\right) + 1 \right\}, \tag{5.1}$$

where f is the frequency of the input, t is time, and I_{A} is the amplitude that corresponds to the target current. The frequency responses were measured for the eight target currents. Then, a gain was calculated according to the following equation:

$$\mathrm{Gain} = 20 \log_{10} \frac{P_{\mathrm{A}}}{P_{\mathrm{static}}}, \tag{5.2}$$

where P_{A} is the amplitude of the measured inner pressure, and P_{static} is the corresponding inner pressure for the static target current. The gain indicates how the inner pressure decreases in comparison to the static response. All measurements were conducted 10 times for each input current.

5.3.2 Results

Fig. 5.3(a) shows the relationship between the input current to the voice coil motor and the inner pressure. The error bars indicate the standard deviation of the 10 measurements. The coefficient of determination was 0.999. Fig. 5.3(b) shows the step responses for different target currents. The mean response curve of 10 measurements is shown for each target. The rising times are longer than the falling times. The rising time, in particular, largely changes according to the target values. The frequency characteristics of the gain for different target currents can be seen in Fig. 5.3(c). The gain decreased by increasing the frequency and also by increasing the target current for frequencies higher than approximately 1 Hz. A bandwidth of the tactile ring was calculated as a limit frequency at which the gain falls below -3 dB for each target pressure, and the result is shown in Fig. 5.3(d). The bandwidth decreased by increasing the target pressure, and the minimum bandwidth was 1.3 Hz at a target pressure of 79.7 kPa.

5.3.3 Discussion

The static relationship between the input current and the inner pressure was almost linear. It is known that the input current to the voice coil motor is linearly related to the force generated. Thus, the inner pressure is related linearly to the pressing force against the aperture. We have assumed that the inner pressure can be calculated from the pressing force and the cross-sectional area of the contact portion between the O-ring and the silicone rubber sheet; that is, the pressing force F is balanced with the force generated by the inner pressure P within the cross-sectional area A. In this case, the diameter of the circular cross-sectional area d is calculated as follows:

$$d = \sqrt{\frac{4A}{\pi}} = \sqrt{\frac{4F}{\pi P}} = \sqrt{\frac{4C_{\mathrm{if}}}{\pi P/I}}, \tag{5.3}$$

where $C_{\mathrm{if}} = 2.0$ N/A is the force sensitivity of the voice coil motor, and I is the input current to the motor. We calculated an equivalent diameter by substituting the slope of the fitted line (41.3 kPa/A) in Fig. 5.3(a) for P/I, and the equivalent diameter was 7.9 mm. The inner and outer diameters of the O-ring were 4.8 and 8.6 mm, respectively.

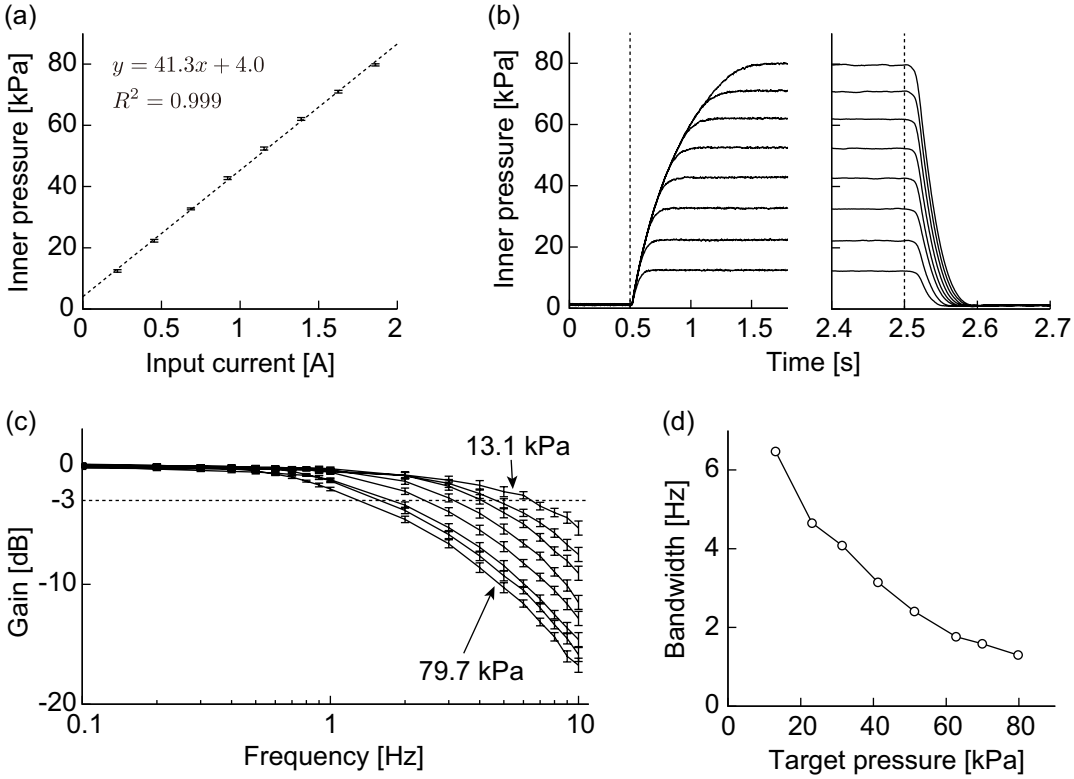

Fig. 5.3: Fundamental performances of the tactile ring. (a) Static relationship between the input current and inner pressure. (b) Step responses of the inner pressure for different target currents. Rising and falling responses are shown at different time scales. (c) Frequency responses of the gain of the inner pressure for different target pressures. (d) Bandwidth of the gain for different target pressures.

The equivalent diameter lies within them. This indicates that the controllable range of the inner pressure depends on the diameter of the O-ring. Moreover, the maximum suppliable pressure depends on the performance of the diaphragm pump. In this study, a pump that can supply a maximum of approximately 90 kPa was used. It was selected based on related studies on a pneumatic tactile display that presents several tens of kPa of air pressure [150, 151]. In this way, the static performance of the drive unit can be designed by selecting a diaphragm pump, a voice coil motor, and an O-ring according to its application.

The step responses of the inner pressure depended on the control direction and the target pressure as shown in Fig. 5.3(b). In particular, the rising response curves for all target pressures overlapped, and the rising time changed according to the target pressure. This is due to the pressure-supply mechanism. The diaphragm pump was directly connected to the tactile ring, and a constant airflow was supplied. Thus, the airflow rate from the diaphragm pump is dominant in the rising responses. On the other hand, the falling responses did not depend as much on the target pressure. This is because the performance of the pump did not affect the falling response, where the air was only discharged. The falling response can, however, be affected by the diameter of the aperture that corresponds to a pneumatic resistance. Thus, the dynamic performance of the drive unit can be designed through the selection of the airflow rate of a diaphragm pump and the diameter of the aperture. Moreover, the inner diameter and the length of the silicone rubber tube strongly affect the dynamic performance [176], and this should be taken into account in the design of the drive unit.

The bandwidth of the device was at least 1.3 Hz. In this study, we aimed to achieve a bandwidth of approximately 1 Hz since the output of our tactile sensor had frequency components lower than roughly 1 Hz when the user scanned the surface of a phantom of the stomach wall containing a typical tumor. Although the typically required bandwidth for a pin-array tactile display with 2 mm spacing is 30 Hz [177], we did not need a bandwidth this large because our device presents only a single pressure.

5.4 Psychophysical experiment

A psychophysical experiment measuring the JNDs of the presented pressure and a localization task of a phantom tumor in a simulated laparoscopic setup was performed. The measurement of the JNDs aimed to quantitatively evaluate how the tactile ring presents the pressure that can be distinguished by the user and validate the empirically determined signal processing to control the tactile ring. Moreover, we aimed to evaluate how the instantaneous tactile feedback through the tactile ring contributes to tumor localization. In laparoscopic resection of an early-stage gastric tumor, surgeons preoperatively acquire information about the tumor such as its dimensions and position using peroral endoscopy. The surgeons then find the accurate position of the

tumor through tactile feedback to determine the appropriate cut-line. Thus, we designed our localization task such that a phantom tumor with constant dimensions was always present, and only its position was changed. This information was provided to the participants before localization trials.

5.4.1 Participants

In this study, we aimed to assess the effectiveness of the tactile ring in a fair manner. Professional surgeons will have a large variation in their surgical skills and experience. Thus, in order to reduce the effect of variation in manipulation skills on our experiment, we employed novice participants and provided them with the same practice trials before the experiment. Twelve persons (9 male and 3 female, age range 18–25, mean 20.4) without any medical background were paid to participate in this experiment. Eleven participants out of the twelve were strongly right-handed, and one participant was strongly left-handed according to Coren's test [125]. They gave their written informed consent before participation. The experimental protocol was conducted in accordance with the ethical standards of the Helsinki Declaration and approved by the Ethical Committee of the Nagoya Institute of Technology.

5.4.2 Feedback signal to tactile ring

We aim to give instantaneous sensory feedback through the tactile ring to the operator of a tactile sensor. We used our proposed tactile sensor employing acoustic sensing principles [15] for the instantaneous feedback (see Fig. 5.4(a)). The sensor has high surgical applicability since it is electrically safe for body tissue, disposable, and sterilizable. The sensor was somewhat improved from [15] for better usability; for instance, the entire length was 50 mm longer than the previous device, and the handle of the sensor was redesigned for better grip. In particular, the position of the sensing area was shifted toward the tip of the sensor, which assists the user in scanning the area of interest accurately. The sensor responds to a normal force applied to the sensing area.

The signal processing of the sensor output that controls the display device is an important design factor. We empirically designed the signal processing according to the results of pilot experiments and comments from clinicians who tested our device.

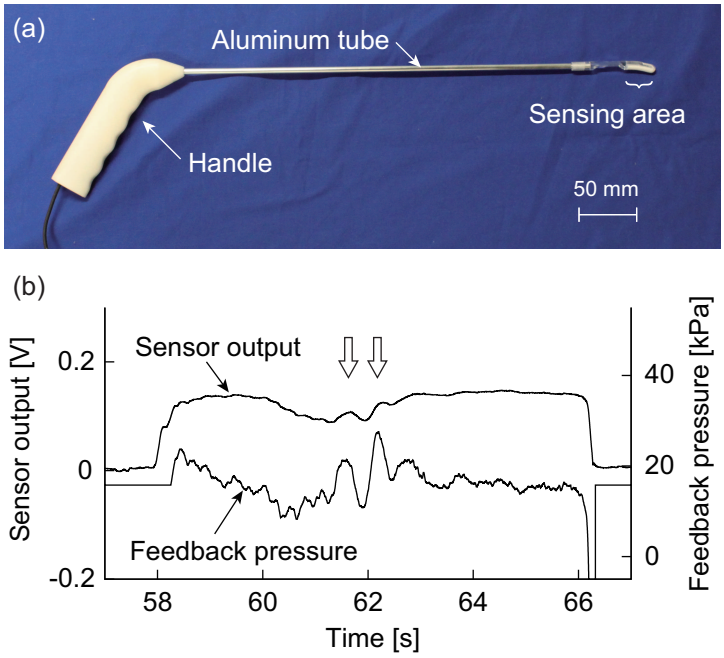

Fig. 5.4: (a) Forceps-type tactile sensor used for the localization test. (b) Typical output from the tactile sensor and the feedback pressure. Open arrows indicate two peaks that mark the tumor.

The typical sensor output and the feedback signal to the tactile ring are shown in Fig. 5.4(b). The sensor output responds with two small peaks since the target tumor has a toroidal shape. The sensor output was firstly filtered by a band-pass filter with a bandwidth of 0.5–10 Hz because the tactile ring aimed to present the relative pressure difference during scanning. Then, a gain of 80.7 kPa/V was applied to the sensor output. However, the gain was reduced to zero over 0.3 s after the initial contact between the sensor and the target object, and subsequently, it was gradually increased to its original value (see Fig. 5.4(b)). The initial contact was detected based on a sensor output threshold (0.01 V). This aspect of the signal processing was added to remove the large pressure feedback due to the initial contact. An offset value corresponding to a pressure of 15.8 kPa was always added, which allowed for a negative feedback signal to be presented. The offset was empirically determined not to be large because, as shown in Fig. 5.3(d), a large pressure results in a smaller dynamic response of the pneumatic

drive unit. The values of the gain and offset were fixed for all of the participants.

5.4.3 Phantom of stomach wall

We aim to localize a 0-IIc (superficial ulcerative) type of early-stage gastric cancer [16], which is located on the mucosal side of the stomach wall and typically has a toroidal shape. We have fabricated a phantom of the stomach wall with the tumor on the basis of the actual dimensions and stiffness of the stomach and the tumor in Chapter 3. In this chapter, although the fabricated phantom was similar, the width was increased to 160 mm to enable the production of stimuli with different tumor positions (see Fig. 5.5(a)). A stimulus for the localization task was prepared by putting the phantom with the mucosal side down on a sponge sheet with a thickness of 10 mm. The two ends of the phantom were supported by rigid semicircular bases and fixed by semicylindrical plates (see Fig. 5.5(b)). Stimuli with different tumor positions were prepared by shifting the position of the phantom on the sponge along the x-direction.

Two different stimulus sets were prepared for practices and localization trials to prevent participants from memorizing the number or the position of the stimuli. As a stimulus set for practices, four stimuli with different tumor position, i.e., two far positions (+5 and +15 mm) from the lateral center of the stimuli and two near positions (-5 and -15 mm), were prepared. An additional set of five stimuli ($-20, -10, 0, +10$, and $+20$ mm) was prepared for the localization trials. Fig. 5.5(c) shows the camera image of the center of the five stimuli.

5.4.4 Setup

Fig. 5.6 shows the setup for the localization experiment. It consisted of a laparoscopic training box (Endowork-Pro II, Kyoto Kagaku Co., Ltd.), a camera, a monitor for displaying the camera image, a 12-mm trocar (ENDOPATH XCEL CB12LT, Ethicon Inc.), the tactile sensor, and the tactile ring. The participants were asked to wear headphones playing white noise to avoid hearing sound from the pneumatic drive unit. They manipulated the tactile sensor with their dominant hand and wore the tactile ring on their middle finger of the dominant hand. For the left-handed participant, the setup was symmetrically rearranged. To avoid visual localization of the tumor, the training

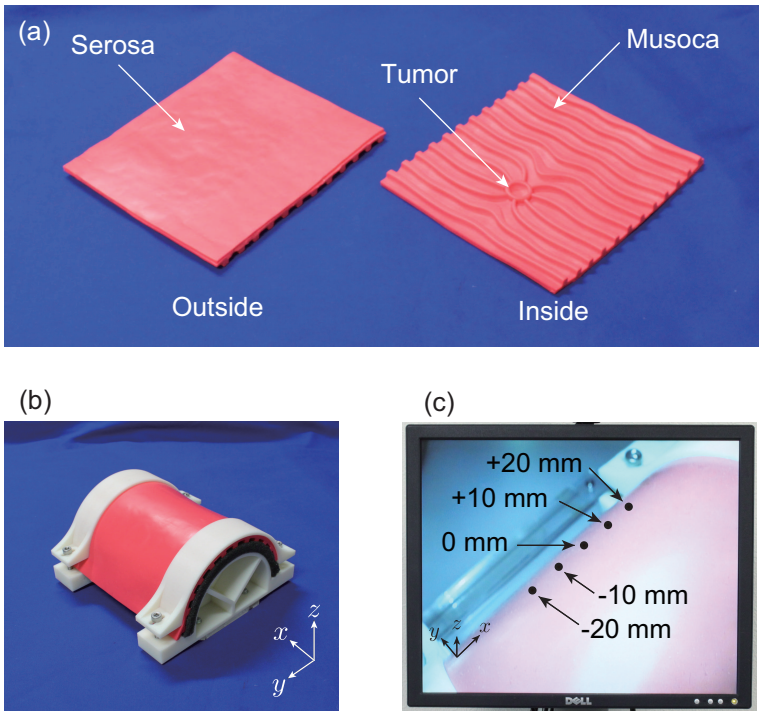

Fig. 5.5: (a) Phantom of stomach wall with tumor. (b) Stimulus for localization test. (c) Camera image of stimulus and five tumor positions presented in localization trials. Black dots show the center of the tumor at each position.

box was covered with a black cloth, and the camera image was blurred slightly.

The stimuli were placed on a three-axis force sensor (Gamma SI-32-2.5, ATI Industrial Automation, Inc.), and they were fixed to the inside of the training box. Exerted force was measured at sampling frequencies of 1 kHz. If the participants applied a larger force than 1 N, an auditory alarm (1 kHz, square wave) was transmitted to the participant through the headphones. The participants were asked to reduce the force if they heard the alarm. The force limitation was to prevent an overload on the stimulus and also imitated real-life conditions since surgeons do not apply a large amount of force to the tissue in clinical situations. As a tool to indicate the position of the tumor, a toroidal marker that has the same diameter as the tumor was prepared. The marker was magnetically connected to a linear encoder that measures its lateral position; thus, the estimated tumor position by the participants was measured through

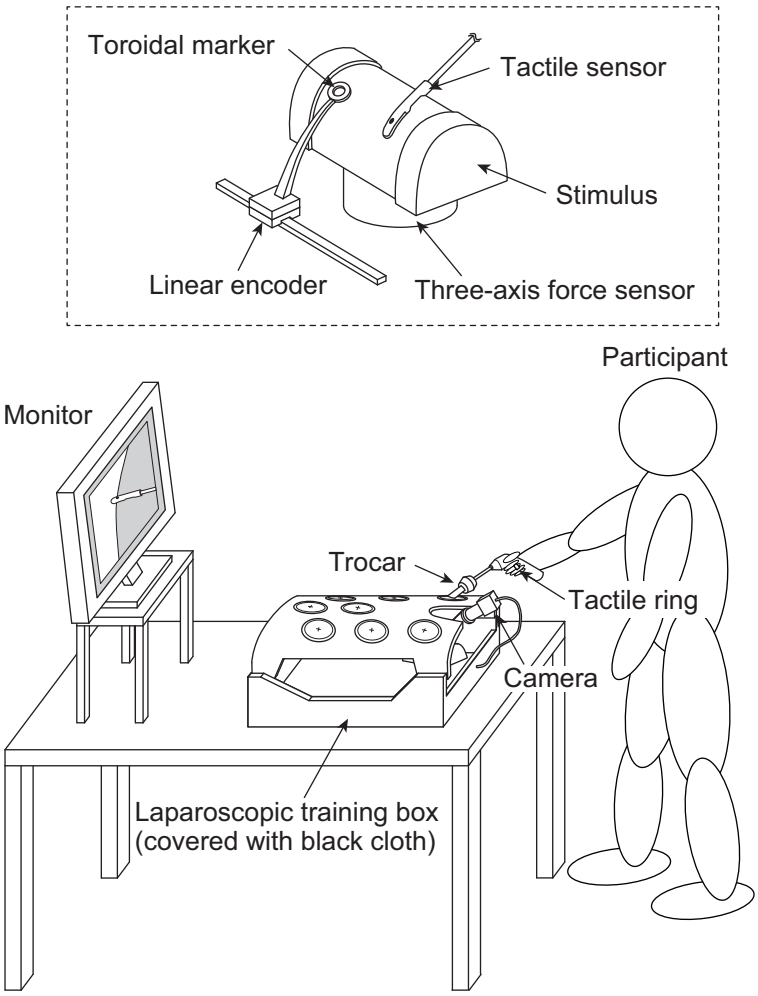

Fig. 5.6: Setup for the localization test. The dashed rectangle details the inside of the training box. For the left-handed participant, the stimulus was symmetrically rearranged.

the position of the marker. While the participants scanned the stimulus surface, the marker was removed from the training box.

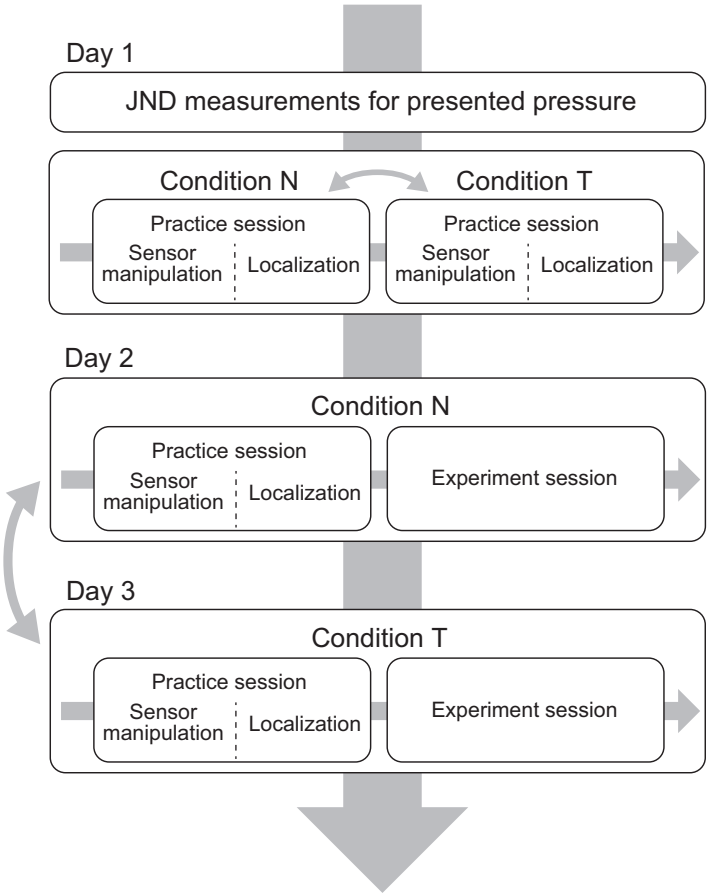

Fig. 5.7: Example of the experimental procedure for each participant. The time interval between each experimental day was more than 24 hours, and the entire procedure was completed within three weeks. Curved arrows indicate that the order of conditions was counterbalanced across the participants.

5.4.5 Experimental procedure

The entire experimental procedure consisted of three days for each participant. Fig. 5.7 shows an example of the detailed procedure. The first day was used for the JND measurements and for practice to become familiar with the sensor manipulation and localization tasks. The remaining two days were used for localization tasks with two experimental conditions. The conditions were set regarding the feedback from the sensor;

no tactile feedback condition (N) and tactile feedback condition (T). Under condition N, the participants did not receive any feedback from the sensor. Under condition T, the participants received the pressure stimulation from the tactile ring according to the sensor output. The time interval of each condition was more than 24 hours to reduce learning effects, and the participants completed the entire experiment within three weeks. The participants wore the tactile ring regardless of the condition. The experiment took 144 ± 16 min, 101 ± 16 min, and 98 ± 22 min for Days $1, 2$, and 3, respectively.

JND measurements

The participants wore the tactile ring but did not manipulate the tactile sensor. Three pressures ($22.7, 42.1$, and 61.4 kPa) were chosen as reference pressures on the basis of the pressure range of the pneumatic drive unit. The reference pressure was presented to the participant for a couple of seconds; then, the pressure was gradually increased/decreased from the reference point, and at the same time, an experimenter gave a cue to the participants. The participants were asked to indicate when they felt a pressure change, and the pressure difference from the reference was recorded as a JND. Each ascending/descending series was alternately conducted six times for each reference pressure. The presenting order of the three references was counterbalanced across the participants.

Localization experiment

After the JND measurements on the first experimental day, the participants practiced the sensor manipulation and localization trials for each condition. The participants were informed that the dimensions of the tumor were always the same and that only the lateral position of the tumor was changed. They were asked to manipulate the sensor as follows. They first made contact with the stimulus, and then laterally slid the sensor in a single direction. After sliding the sensor, they lifted up the sensor. They were instructed not to slide the sensor back and forth. These instructions regarding the manipulation were provided to control the participants' scanning strategy during the localization trials to ensure a fair comparison across the participants.

The participants were forced to practice for at least 4 min against the stimulus with the tumor located at the lateral center (0 mm), and they were given the correct position of the tumor with the toroidal marker before the practice. If they wanted more practice time, they were allowed to practice for an additional 1 min. Then, each tumor position from $-15, -5, +5$, and $+15$ mm was randomly presented, and the participants were forced to practice in the same way.

After the participants practiced the sensor manipulation, they had eight practice localization trials. Two of each tumor position from $-15, -5, +5$, and $+15$ mm were randomly presented. The participants were asked to localize the position of the tumor as quickly and accurately as possible within 180 s in each trial. When they found the position of the tumor or reached the time limit, they were asked to indicate the estimated tumor position with the tip of the sensor and grade confidence in their estimated position on a scale between 1 (not confident at all) to 100 (very confident). The response time was measured with a stopwatch. The toroidal marker was put on the position indicated by the participants with the sensor tip. Then, the marker was shifted to the true position to give the participants feedback about their setting.

Each subsequent experimental day consisted of a practice session and an experimental session. The practice session was similar to practices in the first day; however, the participants were forced to practice sensor manipulation for at least 2 min for five tumor positions (the tumor position of 0 mm followed by positions of $-15, -5, +5$, and $+15$ mm). Then, four practices for tumor localization with feedback about the correctness of their setting were conducted (one for each randomly presented position from $-15, -5, +5$, and $+15$ mm). In the experimental session, the participants conducted the localization trial 20 times, for four of the randomly presented tumor positions from $-20, -10, 0, +10$, and $+20$ mm. The protocol was the same as that for the localization practice; however, the participants did not receive any feedback about the true tumor position.

5.4.6 Data analysis

Localization performances

The absolute error between the estimated and the true position of the tumor, the confidence rating, and the response time were recorded for each localization trial. As an average value of localization performance for each participant, the median of each parameter was calculated instead of the mean because it was found that the raw data were not normally distributed according to Shapiro–Wilk tests.

To quantitatively assess how well the participants localized the tumor, we calculated an expected value of the absolute error for a random tumor localization. Let L be the maximum lateral length that can be scanned by the tactile sensor, and $x_{\mathrm{t}j}$, $(j = 1, 2, \cdots, 5)$ be the prepared positions of the tumor. At first, the length L was divided into a large number of N segments. We assumed that the participants randomly chose one segment from N discrete segments, and the probability of segment selection was uniform within L. The probability that one of each tumor position is randomly presented, and one of each discrete segment is randomly selected is $1/(5N)$. In this case, the expected value E is calculated according to the definition that a summation of each product between a probability and an outcome is as follows:

$$\begin{aligned} E &= \lim_{N\to\infty} \sum_{i=0}^{N} \sum_{j=1}^{5} \frac{\Delta x}{5L} \left| x_i - x_{\mathrm{t}j} \right| \\ &= \frac{1}{5L} \sum_{j=1}^{5} \int_0^L \left| x - x_{\mathrm{t}j} \right| \mathrm{d}x \\ &= \frac{1}{5L} \sum_{j=1}^{5} x_{\mathrm{t}j}^2 - \frac{1}{5} \sum_{j=1}^{5} x_{\mathrm{t}j} + \frac{L}{2}, \end{aligned} \tag{5.4}$$

where $x_i = (L/N)i$ is the position of the i-th discrete segment $(i = 0, 1, \cdots, N)$ from the origin, and $\Delta x = L/N$ is the width of each discrete segment, as shown in Fig. 5.8. The length that can be indicated (L) is 80 mm because the entire length is 100 mm, and the diameter of the tumor is 20 mm. The tumor positions are $20, 30, 40, 50$, and 60 mm from the left side (corresponding to $-20, -10, 0, +10$, and $+20$ mm from the center). We substituted these values into Eq. (5.4) and obtained an expected value of absolute error as 22.5 mm.

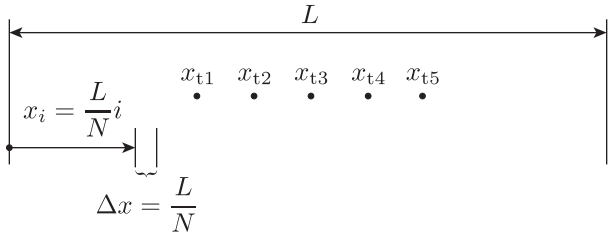

Fig. 5.8: Calculation of expected value of absolute localization error.

Statistical test

Effects of the tactile feedback and the tumor position on the performance indices were investigated through statistical tests. The significance level was set to 0.05. Before analyses, a Shapiro–Wilk test was conducted to check whether all the dependent parameters were distributed normally. For each index in all participants, a two-way repeated measures ANOVA with the conditions (N and T) and the tumor positions ($-20, -10, 0, +10$, and $+20$ mm) as factors was conducted. Before the ANOVAs, a Mauchly's sphericity test was conducted to confirm the assumption of the homogeneity of the variance. If the assumption of the homogeneity of the variance was violated, the Greenhouse–Geisser correction was applied. In the case where a significant influence of the tumor position was shown, post-hoc paired t-tests for all possible combinations of the tumor positions were conducted with Bonferroni correction. If the assumption of a normal distribution was violated, we used the aligned rank transform [178] for non-parametric factorial analyses before the ANOVAs. If a significant influence of the tumor position was confirmed, post-hoc Wilcoxon signed rank tests for all possible combinations were conducted with Bonferroni correction.

5.5 Results

5.5.1 Weber ratio

Fig. 5.9(a) shows the result of JND measurements. The open circles and error bars show the mean and standard deviation of the JNDs for 12 participants at each reference, respectively. A linear function was fitted to the mean JNDs to reveal the Weber ratio

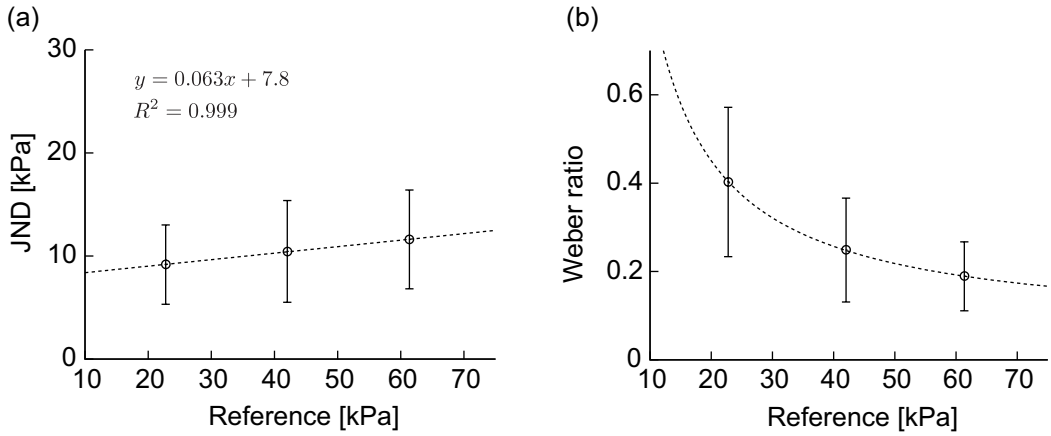

Fig. 5.9: Results of JND measurements. Open circles and error bars indicate the means and standard deviations of the data for 12 participants, respectively. (a) JND for reference pressure. The dashed line shows the fitted linear function. (b) Weber ratio calculated from the JNDs for each reference. The dashed curve was drawn from coefficients of the linear function.

of the pressure (the dashed line in Fig. 5.9(a)). The slope of the fitted line is 0.063, and the intercept is 7.8. The coefficient of determination is 0.999. We also directly calculated the Weber ratio (each JND was divided by the corresponding reference) for each reference (see Fig. 5.9(b)). The dashed curve was drawn on the basis of coefficients for the fitted linear function in Fig. 5.9(a). It was observed that the Weber ratio decreased according to the increasing reference pressure. The Weber ratio was at least 0.40 at the reference pressure of 22.7 kPa.

5.5.2 Localization performances

Fig. 5.10 shows the absolute error, the confidence in the participants' answer, and the response time for the presented tumor positions under each experimental condition. Fig. 5.11 shows the performance indices for each participant under each condition.

An ANOVA showed a significant influence of the condition on the absolute error ($F(1, 11) = 6.2, p = 0.030$). This result indicates that the mean absolute error for condition T is significantly smaller than that for condition N. The ANOVA also showed

a significant influence of tumor position on the error ($F(2.5, 28) = 14, p = 2.3 \times 10^{-5}$). Paired t-tests showed significant differences between tumor positions -20 and $+20$ mm ($p = 7.2 \times 10^{-4}$), -10 and $+20$ mm ($p = 0.049$), 0 and $+20$ mm ($p = 0.015$), and $+10$ and $+20$ mm ($p = 3.2 \times 10^{-4}$). These results indicate that the mean absolute error for the localization of the tumor at $+20$ mm is significantly larger than for other positions. There were no significant interactions between the condition and tumor position ($F(1.6, 17) = 0.28, p = 0.71$).

An ANOVA with the aligned rank transform showed a significant influence of the condition on the participants' confidence ($F(1, 99) = 190, p = 2.2 \times 10^{-16}$). This result indicates that the median of the confidence for condition T is significantly greater than that for condition N. The ANOVA also showed a significant influence of tumor position on the confidence ($F(4, 99) = 7.0, p = 5.0 \times 10^{-5}$). Wilcoxon signed rank tests showed significant differences between tumor positions -20 and $+20$ mm ($p = 0.0057$), -10 and $+20$ mm ($p = 4.4 \times 10^{-4}$), 0 and $+20$ mm ($p = 4.8 \times 10^{-6}$), and $+10$ and $+20$ mm ($p = 6.7 \times 10^{-4}$). These results indicate that the median of confidence for the tumor at $+20$ mm is significantly smaller than for other positions. There were no significant interactions ($F(4, 99) = 1.8, p = 0.13$).

An ANOVA with the aligned rank transform showed no significant influence of the condition on the response time ($F(1, 99) = 3.2, p = 0.078$). The ANOVA also showed a significant influence of tumor position on the time ($F(4, 99) = 7.1, p = 4.9 \times 10^{-5}$). Wilcoxon signed rank tests showed significant differences between tumor positions -20 and $+20$ mm ($p = 0.0021$), -10 and $+20$ mm ($p = 4.8 \times 10^{-6}$), 0 and $+20$ mm ($p = 2.1 \times 10^{-4}$), and $+10$ and $+20$ mm ($p = 0.010$). These results indicate that the median of time for $+20$ mm is significantly larger than for other positions. There were no significant interactions ($F(4, 99) = 1.3, p = 0.27$).

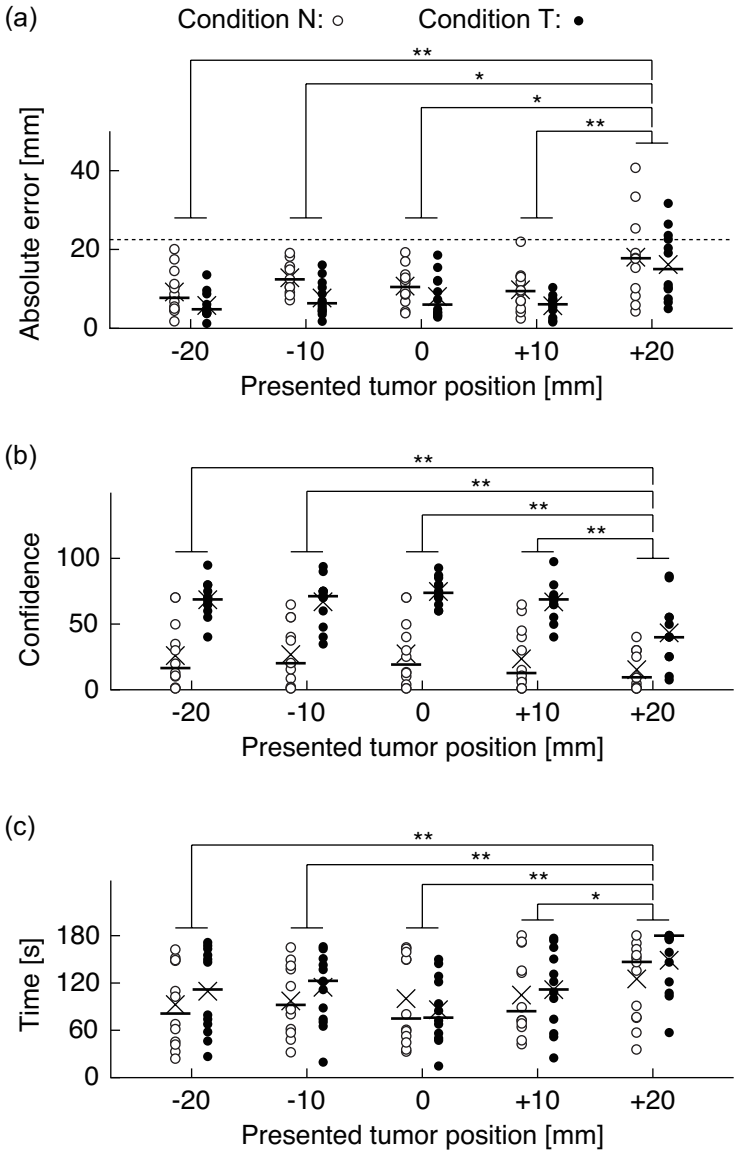

Fig. 5.10: Localization performances for the condition and presented tumor position. Open and filled circles indicate the data for the no feedback (N) and the tactile feedback (T) conditions, respectively. The results for 12 participants are shown. Cross marks and horizontal lines show the means and medians of the data, respectively. * indicates $p < 0.05$ and ** $p < 0.01$ with post-hoc t-tests or Wilcoxon signed rank tests with Bonferroni correction. (a) Absolute error. The dashed line shows the expected value of random localization. (b) Confidence of participant's answer. (c) Response time.

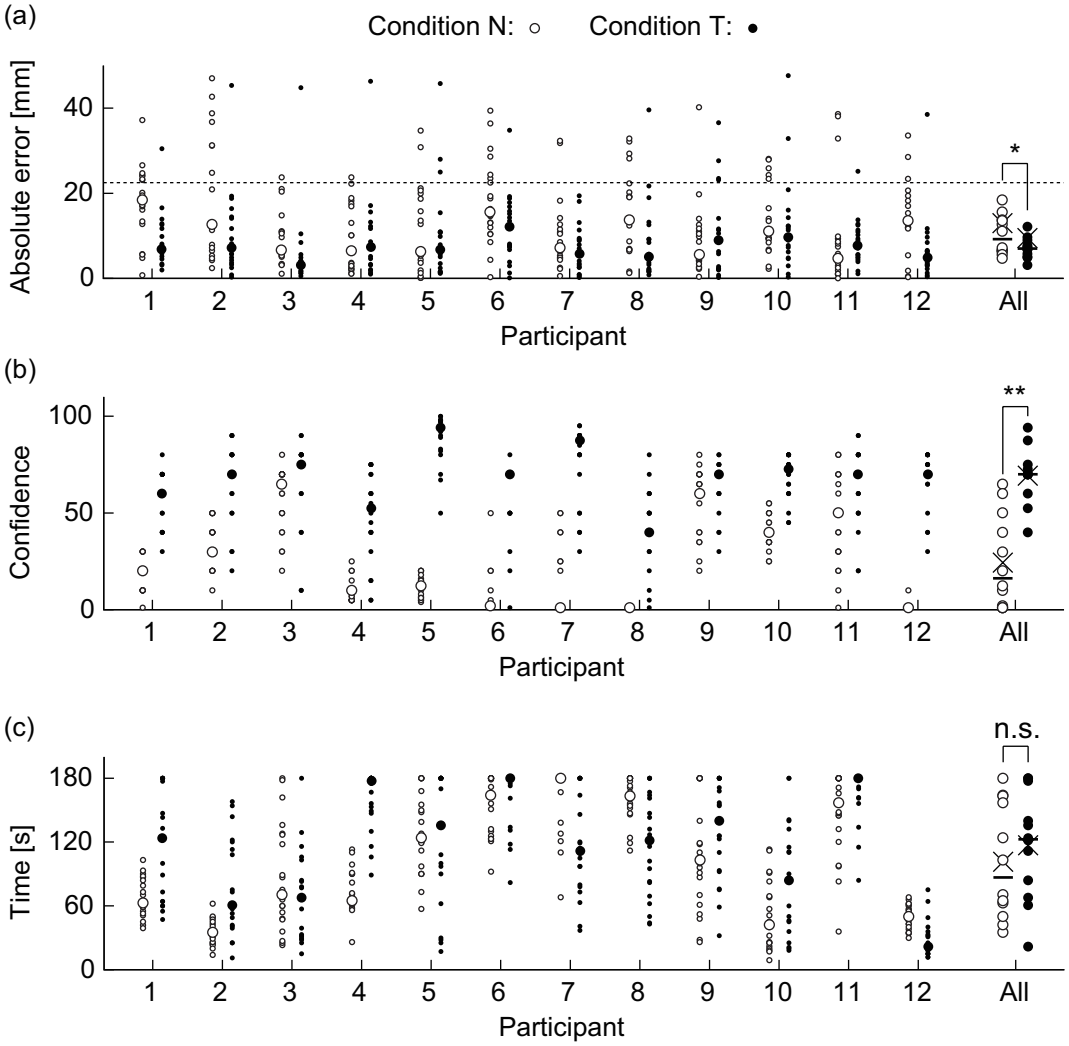

Fig. 5.11: Localization performances of individual participants. Open and filled circles indicate the data for the no feedback (N) and the tactile feedback (T) conditions, respectively. Small circles show the raw data for 20 localization trials. Large circles show the median of the raw data. On the right, the median of the data for each participant is summarized. Cross marks and horizontal lines show means and medians of the summarized data, respectively. * indicates $p < 0.05$ and ** $p < 0.01$ with ANOVAs on condition. (a) Absolute error. The dashed line shows the expected value for random localization. (b) Confidence of participant's answer. (c) Response time.

5.6 Clinical tests on patients

To evaluate the clinical applicability and the effectiveness of the tactile ring in laparoscopic surgery, clinical tests on patients with early-stage gastric tumors were conducted.

The localization tests were conducted immediately before the resection of the tumor. If the tumor had small size and shallow invasion depth, and it was difficult to localize it through palpation, surgical clips were used to indicate the tumor position from the mucosal surface via peroral endoscopy. Before the tests, the tactile sensor and the tactile ring were sterilized using ethylene oxide gas. A surgeon wore the tactile ring on his/her preferred finger and manipulated the sensor to scan the surface of the stomach wall. The sensor was inserted through a 12-mm trocar. An experimental assistant communicated with the surgeon verbally and adjusted the gain and offset of the signal processing according to the surgeon's preference. When the surgeon found the position of the tumor or clips, the position was marked by a clip from the serosal surface, and then, the correctness of the marked position was investigated postoperatively or intraoperatively using an ultrasound probe.

Ten tests were conducted in total. Five cases of the ten were the detection of the tumor itself, and the remaining five cases were the detection of the clips. The intraoperative localization of the tumor or the clip could be achieved according to the feedback through the tactile ring. In two cases of the tumor localizations, the tumors could be found through the laparoscopic image because they had a deeper invasion depth than the preoperative estimations. Although they could be localized visually, the surgeon could also feel a pressure change owing to the presence of the tumor when the surgeon scanned the tumor itself with the sensor. In another case, a nasotracheal tube was detected instead of the tumor.

5.7 Discussion

We will firstly discuss the performance of the tactile ring for presentation of pressure. The Weber ratio of pressure was 0.40 at the reference pressure of 22.7 kPa. This value is comparable to the value obtained for the similar tactile device that presents a force to the user's finger pad [171]. However, Fig. 5.9(b) shows that the Weber ratio

is not constant for the reference pressures; thus, Weber's law does not hold for the pressure presented by the tactile ring. Similar behavior of the Weber ratio has also been reported in intensity discrimination of sound [179]. This is referred to as a near miss to Weber's law. The modification of Weber's law is described as follows [180]:

$$\Delta I = k(I + I_0) \tag{5.5}$$

where ΔI is the JND of a stimulus, I is the reference stimulus, k is the Weber ratio, and I_0 is a constant value. This equation indicates that if the reference stimulus is larger than I_0, the JND is almost proportional to the reference. Alternatively, if the reference has a value close to I_0, the JND is also affected by I_0. The existence of I_0 might be due to noise during the perceptual process [180]. In this study, the diaphragm pump is a possible source of a perceptual noise. The pump supplies pressure with subtle pulsation due to its driving mechanism. When the pressure intensity is relatively small, the subtle pulsative pressure might degrade the perception of the change in pressure. If the pulsative pressure could be reduced, the Weber ratio might not increase even for smaller reference stimuli.

The tactile ring always presented an offset pressure of 15.8 kPa as described in Section 5.4.2. The offset was added to allow for the presentation of the negative feedback direction. The offset should not be large because a large pressure results in a smaller dynamic response of the pneumatic drive unit as shown in Fig. 5.3(d) and might also result in lowered sensitivity to pressure change due to adaptation [181, 182]. The empirically determined offset might actually lie within an appropriate range considering the factors mentioned above. Moreover, it can be seen that the Weber ratio was 0.55 for 15.8 kPa in Fig. 5.9(b). The typical feedback obtained by the user while scanning the phantom tumor is shown in Fig. 5.4(b). The ratio between the peak-to-peak value that marks the tumor (about 16.7 kPa from Fig. 5.4(b)) and the offset pressure (15.8 kPa) was 1.06. Thus, the pressure change due to the tumor was sufficiently perceivable, and it indicates that the gain applied to the sensor output was appropriate.

Next, we will discuss how the tactile ring contributes to tumor localization. The localization error was significantly reduced by providing tactile feedback. Although the tactile feedback gave only simple information to the user, it was effective in intraoperative tumor localization in laparoscopic surgery. Fig. 5.11(a) shows that the median of

the error for each participant lies below the estimated maximal value of 22.5 mm; thus, the participants performed better than random localizations even under condition N. This implies that the participants could utilize other information such as direct haptic information or visual information from the camera monitor. These results are similar to those obtained in Chapter 3, where participants achieved better detection performance (discrimination between phantoms with/without the tumor) than chance level under the no feedback condition. This might imply that direct haptic information and visual information are somewhat informative in detection, but they cannot largely contribute to the localization. Tactile feedback, however, contributed to the localization. This might be because of the high wearability of the tactile ring and the spatial coincidence between the manipulating hand and the feedback site. The high wearability and the spatial coincidence might have effectively facilitated the sensory-motor integration and the interpretation of the tactile feedback for tumor localization. Tactile feedback is also effective in the enhancement of the participants' confidence. Although the localization errors for some participants were not reduced by providing tactile feedback, the confidence was enhanced for all participants. The participants could receive direct haptic information and visual information in condition N; however, they could not fully rely on this information to make decisions. Tactile feedback also contributed to the reliability of the participants' decisions. Tactile feedback had no significant effect on response time. This might be because of the different localization strategies used by the various participants. For instance, under condition N, some participants fully used the maximum time because they could not receive any reliable information. On the other hand, some participants stopped the manipulation early when they could not find the tumor.

In this study, we focused on temporal information-based palpation, in which only a single sensor output was measured and instantaneously fed back to the user. The main characteristic of temporal information-based palpation is that the user should dynamically scan the target surface. Fig. 5.10(a) shows that the localization error for the tumor at +20 mm was significantly greater than that for other positions. In addition, the confidence (the response time) for the tumor at +20 mm was significantly smaller (longer) than those for the other tumor positions. This indicates that the participants achieved worse localization performance for the tumor located at the farthest position.

This might be due to the loss of depth information in the camera image; that is, the resolution of position information on the monitor is more reduced for the farther position as shown in Fig. 5.5(c). The appropriate manipulation of the sensor might be difficult for the participants at the farther position. On the other hand, the surgeon can move the target tissue so that they could appropriately scan the target surface; thus, the worsened localization error due to scanning the farther position might be reduced in surgical situations. In future work, we will investigate how well laparoscopic surgeons conduct the tumor localization using our temporal information-based palpation system in an in-vivo situation.

Finally, we will discuss advantages and issues in clinical applications. The results of the clinical tests validated the clinical applicability of the tactile ring and revealed that the feedback through the ring is also effective in the localization of the tumor or the clip as a marker. This exhibits a valuable example of effective clinical devices validated with clinical tests on actual patients. Moreover, the results showed the effectiveness for the localization of the various targets from a clip (difficult to find via direct haptic information) to a tumor with a deeper invasion depth (visually detectable). For the visible tumor, the surgeons can receive subtle direct haptic information via the rigid sensor probe even without the feedback; however, the tactile feedback might contribute to augment their haptic perception, and it help the surgeons make decision with their higher confidence. Although the localization tests were mostly successful, a nasotracheal tube, which was inserted into the stomach, was detected instead of the tumor in one case. This result indicates that it is difficult to distinguish the quantitative difference (i.e., dimensions and shape) of a hard mass in the soft tissue on the basis of the tactile feedback. It is another limitation of temporal information-based palpation, in which only single sensing information is acquired and fed back to the surgeon. A human being can distinguish the quantitative differences of embedded hard masses owing to spatially distributed information within the finger pad [11]. A solution is, therefore, to use the spatially distributed sensing information; however, this will degrade the simplicity of the entire palpation system. Another possible solution is utilizing a DNN technology to assist the surgeon with the quantitative assessment of the target hard mass. Chapter 4 detailed the detection assistance algorithm based on DNN, and it was shown that the algorithm can detect the feature of the sensor output related to the

tumor. We will try to expand the algorithm for the quantitative evaluation of the sensor output as well as the binary decision. In addition, the surgeon who participated in the tests commented that the subtle pulsative pressure always presented by the tactile ring causes some confusion with the pressure difference due to the tumor. This issue will be addressed in future studies. Another issue that still needs attention is that the signal processing implemented to control the tactile ring was determined empirically. Currently, there is no systematic method to optimize the parameters such as the values of the gain and offset. In future work, we will investigate how these parameters affect performance in tumor localization.

5.8 Summary

In this chapter, we developed and evaluated a pneumatic tactile ring, which is a clinically applicable tactile device to provide instantaneous sensory feedback in laparoscopic tumor localization. We designed a ring-type device to achieve high wearability. The pneumatic tactile ring has high applicability to surgical situations because it is lightweight, cost-effective, sterilizable, and disposable. We also developed a pneumatic drive unit that consists of a diaphragm pump and a voice coil motor to supply the pressure to the tactile ring. The fundamental analysis of the tactile ring revealed that the inner pressure could be controlled linearly based on the input current to the voice coil motor, and it has the bandwidth of at least 1.3 Hz. Moreover, a psychophysical experiment was also conducted to assess the pressure that could be distinguished by the user and how the sensory feedback through the tactile ring contributes to tumor localization performance. It was found that the Weber ratio of the pressure is at least 0.40. Moreover, the tactile feedback significantly reduced the localization error and improved participants' confidence in their estimation of the tumor position. Thus, the tactile ring is effective for intraoperative tumor localization in laparoscopic surgery. In addition, clinical tests on patients with early-stage gastric tumor exhibited its applicability to surgical situations and its effectiveness on the localization of actual tumor.

Chapter 6

Conclusion

This study aimed at achieving the intraoperative localization of early-stage gastric tumors, which cannot be detected visually in laparoscopic surgery. The ultimate goal was the harmonization between a surgeon and the system, that is, to maximize both the performance of the surgeon and the system by utilizing their characteristics in information processing. Moreover, it also aimed to enhance the surgeon's confidence over and above the enhancement of functional performances such as the reduction in localization errors.

The focus in this thesis was on temporal information-based palpation, in which a single output is acquired by a tactile sensor that is directly manipulated by the surgeon and then presented to the surgeon. The main advantage of this type of palpation is the simplicity of the entire system owing to the use of only a single output. Moreover, the direct manipulation of the sensor by the surgeon is also advantageous because stable and pliable control of the sensor is assured by the surgeon even during a laparoscopic surgery, which is quite a complex sensing environment. Moreover, the presentation of the acquired information to the surgeon was aimed at assisting with effective decision-making on the part of the surgeon. In this thesis, the display technologies of the sensor output were designed and evaluated for intraoperative tumor localization according to this focus.

Firstly, visual and tactile feedback of the sensor output were characterized. As the visual feedback, a line graph of the time series of the sensor output on a monitor was prepared. To provide tactile feedback, a device to present a force against the surgeon's foot was assembled. Then, a psychophysical experiment was performed to investigate the effect of each type of feedback on participants' performance of phantom tumor detection and their behavior during detection. The results of the experiment revealed that providing visual feedback significantly enhanced detection performance and par-

ticipants' confidence in their detection in comparison with no feedback. However, the tactile feedback did not significantly enhance the detection performance. Regarding the behavior during detection, the visual and tactile feedback had positive effects with significantly smaller load and lower scanning speed, respectively. These findings show that visual feedback is useful for laparoscopic palpation and that tactile feedback must be improved for effective palpation.

An assistance system using a deep neural network as the replacement for the surgeon's visual-based decision was then proposed. Although the previous psychophysical experiment revealed that the visual feedback of the time series of the sensor output is significantly effective in detection, there is the possibility of visual sensory overload since the surgeons should primarily concentrate on the laparoscopic image. The proposed algorithm was designed so that it analyzes the time-series sensor output and provides a detection result independent of the surgeon. This method is advantageous because the reliability and safety of the manipulation are ensured by a human operator, but a more effective detection might be expected from the collaboration between a human operator and the algorithm. The feasibility of the algorithm was validated using the data obtained in the previous experiment. The proposed algorithm allows the removal of the visual feedback that can cause the sensory overload while utilizing the effectiveness of the time-series sensor output in detection.

Finally, a pneumatic tactile ring, which is a clinically applicable device to present pressure according to the sensor output, was developed. The previous psychophysical experiment suggested the need for the improvement of the tactile display, which has been designed to present a pressure against the foot. It was assumed that the main issue of the previous tactile display was the inferior spatial coincidence between the manipulating hand of the sensor and the presenting site. Thus, the tactile ring was designed to wear on one of the fingers on the manipulating hand. It is lightweight, cost-effective, disposable, and sterilizable owing to the pneumatic actuation principle. The fundamental performance of the tactile ring was investigated, and it was validated that the tactile ring performs sufficiently for palpation. A psychophysical experiment was also conducted to reveal how the tactile ring contributes to the localization of a phantom tumor. The experimental results showed that the feedback through the tactile ring significantly reduced the localization error and enhanced the participants'

confidence in their answers. Thus, it was shown that the tactile ring is an effective device to provide feedback from the sensor for laparoscopic tumor localization. Moreover, clinical tests on patients with an early-stage gastric tumor were conducted to validate the applicability to surgical environments as well as the effectiveness of the tactile ring. The position of the tumor was found successfully through the detection of the tumor itself or the clips placed preoperatively using peroral endoscopy. It was also shown that the tactile ring has surgical applicability and that the feedback through it is effective in actual tumor localization.

In summary, this thesis characterized the visual and tactile feedback of the time-series sensor output. On the basis of investigated and discussed characteristics of each feedback method, a novel assistance algorithm was proposed as a replacement for the visual feedback to surgeons, and the pneumatic tactile ring was developed to improve the previous tactile display. Consequently, the current palpation system mainly consists of our developed tactile sensor and the pneumatic tactile ring. The surgeon scans the target surface with the sensor, receives the feedback from the tactile ring, and localizes the tumor according to the feedback. The feedback might also contribute to improving the sensor manipulation by the surgeon. At the same time, the assistance algorithm can provide an independent detection result based on the sensor output. Thus, the surgeon can take the result from the assistant into account for more effective tumor localization. This thesis details the first step towards the ultimate goal of the harmonization between the surgeon and the system.

There are several issues that should be addressed in future. Firstly, the signal processing applied to the sensor output for driving the tactile ring is determined experimentally. Thus, the effect of the signal processing on localization and confidence in the surgeons' confidence should be investigated. On the basis of the result, the systematic method to determine each parameter of the signal processing such as the gain and offset should be established while considering a human perceptual mechanism. Moreover, how the assistance algorithm can actually assist the surgeon's decision has still not been investigated; thus, the effect of the assistance algorithm on not only tumor localization performance by the surgeon but also on their confidence will be investigated in future. Finally, we will expand the applications of the palpation system to different target tissue and surgical procedures.

References

[1] P. C. Grammaticos and A. Diamantis: "Useful known and unknown views of the father of modern medicine, Hippocrates and his teacher Democritus", *Hellenic Journal of Nuclear Medicine*, Vol. 11, No. 1, pp.2–4, 2008.

[2] A. Castiglioni: "The golden age of Greek medicine: Hippocratic medicine–biologic and synthetic concept", In: *A History of Medicine*, E. B. Krumbhaar ed., New York: Alfred A. Knopf, pp. 148–178, 1941.

[3] E. S. Vasiliadis, T. B. Grivas, and A. Kaspiris: "Historical overview of spinal deformities in ancient Greece", *Scoliosis and Spinal Disorders*, Vol. 4, No. 6, 2009.

[4] Y. M. Bhat, B. K. A. Dayyeh, S. S. Chauhan, K. T. Gottlieb, J. H. Hwang, S. Komanduri, V. Konda, S. K. Lo, M. A. Manfredi, J. T. Maple, F. M. Murad, U. D. Siddiqui, S. Banerjee, and M. B. Wallace: "High-definition and high-magnification endoscopes", *Gastrointestinal Endoscopy*, Vol. 80, Issue 6, pp. 919–927, 2014.

[5] K. Schwab, R. Smith, V. Brown, M. Whyte, and I. Jourdan: "Evolution of stereoscopic imaging in surgery and recent advances", *World Journal of Gastrointestinal Endoscopy*, Vol. 9, Issue 8, pp. 368–377, 2017.

[6] G. S. Guthart and J. K. Salisbury: "The Intuitive^{TM} telesurgery system: Overview and application", In: *Proceedings of the 2000 IEEE International Conference on Robotics and Automation*, pp. 618–621, 2000.

[7] G.-Z. Yang, J. Cambias, K. Cleary, E. Daimler, J. Drake, P. E. Dupont, N. Hata, P. Kazanzides, S. Martel, R. V. Patel, V. J. Santos, and R. H. Taylor: "Medical robotics–Regulatory, ethical, and legal considerations for increasing levels of autonomy", *Science Robotics*, Vol. 2, Issue 4, Article no. eaam8638, 2017.

[8] S. A. Bowyer, B. L. Davies, and F. R. y Baena: "Active constraints/virtual fixtures: A survey", *IEEE Transactions on Robotics*, Vol. 30, Issue 1, pp. 138–157, 2014.

[9] S. A. Pedram, P. Ferguson, J. Ma, E. Dutson, and J. Rosen: "Autonomous suturing via surgical robot: An algorithm for optimal selection of needle diameter, shape, and path", In: *Proceedings of the 2017 IEEE International Conference on Robotics and Automation*, pp. 2391–2398, 2017.

[10] K. O. Johnson: "The roles and functions of cutaneous mechanoreceptors", *Current Opinion in Neurobiology*, Vol. 11, Issue 4, pp. 455–461, 2001.

[11] J. C. Gwilliam, T. Yoshioka, A. M. Okamura, and S. S. Hsiao: "Neural coding of passive lump detection in compliant artificial tissue", *Journal of Neurophysiology*, Vol. 112, Issue 5, pp. 1131–1141, 2014.

[12] J. Konstantinova, M. Li, G. Mehra, P. Dasgupta, K. Althoefer, and T. Nanayakkara: "Behavioral characteristics of manual palpation to localize hard nodules in soft tissues", *IEEE Transactions on Biomedical Engineering*, Vol. 61, Issue 6, pp. 1651–1659, 2014.

[13] A. Garg, S. Sen, R. Kapadia, Y. Jen, S. McKinley, L. Miller, and K. Goldberg: "Tumor localization using automated palpation with Gaussian process adaptive sampling", In: *Proceedings of the 2016 IEEE International Conference on Automation Science and Engineering*, pp. 194–200, 2016.

[14] J. Konstantinova, G. Cotugno, P. Dasgupta, K. Althoefer, and T. Nanayakkara: "Palpation force modulation strategies to identify hard regions in soft tissue organs", *PLoS ONE*, Vol. 12, No. 2, Article no. e0171706, 2017.

[15] Y. Tanaka, T. Fukuda, M. Fujiwara, and A. Sano: "Tactile sensor using acoustic reflection for lump detection in laparoscopic surgery", *International Journal of Computer Assisted Radiology and Surgery*, Vol. 10, Issue 2, pp. 183–193, 2015.

[16] Japanese Gastric Cancer Association: "Japanese classification of gastric carcinoma: 3rd English edition", *Gastric Cancer*, Vol. 14, Issue 2, pp. 101–112, 2011.

[17] M. S. Cappell J. T. Courtney, and M. Amin: "Black macular patches on parietal peritoneum and other extraintestinal sites from intraperitoneal spillage and spread of India ink from preoperative endoscopic tattooing: An endoscopic, surgical, gross pathologic, and microscopic study", *Digestive Diseases and Sciences*, Vol. 55, Issue 9, pp. 2599–2605, 2010.

[18] W. J. Hyung, J. S. Lim, J. H. Cheong, J. Kim, S. H. Choi, S. Y. Song, and S. H. Noh: "Intraoperative tumor localization using laparoscopic ultrasonography in laparoscopic-assisted gastrectomy", *Surgical Endoscopy*, Vol. 19, Issue 10, pp. 1353–1357, 2005.

[19] H.-I. Kim, W. J. Hyung, C. R. Lee, J. S. Lim, J. Y. An, J.-H. Cheong, S. H. Choi, and S. H. Noh: "Intraoperative portable abdominal radiograph for tumor localization: A simple and accurate method for laparoscopic gastrectomy", *Surgical Endoscopy*, Vol. 25, Issue 3, pp. 958–963, 2011.

[20] H. Hur, S.-Y. Son, Y. K. Cho, and S.-U. Han: "Intraoperative gastroscopy for tumor localization in laparoscopic surgery for gastric adenocarcinoma", *Journal of Visualized Experiments*, Issue 114, Article no. e53170, 2016.

[21] A. M. Okamura, C. Basdogan, S. Baillie, and W. S. Harwin: "Haptics in medicine and clinical skill acquisition", *IEEE Transactions on Haptics*, Vol. 4, Issue 3, pp. 153–154, 2011.

[22] E. Samur, M. Sedef, C. Basdogan, L. Avtan, and O. Duzgun: "A robotic indenter for minimally invasive measurement and characterization of soft tissue response", *Medical Image Analysis*, Vol. 11, Issue 4, pp. 361–373, 2007.

[23] H. Liu, D. P. Noonan, B. J. Challacombe, P. Dasgupta, L. D. Seneviratne, and K. Althoefer: "Rolling mechanical imaging for tissue abnormality localization during minimally invasive surgery", *IEEE Transactions on Biomedical Engineering*, Vol. 57, Issue 2, pp. 404–414, 2010.

[24] J.-H. Hwang, J. H. Kwon, T.-K. Kim, and D. Hong: "Design of simple structured tactile sensor for the minimally invasive robotic palpation", In: *Proceedings of*

the 2013 IEEE/ASME International Conference on Advanced Intelligent Mechatronics, pp. 1296–1299, 2013.

[25] T. Yoneyama, T. Watanabe, H. Kagawa, J. Hamada, Y. Hayashi, and M. Nakada: "Force-detecting gripper and force feedback system for neurosurgery applications", *International Journal of Computer Assisted Radiology and Surgery*, Vol. 8, Issue 5, pp. 819–829, 2013.

[26] A. L. Trejos, A. Escoto, D. Hughes, M. D. Naish, and R. V. Patel: "A sterilizable force-sensing instrument for laparoscopic surgery", In: *Proceedings of the 5th IEEE RAS/EMBS International Conference on Biomedical Robotics and Biomechatronics*, pp. 157–162, 2014.

[27] J. B. Gafford, S. B. Kesner, A. Degirmenci, R. J. Wood, R. D. Howe, and C. J. Walsh: "A monolithic approach to fabricating low-cost, millimeter-scale multi-axis force sensors for minimally-invasive surgery", In: *Proceeding of the 2014 IEEE International Conference on Robotics and Automation*, pp. 1419–1425, 2014.

[28] M. M. Dalvand, B. Shirinzadeh, A. H. Shamdani, J. Smith, and Y. Zhong: "An actuated force feedback-enabled laparoscopic instrument for robotic-assisted surgery", *The International Journal of Medical Robotics and Computer Assisted Surgery*, Vol. 10, Issue 1, pp. 11–21, 2014.

[29] J. Dargahi, S. Payandeh, and M. Parameswaran: "A micromachined piezoelectric teeth-like laparoscopic tactile sensor: Theory, fabrication and experiments", In: *Proceeding of the 1999 IEEE International Conference on Robotics and Automation*, pp. 299–304, 1999.

[30] R. Sedaghati, J. Dargahi, and H. Singh: "Design and modeling of an endoscopic piezoelectric tactile sensor", *International Journal of Solids and Structures*, Vol. 42, Issues 21–22, pp. 5872–5886, 2005.

[31] S. Sokhanvar, M. Packirisamy, and J. Dargahi: "A multifunctional PVDF-based tactile sensor for minimally invasive surgery", *Smart Materials and Structures*, Vol. 16, No. 4, pp. 989–998, 2007.

[32] A. M. Hamed, Z. T. H. Tse, I. Young, B. L. Davies, and M. Lampérth: "Applying tactile sensing with piezoelectric materials for minimally invasive surgery and magnetic-resonance-guided interventions", In: *Proceedings of the Institution of Mechanical Engineers, Part H: Journal of Engineering in Medicine*, Vol. 223, Issue 1, pp. 99–110, 2009.

[33] H. Leng and Y. Lin: "Development of a novel deformation-based tissue softness sensor", *IEEE Sensors Journal*, Vol. 9, Issue 5, pp. 548–554, 2009.

[34] U. Kim, D.-H. Lee, W. J. Yoon, B. Hannaford, and H. R. Choi: "Force sensor integrated surgical forceps for minimally invasive robotic surgery", *IEEE Transactions on Robotics*, Vol. 31, Issue 5, pp. 1214–1224, 2015.

[35] S. McKinley, A. Garg, S. Sen, R. Kapadia, A. Murali, K. Nichols, S. Lim, S. Patil, P. Abbeel, A. M. Okamura, and K. Goldberg: "A single-use haptic palpation probe for locating subcutaneous blood vessels in robot-assisted minimally invasive surgery", In: *Proceeding of the 2015 IEEE International Conference on Automation Science and Engineering*, pp. 1151–1158, 2015.

[36] B. Darvish, S. Najarian, E. Shirzad, and R. Khodambashi: "A novel tactile force probe for tissue stiffness classification", *American Journal of Applied Sciences*, Vol. 6, Issue 3, pp. 512–517, 2009.

[37] P. Peng, A. S. Sezen, R. Rajamani, and A. G. Erdman: "Novel MEMS stiffness sensor for in-vivo tissue characterization measurement", In: *Proceeding of the 2009 Annual International Conference of the IEEE Engineering in Medicine and Biology Society*, pp. 6640–6643, 2009.

[38] S. Sokhanvar, M. Packirisamy, and J. Dargahi: "MEMS endoscopic tactile sensor: Toward in-situ and in-vivo tissue softness characterization", *IEEE Sensors Journal*, Vol. 9, Issue 12, pp. 1679–1687, 2009.

[39] K. Kuwana, A. Nakai, K. Masamune, and T. Dohi: "A grasping forceps with a triaxial MEMS tactile sensor for quantification of stresses on organs", In: *Proceeding of the 2013 Annual International Conference of the IEEE Engineering in Medicine and Biology Society*, pp. 4490–4493, 2013.

[40] M. T. Perri, A. L. Trejos, M. D. Naish, R. V. Patel, and R. A. Malthaner: "New tactile sensing system for minimally invasive surgical tumour localization", *The International Journal of Medical Robotics and Computer Assisted Surgery*, Vol. 6, Issue 2, pp. 211–220, 2010.

[41] A. Escoto, S. Bhattad, A. Shamsil, A. Sanches, A. L. Trejos, M. D. Naish, R. A. Malthaner, and R. V. Patel: "A multi-sensory mechatronic device for localizing tumors in minimally invasive interventions", In: *Proceeding of the 2015 IEEE International Conference on Robotics and Automation*, pp. 4742–4747, 2015.

[42] C. Wiederer, M. Frohlich, and M. W. Strohmayr: "Improving tactile sensation in laparoscopic surgery by overcoming size restrictions", *Current Directions in Biomedical Engineering*, Vol. 1, Issue 1, pp. 135–139, 2015.

[43] A. S. Naidu, A. Escoto, O. Fahmy, R. V. Patel, and M. D. Naish: "An autoclavable wireless palpation instrument for minimally invasive surgery", In: *Proceeding of the 2016 38th Annual International Conference of the IEEE Engineering in Medicine and Biology Society*, pp. 6489–6492, 2016.

[44] B. Li, Y. Shi, A. Fontecchio, and Y. Visell: "Mechanical imaging of soft tissues with a highly compliant tactile sensing array", *IEEE Transactions on Biomedical Engineering*, Vol. 65, Issue 3, pp. 687–697, 2018.

[45] K. Takashima, K. Yoshinaka, and K. Ikeuchi: "Vision-based tactile sensor for endoscopy", In: *Complex Medical Engineering*, J. L. Wu et al. eds., Tokyo: Springer, pp. 13–23, 2007.

[46] T. Watanabe, T. Iwai, Y. Fujihira, L. Wakako, H. Kagawa, and T. Yoneyama: "Force sensor attachable to thin fiberscopes/endoscopes utilizing high elasticity fabric", *Sensors*, Vol. 14, Issue 4, pp. 5207–5220, 2014.

[47] A. Faragasso, A. Stilli, J. Bimbo, Y. Noh, H. Liu, T. Nanayakkara, P. Dasgupta, H. A. Wurdemann, and K. Althoefer: "Endoscopic add-on stiffness probe for real-time soft surface characterisation in MIS", In: *Proceeding of the 2014*

36th Annual International Conference of the IEEE Engineering in Medicine and Biology Society, pp. 6517–6520, 2014.

[48] A. Faragasso, A. Stilli, J. Bimbo, H. A. Wurdemann, and K. Althoefer: "Multi-axis stiffness sensing device for medical palpation", In: *Proceeding of the 2015 IEEE/RSJ International Conference on Intelligent Robots and Systems*, pp. 2711–2716, 2015.

[49] T. Kawahara and M. Kaneko: "Non-contact stiffness imager for medical application", In: *Proceeding of the 2005 IEEE International Conference on Information Acquisition*, pp. 350–355, 2005.

[50] J. Li, H. Liu, K. Althoefer, and L. D. Seneviratne: "A stiffness probe based on force and vision sensing for soft tissue diagnosis", In: *Proceeding of the 2012 Annual International Conference of the IEEE Engineering in Medicine and Biology Society*, pp. 944–947, 2012.

[51] X. Jia, R. Li, M. A. Srinivasan, and E. H. Adelson: "Lump detection with a GelSight sensor", In: *Proceeding of the 2013 IEEE World Haptics Conference*, pp. 175–179, 2013.

[52] J.-H. Lee, Y. N. Kim, J. Ku, and H.-J. Park: "Optical-based artificial palpation sensors for lesion characterization", *Sensors*, Vol. 13, Issue 8, pp. 11097–11113, 2013.

[53] M. Blank and J. F. Antaki: "Low-cost quantitative palpation device for breast lesion tracking and telehealth", In: *Proceeding of the 2014 IEEE Healthcare Innovation and Point-of-Care Technologies Conference*, pp. 280–283, 2014.

[54] K. M. Kennedy, S. Es'haghian, L. Chin, R. A. McLaughlin, D. D. Sampson, and B. F. Kennedy: "Optical palpation: Optical coherence tomography-based tactile imaging using a compliant sensor", *Optics Letters*, Vol. 30, Issue 10, pp. 3014–3017, 2014.

[55] T. Watanabe, T. Iwai, T. Koyama, and T. Yoneyama: "Stiffness measurement system using endoscopes with a visualization method", *IEEE Sensors Journal*, Vol. 16, Issue 15, pp. 5889–5897, 2016.

[56] M. M. Gubenko, A. V. Morozov, A. N. Lyubicheva, I. G. Goryacheva, M. Z. Dosaev, M.-Sh. Ju, Ch.-H. Yeh, and F.-Ch. Su: "Video-tactile pneumatic sensor for soft tissue elastic modulus estimation", *BioMedical Engineering Online*, Vol. 16, Article no. 94, 2017.

[57] K. Althoefer, D. Zbyszewski, H. Liu, P. Puangmali, L. Seneviratne, B. Challacombe, P. Dasgupta, and D. Murphy: "Air-cushion force sensitive probe for soft tissue investigation during minimally invasive surgery", In: *Proceeding of the 2008 IEEE Sensors*, pp. 827–830, 2008.

[58] M. Ayyildiz, B. Guclu, M. Z. Yildiz, and C. Basdogan: "A novel tactile sensor for detecting lumps in breast tissue", In: *Haptics: Generating and Perceiving Tangible Sensations. EuroHaptics 2010. Lecture Notes in Computer Science*, Vol. 6191, A. M. L. Kappers et al. eds., Berlin, Heidelberg: Springer, pp. 367–372, 2010.

[59] J. Peirs, J. Clijnen, D. Reynaerts, H. V. Brussel, P. Herijgers, B. Corteville, and S. Boone: "A micro optical force sensor for force feedback during minimally invasive robotic surgery", *Sensors and Actuators A: Physical*, Vol. 115, Issues 2–3, pp. 447–455 , 2004.

[60] H. Liu, J. Li, X. Song, L. D. Senevirante, and K. Althoefer: "Rolling indentation probe for tissue abnormality identification during minimally invasive surgery", *IEEE Transactions on Robotics*, Vol. 27, Issue 3, pp. 450–460 , 2011.

[61] I. B. Wanninayake, P. Dasgupta, L. D. Seneviratne, and K. Althoefer: "Air-float palpation probe for tissue abnormality identification during minimally invasive surgery", *IEEE Transactions on Biomedical Engineering*, Vol. 60, Issue 10, pp. 2735–2744 , 2013.

[62] P. Puangmali, H. Liu, L. D. Seneviratne, P. Dasgupta, and K. Althoefer: "Miniature 3-axis distal force sensor for minimally invasive surgical palpation", *IEEE/ASME Transactions on Mechatronics*, Vol. 17, Issue 4, pp. 646–656 , 2012.

[63] H. Xie, H. Liu, L. D. Seneviratne, and K. Althoefer: "An optical tactile array probe head for tissue palpation during minimally invasive surgery", *IEEE Sensors Journal*, Vol. 14, Issue 9, pp. 3283–3291 , 2014.

[64] J. Back, P. Dasgupta, L. Seneviratne, K. Althoefer, and H. Liu: "Feasibility study–novel optical soft tactile array sensing for minimally invasive surgery", In: *Proceeding of the 2015 IEEE/RSJ International Conference on Intelligent Robots and Systems*, pp. 1528–1533 , 2015.

[65] J. Li, S. J. Hammer, W. M. Shu, R. R. J. Maier, D. P. Hand, R. L. Reuben, and W. N. MacPherson: "An optical fibre dynamic instrumented palpation sensor for the characterisation of biological tissue", *Sensors and Actuators A: Physical*, Vol. 225, pp. 53–60, 2015.

[66] T. Sasaki, M. Hebisawa, Y. Mito, K. Dohda, and S. Kuroda: "Force measurement of blood vessel gripping by hydraulic-driven forceps", *Procedia CIRP*, Vol. 65, pp. 84–87 , 2017.

[67] C. Gaudeni, L. Meri, and D. Prattichizzo: "A novel pneumatic force sensor for robot-assisted surgery", In: *Haptics: Science, Technology, and Applications. EuroHaptics 2018. Lecture Notes in Computer Science*, Vol. 10894, D. Prattichizzo et al. eds., Cham: Springer International Publishing AG, pp. 587–599 , 2018.

[68] T. Takaki, Y. Omasa, I. Ishii, T. Kawahara, and M. Okajima: "Force visualization mechanism using a Moiré fringe applied to endoscopic surgical instruments", In: *Proceeding of the 2010 IEEE International Conference on Robotics and Automation*, pp. 3648–3653 , 2010.

[69] T. Watanabe, T. Koyama, T. Yoneyama, and M. Nakada: "Force-sensing silicone retractor for attachment to surgical suction pipes", *Sensors*, Vol. 16, Issue 7, Article no. 1133, 2016.

[70] H. I. Son, T. Bhattacharjee, and D. Y. Lee: "Estimation of environmental force for the haptic interface of robotic surgery", *The International Journal of Medical Robotics and Computer Assisted Surgery*, Vol. 6, Issue 2, pp. 221–230, 2010.

[71] M. C. Lee, C. Y. Kim, B. Yao, W. J. Peine, and Y. E. Song: "Reaction force estimation of surgical robot instrument using perturbation observer with SMCSPO algorithm", In: *Proceeding of the 2010 IEEE/ASME International Conference on Advanced Intelligent Mechatronics*, pp. 181–186, 2010.

[72] B. Zhao and C. A. Nelson: "Sensorless force sensing for minimally invasive surgery", *Journal of Medical Devices*, Vol. 9, No. 4, Article no. 041012, 2015.

[73] S. Schostek, C.-N. Ho, D. Kalanovic, and M. O. Schurr: "Artificial tactile sensing in minimally invasive surgery–a new technical approach", *Minimally Invasive Therapy & Allied Technologies*, Vol. 15, Issue 5, pp. 296–304, 2006.

[74] S. Sokhanvar, M. Ramezanifard, J. Dargahi, and M. Packirisamy: "Graphical rendering of localized lumps for MIS applications", *Journal of Medical Devices*, Vol. 1, Issue 3, pp. 217–224, 2007.

[75] M. D. Naish, M. T. Perri, D. A. Bottoni, A. L. Trejos, R. V. Patel, and R. A. Malthaner: "Palpation system for minimally invasive localization of occult tumors", In: *Proceedings of the 2010 3rd IEEE RAS & EMBS International Conference on Biomedical Robotics and Biomechatronics*, pp. 662–667, 2010.

[76] A. Talasaz and R. V. Patel: "Remote palpation to localize tumors in robot-assisted minimally invasive approach", In: *Proceedings of the 2012 IEEE International Conference on Robotics and Automation*, pp. 3719–3724, 2012.

[77] M. Mahvash, J. Gwilliam, R. Agarwal, B. Vagvolgyi, L.-M. Su, D. D. Yuh, and A. M. Okamura: "Force-feedback surgical teleoperator: Controller design and palpation experiments", In: *Proceedings of the 2008 IEEE Symposium on Haptic Interfaces for Virtual Environments and Teleoperator Systems*, pp. 465–471, 2008.

[78] M. E. Currie, A. Talasaz, R. Rayman, M. W. A. Chu, B. Kiaii, T. Peters, A. L. Trejos, and R. Patel: "The role of visual and direct force feedback in robotics-assisted mitral valve annuloplasty", *The International Journal of Medical Robotics and Computer Assisted Surgery*, Vol. 13, Issue 3, Article no. e1787, 2017.

[79] M. Tavakoli, A. Aziminejad, R. V. Patel, and M. Moallem: "Methods and mechanisms for contact feedback in a robot-assisted minimally invasive environment", *Surgical Endoscopy*, Vol. 20, Issue 10, pp. 1570–1579, 2006.

[80] A. P. Miller, W. J. Peine, J. S. Son, and Z. T. Hammonud: "Tactile imaging system for localizing lung nodules during video assisted thoracoscopic surgery", In: *Proceedings of the 2007 IEEE International Conference on Robotics and Automation*, pp. 2996–3001, 2007.

[81] T. Yamamoto B. Vagvolgyi, K. Balaji, L. L. Whitcomb, and A. M. Okamura: "Tissue property estimation and graphical display for teleoperated robot-assisted surgery", In: *Proceedings of the 2009 IEEE International Conference on Robotics and Automation*, pp. 4239–4245, 2009.

[82] P. Richard and P. Coiffet: "Human perceptual issues in virtual environments: sensory substitution and information redundancy", In: *Proceedings of the 4th IEEE International Workshop on Robot and Human Communication*, pp. 301–306, 1995.

[83] E. U. Braun, H. Mayer, A. Knoll, R. Lange, and R. Bauernschmitt: "The must-have in robotic heart surgery: Haptic feedback", In: *Medical robotics*, V. Bozovic ed., Croatia: I-Tech Education and Publishing, pp. 9–20, 2008.

[84] J. Rosen, B. Hannaford, M. P. MacFarlane, and M. N. Sinanan: "Force controlled and teleoperated endoscopic grasper for minimally invasive surgery–experimental performance evaluation", *IEEE Transactions on Biomedical Engineering*, Vol. 46, Issue 10, pp. 1212–1221, 1999.

[85] G. L. McCreery, A. L. Trejos, M. D. Naish, R. V. Patel, and R. A. Malthaner: "Feasibility of locating tumours in lung via kinaesthetic feedback", *The International Journal of Medical Robotics and Computer Assisted Surgery*, Vol. 4, Issue 1, pp. 58–68, 2008.

[86] E. P. W. Putten, J. J. Dobbelsteen, R. H. M. Goossens, J. J. Jakimowicz, and J. Dankelman: "Force feedback requirements for efficient laparoscopic grasp control", *Ergonomics*, Vol. 52, Issue 9, pp. 1055–1066, 2009.

[87] H. Li, K. Tadano, and K. Kawashima: "Achieving force perception in master-slave manipulators using pneumatic artificial muscles", In: *Proceeding of the SICE Annual Conference 2012*, pp. 1342–1345, 2012.

[88] T. L. Gibo, D. R. Deo, Z. F. Quek, and A. M. Okamura: "Effect of load force feedback on grip force control during teleoperation: A preliminary study", In: *Proceeding of the 2014 IEEE Haptics Symposium*, pp. 379–383, 2014.

[89] F. Bechet, K. Ogawa, E. Sariyildiz, and K. Ohnishi: "Electro-hydraulic transmission system for minimally invasive robotics", *IEEE Transactions on Industrial Electronics*, Vol. 62, Issue 12, pp. 7643–7654, 2015.

[90] E. Beretta, F. Nessi, G. Ferrigno, and E. D. Momi: "Force feedback enhancement for soft tissue interaction tasks in cooperative robotic surgery", In: *Proceeding of the 2015 IEEE/RSJ International Conference on Intelligent Robots and Systems*, pp. 209–215, 2015.

[91] C. Pacchierotti, L. Meli, F. Chinello, M. Malvezzi, and D. Prattichizzo: "Cutaneous haptic feedback to ensure the stability of robotic teleoperation systems", *The International Journal of Robotics Research*, Vol. 34, Issue 14, pp. 1773–1787, 2015.

[92] C. R. Wottawa, J. R. Cohen, R. E. Fan, J. W. Bisley, M. O. Culjat, W. S. Grundfest, and E. P. Dutson: "The role of tactile feedback in grip force during laparoscopic training tasks", *Surgical Endoscopy*, Vol. 27, Issue 4, pp. 1111–1118, 2013.

[93] J. Dargahi, D. Arbatani, S. Sokhanvar, W.-F. Xie, and R. Ramezanifard: "A novel tactile softness display for minimally invasive surgery", *Mechatronics*, Vol. 24, Issue 8, pp. 1144–1156, 2014.

[94] S.-C. Lim, H.-K. Lee, E. Doh, K.-S. Yun, and J. Park: "Tactile display with tangential and normal skin displacement for robot-assisted surgery", *Advanced Robotics*, Vol. 28, Issue 13, pp. 859–868, 2014.

[95] M. V. Ottermo, Ø. Stavdahl, and T. A. Johansen: "A remote palpation instrument for laparoscopic surgery: Design and performance", *Minimally Invasive Therapy & Allied Technologies*, Vol. 18, Issue 5, pp. 259–272, 2009.

[96] C.-H. King, M. O. Culjat, M. L. Franco, J. W. Bisley, G. P. Carman, E. P. Dutson, and W. S. Grundfest: "A multielement tactile feedback system for robot-assisted minimally invasive surgery", *IEEE Transactions on Haptics*, Vol. 2, Issue 1, pp. 52–56, 2009.

[97] C. Roke, C. Melhuish, T. Pipe, D. Drury, and C. Chorley: "Deformation-based tactile feedback using a biologically-inspired sensor and a modified display", In: *Towards Autonomous Robotic Systems. TAROS 2011. Lecture Notes in Computer Science*, Vol. 6856, R. Groß et al. eds., Berlin, Heidelberg: Springer, pp. 114–124, 2011.

[98] P. Goethals, D. Reynaerts, and H. V. Brussel: "Pneumatic tactile display controlled by a miniaturised proportional valve", In: *Proceeding of the 9th National Congress on Theoretical and Applied Mechanics*, pp. 1–4, 2012.

[99] J.-S. Oh, J.-K. Kim, and S.-B. Choi: "Experimental test of MR fluid based tactile device for minimally invasive surgery", In: *Proceedings SPIE 8688, Active and Passive Smart Structures and Integrated Systems 2013*, Article no. 86882C, 2013.

[100] N. Gurari, K. Smith, M. Madhav, and A. M. Okamura: "Environment discrimination with vibration feedback to the foot, arm, and fingertip", In: *Proceeding of the 2009 IEEE International Conference on Rehabilitation Robotics*, pp. 343–348, 2009.

[101] M. Zhou and C. G. L. Cao: "Vibrotactile feedback improves laparoscopic palpation skills", In: *Proceeding of the Human Factors and Ergonomics Society Annual Meeting*, Vol. 53, Issue 11, pp. 738–742, 2009.

[102] W. McMahan, J. Gewirtz, D. Standish, P. Martin, J. A. Kunkel, M. Lilavois, A. Wedmid, D. I. Lee, and K. J. Kuchenbecker: "Tool contact acceleration feedback for telerobotic surgery", *IEEE Transactions on Haptics*, Vol. 4, Issue 3, pp. 210–220, 2011.

[103] K. Bark, W. McMahan, A. Remington, J. Gewirtz, A. Wedmid, D. I. Lee, and K. J. Kuchenbecker: "In vivo validation of a system for haptic feedback of tool vibrations in robotic surgery", *Surgical Endoscopy*, Vol. 27, Issue 2, pp. 656–664, 2013.

[104] C. Pacchierotti, A. Tirmizi, G. Bianchini, and D. Prattichizzo: "Improving transparency in passive teleoperation by combining cutaneous and kinesthetic force feedback", In: *Proceeding of the 2013 IEEE/RSJ International Conference on Intelligent Robots and Systems*, pp. 4958–4963, 2013.

[105] N. Cutler, M. Balicki, M. Finkelstein, J. Wang, P. Gehlbach, J. McGready, I. Iordachita, R. Taylor, and J. T. Hanada: "Auditory force feedback substitution improves surgical precision during simulated ophthalmic surgery", *Investigative Ophthalmology & Visual Science*, Vol. 54, Issue 2, pp. 1316–1324, 2013.

[106] K. Haraguchi, S. Miyachi, N. Matsubara, Y. Nagano, H. Yamada, N. Marui, A. Sano, H. Fujimoto, T. Izumi, T. Yamanouchi, T. Asai, and T. Wakabayashi: "A mechanical coil insertion system for endovascular coil embolization of intracranial aneurysms", *Interventional Neuroradiology*, Vol. 19, Issue 2, pp. 159–166, 2013.

[107] J. K. Koehn and K. J. Kuchenbecker: "Surgeons and non-surgeons prefer haptic feedback of instrument vibrations during robotic surgery", *Surgical Endoscopy*, Vol. 29, Issue 10, pp. 2970–2983, 2015.

[108] M. Akamatsu, I. S. Mackenzie, and T. Hasbroucq: "A comparison of tactile, auditory, and visual feedback in a pointing task using a mouse-type device", *Ergonomics*, Vol. 38, Issue 4, pp. 816–827, 1995.

[109] Y. Wan, J. C. Prinet, and N. Sarter: "Visual and auditory feedback to improve touchscreen usability in turbulence", In: *Proceedings of the Human Factors and Ergonomics Society Annual Meeting*, Vol. 61, Issue 1, pp. 89–93, 2017.

[110] Y. Monai, K. Hasegawa, M. Fujiwara, K. Yoshino, S. Inoue, and H. Shinoda: "HaptoMime: Mid-air haptic interaction with a floating virtual screen", In: *Pro-*

ceedings of the 27th Annual ACM Symposium on User Interface Software and Technology, pp. 663–668, 2014.

[111] M. S. Prewett, L. R. Elliott, A. G. Walvoord, and M. D. Coovert: "A meta-analysis of vibrotactile and visual information displays for improving task performance", *IEEE Transactions on Systems, Man, and Cybernetics–Part C (Applications and Reviews)*, Vol. 42, Issue 1, pp. 123–132, 2012.

[112] J. M. Walker, A. A. Blank, P. A. Shewokis, and M. K. O'Malley: "Tactile feedback of object slip improves performance in a grasp and hold task", In: *Proceedings of the 2014 IEEE Haptics Symposium*, pp. 461–466, 2014.

[113] E. Tzorakoleftherakis, F. A. Mussa-Ivaldi, R. A. Scheidt, and T. D. Murphey: "Effects of optimal tactile feedback in balancing tasks: A pilot study", In: *Proceedings of the 2014 American Control Conference*, pp. 778–783, 2014.

[114] M. M. Ankarali, H. T. Şen, A. De, A. M. Okamura, and N. J. Cowan: "Haptic feedback enhances rhythmic motor control by reducing variability, not improving convergence rate", *Journal of Neurophysiology*, Vol. 111, Issue 6, pp. 1286–1299, 2014.

[115] M. Furukawa, H. Yoshikawa, T. Hachisu, S. Fukushima, and H. Kajimoto: ""Vection field" for pedestrian traffic control", In: *Proceedings of the 2nd Augmented Human International Conference*, Article no. 19, 2011.

[116] A. Ishii, I. Suzuki, S. Sakamoto, K. Kanai, K. Takazawa, H. Doi, and Y. Ochiai: "Graphical manipulation of human's walking direction with visual illusion", In: *Proceedings of the ACM SIGGRAPH 2016 Posters*, Article no. 9, 2016.

[117] M. Pielot, B. Poppinga, W. Heuten, and S. Boll: "A tactile compass for eyes-free pedestrian navigation", In: *Human-Computer Interaction–INTERACT 2011. Lecture Notes in Computer Science*, Vol. 6947, P. Campos et al. eds., Berlin, Heidelberg: Springer, pp. 640–656, 2011.

[118] T. S. Filgueiras, A. C. O. Lima, R. L. Baima, G. T. R. Oka, L. A. Q. Cordovil, and M. P. Bastos: "Vibrotactile sensory substitution on personal navigation:

Remotely controlled vibrotactile feedback wearable system to aid visually impaired", In: *Proceedings of the 2016 IEEE International Symposium on Medical Measurements and Applications*, pp. 1–5, 2016.

[119] T. Amemiya and H. Gomi: "Buru-Navi3: Behavioral navigations using illusory pulled sensation created by thumb-sized vibrator", In: *Proceedings of the ACM SIGGRAPH 2014 Emerging Technologies*, Article no. 4, 2014.

[120] P. Culmer, J. Barrie, R. Hewson, M. Levesley, M. Mon-Williams, D. Jayne, and A. Neville: "Reviewing the technological challenges associated with the development of a laparoscopic palpation device", *The International Journal of Medical Robotics and Computer Assisted Surgery*, Vol. 8, Issue 2, pp. 146–159, 2012.

[121] J. C. Gwilliam, M. Mahvash, B. Vagvolgyi, A. Vacharat, D. D. Yuh, and A. M. Okamura: "Effects of haptic and graphical force feedback on teleoperated palpation", In: *Proceeding of the 2009 IEEE International Conference on Robotics and Automation*, pp. 677–682, 2009.

[122] R. E. Schoonmaker and C. G. L. Cao: "Vibrotactile force feedback system for minimally invasive surgical procedures", In: *Proceeding of the 2006 IEEE International Conference on Systems, Man, and Cybernetics*, pp. 2464–2469, 2006.

[123] M. Dohi, M. Mochimaru, and M. Kouchi: "Distribution of tactile sensitivity and elasticity in Japanese foot sole", *Kansei Engineering International Journal*, Vol. 5, Issue 2, pp. 9–14, 2004.

[124] E. R. Kandel, J. H. Schwartz, and T. M. Jessell: *Principles of neural science*, 4th ed., New York: McGraw-Hill, 2000.

[125] S. Coren: *The left-hander syndrome: The causes and consequences of left-handedness*, New York: McGraw-Hill, 2000.

[126] N. A. Macmillan and C. D. Creelman: *Detection theory: A user's guide*, 2nd ed., New York: Lawrence Erlbaum Associates, 2005.

[127] P. Irwin and H. Robert: "Sampling variability of the area under the ROC-curve and of d'e", *Psychological Bulletin*, Vol. 71, No. 3, pp. 161–173, 1969.

[128] C. R. Wagner and R. D. Howe: "Force feedback benefit depends on experience in multiple degree of freedom robotic surgery task", *IEEE Transactions on Robotics*, Vol. 23, Issue 6, pp. 1235–1240, 2007.

[129] M. A. Pastor, B. L. Day, E. Macaluso, K. J. Friston, and R. S. J. Frackowiak: "The functional neuroanatomy of temporal discrimination", *Journal of Neuroscience*, Vol. 24, Issue 10, pp. 2585–2591, 2004.

[130] M. O. Ernst and M. S. Banks: "Humans integrate visual and haptic information in a statistically optimal fashion", *Nature*, Vol. 415, Issue 6870, pp. 429–433, 2002.

[131] M. Ide and S. Hidaka: "Tactile stimulation can suppress visual perception", *Scientific Reports*, Vol. 3, Article no. 3453, 2013.

[132] H.-C. Shin, K. Roberts, L. Lu, D. Demmer-Fushman, J. Yao, and R. M. Summers: "Learning to read chest X-rays: Recurrent neural cascade model for automated image annotation", In: *Proceeding of the 2016 IEEE Conference on Computer Vision and Pattern Recognition*, pp. 2497–2506, 2016.

[133] Q. Dou, H. Chen, L. Yu, L. Zhao, J. Qin, D. Wang, V. C. T. Mok, L. Shi, and P.-A. Heng: "Automatic detection of cerebral microbleeds from MR images via 3D convolutional neural networks", *IEEE Transactions on Medical Imaging*, Vol. 35, Issue 5, pp. 1182–1195, 2016.

[134] J. Kleesiek, G. Urban, A. Hubert, D. Schwarz, K. Maier-Hein, M. Bendszus, and A. Biller: "Deep MRI brain extraction: A 3D convolutional neural network for skull stripping", *Neuroimage*, Vol. 129, pp. 460–469, 2016.

[135] S. Pereira, A. Pinto, V. Alves, and C. A. Silva: "Brain tumor segmentation using convolutional neural networks in MRI images", *IEEE Transactions on Medical Imaging*, Vol. 35, Issue 5, pp. 1240–1251, 2016.

[136] A. A. A. Setio, F. Ciompi, G. Litjens, P. Gerke, C. Jacobs, S. J. van Riel, M. M. W. Wille, M. Naqibullah, C. I. Sánchez, and B. van Ginneken: "Pulmonary nodule detection in CT images: False positive reduction using multi-

view convolutional networks", *IEEE Transactions on Medical Imaging*, Vol. 35, Issue 5, pp. 1160–1169, 2016.

[137] M. Havaei, A. Davy, D. Warde-Farley, A. Biard, A. Courville, Y. Bengio, C. Pal, P.-M. Jodoin, and H. Larochelle: "Brain tumor segmentation with deep neural networks", *Medical Image Analysis*, Vol. 35, pp. 18–31, 2017.

[138] W. Shen, M. Zhou, F. Yang, C. Yang, and J. Tian: "Multi-scale convolutional neural networks for lung nodule classification", In: *Proceeding of the International Conference on Information Processing in Medical Imaging*, pp. 588–599, 2015.

[139] H.-I. Suk, D. Shen, and Alzheimer's Disease Neuroimaging Initiative: "Deep learning in diagnosis of brain disorders", In: *Recent Progress in Brain and Cognitive Engineering. Trends in Augmentation of Human Performance*, Vol. 5, S.-W. Lee et al. eds., Dordrecht: Springer, pp. 203–213, 2015.

[140] J.-Z. Cheng, D. Ni, Y.-H. Chou, J. Qin, C.-M. Tiu, Y.-C. Chang, C.-S. Huang, D. Shen, and C.-M. Chen: "Computer-aided diagnosis with deep learning architecture: Applications to breast lesions in US images and pulmonary nodules in CT scans", *Scientific Reports*, Vol. 6, Article no. 24454, 2016.

[141] C. Varytimidis, K. Rapantzikos, C. Loukas, and S. Kollias: "Surgical video retrieval using deep neural networks", In: *Proceeding of the Workshop and Challenges on Modeling and Monitoring of Computer Assisted Interventions*, pp. 1–11, 2016.

[142] S. Petscharing and K. Schöffmann: "Learning laparoscopic video shot classification for gynecological surgery", *Multimedia Tools and Applications*, Vol. 77, Issue 7, pp. 8061–8079, 2017.

[143] S. Wang, A. Raju, and J. Huang: "Deep learning based multi-label classification for surgical tool presence detection in laparoscopic videos", In: *Proceeding of the 2017 IEEE 14th International Symposium on Biomedical Imaging*, pp. 620–623, 2017.

[144] Z. Zhao, S. Voros, Y. Weng, F. Chang, and R. Li: "Tracking-by-detection of surgical instruments in minimally invasive surgery via the convolutional neural network deep learning-based method", *Computer Assisted Surgery*, Vol. 22, pp. 26–35, 2017.

[145] P. L. Jia, P. F. Zhang, H. D. Li, L. H. Zhang, Y. Chen, and M. M. Zhang: "Literature review on clinical decision support system reducing medical error", *Journal of Evidence-Based Medicine*, Vol. 7, Issue 3, pp. 219–226, 2014.

[146] V. Nair and G. E. Hinton: "Rectified linear units improve restricted Boltzmann machines", In: *Proceedings of the 27th International Conference on Machine Learning*, pp. 807–814, 2010.

[147] S. Tokui, K. Oono, S. Hido, and J. Clayton: "Chainer: A next-generation open source framework for deep learning", In: *Proceedings of Workshop on Machine Learning Systems in the 29th Annual Conference on Neural Information Processing Systems*, Vol. 5, pp. 1–6, 2015.

[148] K. He, X. Zhang, S. Ren, and J. Sun: "Delving deep into rectifiers: Surpassing human-level performance on ImageNet classification", In: *Proceeding of the 2015 IEEE International Conference on Computer Vision*, pp. 1026–1034, 2015.

[149] D. P. Kingma and J. Ba: "Adam: A method for stochastic optimization", In: *Proceedings of the 3rd International Conference on Learning Representations*, pp. 1–15, 2015.

[150] C.-H. King, M. O. Culjat, M. L. Franco, C. E. Lewis, E. P. Dutson, W. S. Grundfest, and J. W. Bisley: "Tactile feedback induces reduced grasping force in robot-assisted surgery", *IEEE Transactions on Haptics*, Vol. 2, Issue 2, pp. 103–110, 2009.

[151] M. Li, S. Luo, T. Nanayakkara, L. D. Seneviratne, P. Dasgupta, and K. Althoefer: "Multi-fingered haptic palpation using pneumatic feedback actuators", *Sensors and Actuators A: Physical*, Vol. 218, pp. 132–141, 2014.

[152] S. Yun, J. Yoo, S. Lim, J. Park, H.-K. Lee, and K.-S. Yun: "Three-axis pneumatic tactile display with integrated capacitive sensors for feedback control", *Microsystem Technologies*, Vol. 22, Issue 2, pp. 275–282, 2016.

[153] M. Li, T. Ranzani, S. Sareh, L. D. Seneviratne, P. Dasgupta, H. A. Wurdemann, and K. Althoefer: "Multi-fingered haptic palpation utilizing granular jamming stiffness feedback actuators", *Smart Materials and Structures*, Vol. 23, No. 9, Article no. 095007, 2014.

[154] M. Bianchi, J. C. Gwilliam, A. Degirmenci, and A. M. Okamura: "Characterization of an air jet haptic lump display", In: *Proceedings of the 2011 Annual International Conference of the IEEE Engineering in Medicine and Biology Society*, pp. 3467–3470, 2011.

[155] C. R. Wagner, S. J. Lederman, and R. D. Howe: "A tactile shape display using RC servomotors", In: *Proceedings of the 10th Symposium on Haptic Interfaces for Virtual Environment and Teleoperator Systems. HAPTICS 2002*, pp. 354–355, 2002.

[156] R. L. Feller, C. K. L. Lau, C. R. Wagner, D. P. Perrin, and R. D. Howe: "The effect of force feedback on remote palpation", In: *Proceedings of the 2004 IEEE International Conference on Robotics and Automation*, pp. 782–788, 2004.

[157] J. Hergenhan, H. Alagi, H. Wörn, M. Uhl, R. Schirren, and S. Reiser: "Prototype of a haptic display for the evaluation of sensible haptic feedback in remote palpation", In: *Proceedings of the 2014 IEEE International Symposium on Medical Measurements and Applications*, pp. 1–6, 2014.

[158] C. Roke, A. Spiers, T. Pipe, and C. Melhuish: "The effects of laterotactile information on lump localization through a teletaction system", In: *Proceedings of the 2013 IEEE World Haptics Conference*, pp. 365–370, 2013.

[159] C. Pacchierotti, D. Prattichizzo, and K. J. Kuchnbecker: "Cutaneous feedback of fingertip deformation and vibration for palpation in robotic surgery", *IEEE Transactions on Biomedical Engineering*, Vol. 63, Issue 2, pp. 278–287, 2016.

[160] R. D. Howe, W. J. Peine, D. A. Kantarinis, and J. S. Son: "Remote palpation technology", *IEEE Engineering in Medicine and Biology Magazine*, Vol. 14, Issue 3, pp. 318–323, 1995.

[161] N. A. Mansour, A. M. R. F. El-Bab, and M. Abdellatif: "Design of a novel multimodal tactile display device for biomedical applications", In: *Proceeding of the 2012 4th IEEE RAS & EMBS International Conference on Biomedical Robotics and Biomechatronics*, pp. 183–188, 2012.

[162] E. P. Scilingo, N. Sgambelluri, D. D. Rossi, and A. Bicchi: "Haptic displays based on magnetorheological fluids: Design, realization and psychophysical validation", In: *Proceedings of the 11th Symposium on Haptic Interfaces for Virtual Environment and Teleoperator Systems. HAPTICS 2003*, pp. 10–15, 2003.

[163] J. S. Oh, J. K. Kim, S. R. Lee, S. B. Choi, and B. K. Song: "Design of tactile device for medical application using magnetorheological fluid", *Journal of Physics: Conference Series*, Vol. 412, No 1, Article no. 012047, 2013.

[164] H. Ishizuka and N. Miki: "Development of a tactile display with 5 mm resolution using an array of magnetorheological fluid", *Japanese Journal of Applied Physics*, Vol. 56, No. 6S1, Article no. 06GN19, 2017.

[165] P. Goethals, H. Lintermans, M. M. Sette, D. Reynaerts, and H. Van Brussel: "Powerful compact tactile display with microhydraulic actuators", In: *Haptics: Perception, Devices and Scenarios. EuroHaptics 2008. Lecture Notes in Computer Science*, Vol. 5024, M. Ferre ed., Berlin, Heidelberg: Springer, pp. 447–457, 2008.

[166] H.-Y. Yao, V. Hayward, and R. E. Ellis: "A tactile enhancement instrument for minimally invasive surgery", *Computer Aided Surgery*, Vol. 10, Issue 4, pp. 233–239, 2005.

[167] D. D. Lorenzo, Y. Koseki, E. D. Momi, K. Chinzei, and A. M. Okamura: "Experimental evaluation of a coaxial needle insertion assistant with enhanced force feedback", In: *Proceedings of the 2011 Annual International Conference of the IEEE Engineering in Medicine and Biology Society*, pp. 3447–3450, 2011.

[168] C. Pacchierotti, S. Sinclair, M. Solazzi, A. Frisoli, V. Hayward, and D. Prattichizzo: "Wearable haptic systems for the fingertip and the hand: Taxonomy, review, and perspectives", *IEEE Transactions on Haptics*, Vol. 10, Issue 4, pp. 580–600, 2017.

[169] K. Minamizawa, S. Fukamachi, H. Kajimoto, N. Kawakami, and S. Tachi: "Gravity grabber: Wearable haptic display to present virtual mass sensation", In: *Proceedings of the ACM SIGGRAPH 2007 Emerging Technologies*, Article no. 8, 2007.

[170] M. Bianchi and A. Serio,: "Design and characterization of a fabric-based softness display", *IEEE Transactions on Haptics*, Vol. 8, Issue 2, pp. 152–163, 2015.

[171] G. Frediani, D. Mazzei, D. E. D. Rossi, and F. Carpi: "Wearable wireless tactile display for virtual interactions with soft bodies", *Frontiers in Bioengineering and Biotechnology*, Vol. 2, Article no. 31, 2014.

[172] T. Aoki, H. Mitake, D. Keoki, S. Hasegawa, and M. Sato: "Wearable haptic device to present contact sensation based on cutaneous sensation using thin wire", In: *Proceedings of the International Conference on Advances in Computer Entertainment Technology*, pp. 115–122, 2009.

[173] G. A. Pradana, A. D. Cheok, M. Inami, J. Tewell, and Y. Choi: "Emotional priming of mobile text messages with ring-shaped wearable device using color lighting and tactile expressions", In: *Proceedings of the 5th Augmented Human International Conference*, Article no. 14, 2014.

[174] S. Je, O. Choi, K. Choi, M. Lee, H.-J. Suk, L. Chan, and A. Bianchi: "Designing skin-dragging haptic motions for wearables", In: *Proceedings of the 2017 ACM International Symposium on Wearable Computers*, pp. 98–101, 2017.

[175] C. Pacchierotti, G. Salvietti, I. Hussain, L. Meli, and D. Prattichizzo: "The hRing: A wearable haptic device to avoid occlusions in hand tracking", In: *Proceedings of the 2016 IEEE Haptics Symposium*, pp. 134–139, 2016.

[176] A. Russomanno, R. B. Gillespie, S. O'Modhrain, and J. Barber: "Modeling pneumatic actuators for a refreshable tactile display", In: *Haptics: Neuroscience, Devices, Modeling, and Applications. EuroHaptics 2014. Lecture Notes in Computer Science*, Vol. 8619, M. Auvray et al. eds., Berlin, Heidelberg: Springer, pp. 385–393, 2014.

[177] W. J. Peine, P. S. Wellman, and R. D. Howe: "Temporal bandwidth requirements for tactile shape displays", In: *Proceedings of the IMECE Haptics Symposium*, pp. 1–16, 1997.

[178] J. O. Wobbrock, L. Findlater, D. Gergle, and J. J. Higgins: "The aligned rank transform for nonparametric factorial analyses using only anova procedures", In: *Proceedings of the SIGCHI Conference on Human Factors in Computing Systems*, pp. 143–146, 2011.

[179] W. Jesteadt, C. C. Wier, and D. M. Green: "Intensity discrimination as a function of frequency and sensation level", *The Journal of the Acoustical Society of America*, Vol. 61, No. 1, pp. 169–177, 1977.

[180] G. A. Gescheider: *Psychophysics: The fundamentals*, 3rd ed., Mahwah, NJ: Lawrence Erlbaum Associates, 1997.

[181] S. J. Bensmaïa, Y. Y. Leung, S. S. Hsiao, and K. O. Johnson: "Vibratory adaptation of cutaneous mechanoreceptive afferents", *Journal of Neurophysiology*, Vol. 94, Issue 5, pp. 3023–3036, 2005.

[182] Y. G. Chung, S. W. Han, H.-S. Kim, S.-C. Chung, J.-Y. Park, C. Wallraven, and S.-P. Kim: "Adaptation of cortical activity to sustained pressure stimulation on the fingertip", *BMC Neuroscience*, Vol. 16, Article no. 71, 2015.

Publications

Journals

1. T. Fukuda, Y. Tanaka, A. M. L. Kappers, M. Fujiwara, and A. Sano: "Visual and tactile feedback for a direct-manipulating tactile sensor in laparoscopic palpation", *The International Journal of Medical Robotics and Computer Assisted Surgery*, Vol. 14, Issue 2, Article no. e1879, 2018, DOI: 10.1002/rcs.1879.

2. T. Fukuda, Y. Tanaka, M. Fujiwara, and A. Sano: "DNN-based assistant in laparoscopic computer-aided palpation", *Frontiers in Robotics and AI*, Vol. 5, Article no. 71, 2018, DOI: 10.3389/frobt.2018.00071.

3. T. Fukuda, Y. Tanaka, A. M. L. Kappers, M. Fujiwara, and A. Sano: "A pneumatic tactile ring for instantaneous sensory feedback in laparoscopic tumor localization", *IEEE Transactions on Haptics*, Vol. 11, Issue 4, pp. 485–497, 2018, DOI: 10.1109/TOH.2018.2854753.

Proceedings of International Conferences

1. T. Fukuda, Y. Tanaka, M. Fujiwara, and A. Sano: "A ring-type tactile display with a compact pneumatic drive unit for a laparoscopic palpation system", In: *Proceedings of the 2017 IEEE/RSJ International Conference on Intelligent Robots and Systems (Abstract-Only)*, p. 2303, 2017.

Proceedings of Domestic Conferences

1. T. Fukuda, Y. Tanaka, M. Fujiwara, and A. Sano: "A study on a sticking type tactile display for a laparoscopic palpation system", In: *Proceedings of the 34th Annual Conference of the Robotics Society of Japan*, Article no. 3F2-08, 2016. (In Japanese)

2. T. Fukuda, Y. Tanaka, M. Fujiwara, and A. Sano: "Ring-type pneumatic tactile display for laparoscopic palpation system", In: *Proceedings of the 17th SICE System Integration Division Annual Conference*, pp. 2149–2150, 2016. (In Japanese)